EXPLORING THE ROLE OF MITOCHONDRIA IN MUSCLE WEAKNESS AND ATROPHY IN A MOUSE MODEL OF CANCER CACHEXIA

LUCA DELFINIS

A THESIS SUBMITTED TO
THE FACULTY OF GRADUATE STUDIES
IN PARTIAL FULFILLMENT OF THE REQUIREMENTS
FOR THE DEGREE OF
MASTER OF SCIENCE

GRADUATE PROGRAM IN KINESIOLOGY
YORK UNIVERSITY
TORONTO, ONTARIO

August 2020

Abstract

Cancer cachexia is a multifactorial syndrome characterized by an ongoing loss of skeletal muscle mass. The focus of this thesis was to determine the degree of skeletal muscle mitochondrial bioenergetic dysfunction in a preclinical model of cancer cachexia as this may reveal impaired energy homeostasis as a mechanism underlying muscle atrophy and muscle weakness. To do this, we used the C26 cancer cachexia model and evaluated mitochondrial bioenergetics in both the quadriceps and diaphragm. Our findings reveal that effects of C26 cancer on mitochondrial bioenergetic differs between diaphragm and quadriceps. In addition, this thesis reports a unique finding whereby mitochondrial ADP sensitivity is increased in C26 cancer cachectic skeletal muscle, suggesting that cancer improves the ability of muscle mitochondria to respond to changes in energy demand. Moreover, these findings also suggest that mitochondria may be more uncoupled in cancer cachexia.

Acknowledgements

I want to thank my supervisor Dr. Christopher Perry for his guidance throughout the course of these 2 years. There's only so many times you can watch someone make a mistake, but you stood by me every time and helped me learn from them… until I made them again. Your patience and commitment towards completing this project with me not only taught me science, but I learned a great deal about life by learning how to be patient, understanding, relentless and most importantly – curious. I also learned that I laugh too much at bad jokes.

I also want to thank Megan Rosa-Caldwell and Dr. Nicholas Greene from the University of Arkansas. It was only with their help that we were able to pioneer a preclinical model of cancer cachexia within this laboratory. Their guidance and knowledge made this work possible and cannot be emphasized enough.

Last, I want to thank all of the labmates that have come and gone: Meg, Pat, Sofhia, Ali, Cat, Sara and Shiv. I've learned so much from all of you and truly made life-long friends along the way. I'm beyond excited to have the opportunity to continue for the next 4 years to pursue a PhD.

Table of Contents

List of Tables

List of Figures

List of Appendices

List of Abbreviations

ADP: Adenosine Diphosphate
AIF: Apoptosis Inducing Factor
AMPK: 5'-Adenosine Monophosphate-Activated Protein Kinase
ANT: Adenine Nucleotide Translocator
APAF-1: Apoptosis-Activating Factor-1
ATP: Adenosine Triphosphate
C26: Colon-26 Adenocarcinoma (Experimental group)
CDNB: 2,4-dinitrochlorobenzene
CRC: Calcium Retention Capacity
Cr: Creatine
CyD: Cyclophilin D
DRP1: Dynamin Related Protein 1
ETC: Electron Transport Chain
$FADH_2$: Flavin Adenine Dinucleotide
FIS1: Mitochondrial Fission Protein 1
gp130: Glycoprotein 130
H_2O_2: Hydrogen Peroxide
IFN-γ: Interferon -γ
IGF-1: Insulin-Like Growth Factor-1
IkBA: Inhibitor of Kappa B Alpha
IL-1: Interleukin – 1
IL-6: Interleukin – 6
IMM: Inner Mitochondrial Membrane
IMS: Intermembrane Space
IP3R: Inositol Triphosphate Receptor
JAK/STAT: Janus Kinases/Signal Transducer and Activator of Transcription Proteins
LC3B: Microtubule-Associated Protein-1
LLC: Lewis Lung Carcinoma
MAFbx: Muscle Atrophy F-box
MCU: Mitochondrial Calcium Uniporter
MFN: Mitofusin
mH_2O_2: Mitochondrial Hydrogen Peroxide
mtCK: Mitochondrial Creatine Kinase
mTOR: Mammalian Target of Rapamycin
MURF-1: Muscle RING Finger 1
NADH: Nicotinamide Adenine Dinucleotide
NCLX: Na^+/Ca^+ exchanger
NF-kB: Nuclear Factor Kappa B
OMM: Outer Mitochondrial Membrane
OPA-1: Optic Atrophy Protein - 1
OXPHOS: Oxidative Phosphorylation
PARP: Poly-ADP Ribose Polymerase
PBS: Phosphate Buffered Saline (Control group)
PCr: Phosphocreatine
P_i: Inorganic Phosphate
PGC-1: Peroxisome Proliferator-Activated Receptor Gamma Coactivator-1

PIF: Proteolysis-Inducing Factor
PTP: Permeability Transition Pore
RCR: Respiratory Control Ratio
REE: Resting Energy Expenditure
RNS: Reactive Nitrogen Species
ROS: Reactive Oxygen Species
RyR: Ryanodine Receptor
SERCA: Sarco/Endoplasmic Reticulum Ca^{2+} ATPase
STAT3: Signal Transducer and Activator of Transcription Protein – 3
SOD: Superoxide Dismutase
TNF-α: Tumour Necrosis Factor-α
UCP: Uncoupling Proteins
VDAC: Voltage Dependent Anion Channel

CHAPTER 1: INTRODUCTION

Cancer is fundamentally understood as continual, unregulated cell proliferation that occurs due to mutations from single cells[1]. Tumours can induce a myriad of harmful alterations to the host, one of which is the tumours ability to provoke specific alterations on skeletal muscle metabolism such that there is a dysregulation of muscle protein synthesis and degradation[2]. This often leads to cancer cachexia. Cancer cachexia is defined as a multifactorial syndrome characterized by an ongoing loss of skeletal muscle mass that cannot be reversed by conventional nutritional support[3]. Nearly one half of Canadians will develop cancer at some point in their lives[4] and 25-80% of cancer patients will develop cachexia throughout the disease depending on the type and stage of cancer[5]. It is thought that cancer induces cachexia through inflammation and activation of proteolytic systems[6], however recent literature suggests skeletal muscle mitochondria may be impaired in cancer.

Mitochondria are organelles within muscle cells that regulate three vital cellular processes: ATP production, reactive oxygen species (ROS) generation and calcium retention capacity (CRC) in relation to triggering of the permeability transition pore prior to apoptosis. ROS generation is a natural by-product of ATP production. In modest concentrations, ROS is vital to maintain cellular processes, but at high concentrations, ROS can trigger protein degradation via proteolytic pathways resulting in cell death[7]. This balance of energy transduction between ATP production and ROS generation within mitochondria is termed mitochondrial bioenergetics and can impact upstream skeletal muscle homeostasis. Therefore, the mitochondrial regulation of energy transduction by balancing ATP and adenosine diphosphate (ADP) homeostasis is a vital process and predictor of skeletal muscle health.

Literature elucidating the role of mitochondrial bioenergetics in cancer skeletal muscle is scarce and inconclusive as cancer may impact mitochondria differentially depending on the model and muscle questioned. Current literature suggests in two models of cancer cachexia that mitochondrial ADP-stimulated respiration is impaired in cancer cachectic skeletal muscle [8,9]. In addition ROS in the form of mitochondrial hydrogen peroxide (mH_2O_2) emission may be increased in cancer cachexia skeletal muscle[9]. However, to our knowledge no researchers to date have evaluated ADP sensitivity in cancer skeletal muscle while evaluating mitochondrial respiration and ROS generation. This gap in knowledge is important to address given ADP is a central governor of mitochondrial bioenergetics, particularly with respect to respiratory control and mH_2O_2 emission given both processes are regulated by mitochondrial membrane potential, as explained below. Therefore, it may be possible that the reports of gross indicators of mitochondrial dysfunction during cancer cachexia may be linked to a unifying impairment in ADP sensitivity – a process that can also be heavily influenced by mitochondrial creatine cycling. In this regard, researchers have yet to compare creatine independent and creatine dependent phosphate shuttling of energy exchange. As dysfunctions in these bioenergetic process can be linked to impaired mitochondrial calcium handling[10], it is also unknown if mitochondrial calcium retention capacity linked to permeability transition pore formation (a regulator of apoptosis) is activated during cancer cachexia. These questions are vital to understanding the role of muscle mitochondrial bioenergetics in cancer as impaired mitochondrial bioenergetics may be a potential therapeutic target for cancer cachexia which currently has no cure. Therefore, the three main purposes of this thesis were to determine if cancer cachexia 1) impairs mitochondrial ADP sensitivity with respect to the regulation of respiration and mH_2O_2 emission, 2) impairs creatine's control of ADP sensitivity during respiration and mH_2O_2 emission and 3) impacts mitochondrial bioenergetics differently in different muscles relative to muscle weakness and/or atrophy.

CHAPTER 2: LITERATURE REVIEW

Section 2.1: Introduction to Cancer Cachexia

2.1.1 Overview of Cancer Cachexia

Cancer is fundamentally understood as continual, unregulated cell proliferation resulting in tumour formation[1,11]. This occurs due to mutations from single cells that divide abnormally[1,11]. Many different types of cancers exist, and no cancer acts the same. Although cancer development is important to elucidate, it is also paramount to understand how cancer affects its host when it manifests as a tumour at a given site. More specifically, it is important to understand how a tumour induces implications to surrounding organs that can compromise the health of the host. Therefore, this thesis is concerned with the repercussions a cancerous tumour has on skeletal muscle. This thesis is interested in how cancer induces cachexia.

The international consensus on the definition of cancer cachexia is "a multifactorial syndrome characterized by an ongoing loss of skeletal muscle mass (with or without fat mass) that cannot be fully reversed by conventional nutritional support and leads to progressive functional impairment"[3]. Cachexia can manifest itself in a myriad of different conditions aside from cancer like chronic renal failure, chronic kidney disease, chronic heart failure and more[12]. In order to assess if a cancer patient is cachectic, physicians are instructed to assess: anorexia or reduced food intake, catabolic drivers, muscle mass/strength and psychosocial effects[3]. Cancer cachectic patients exhibit reduced physical function,[13] reduced tolerance to anticancer therapies,[14] and reduced survival[15]. As of 2019, it is estimated that nearly one half of Canadians will develop cancer at some point in their lives[4], while 25-80% of cancer patients will develop cachexia throughout the disease depending on the type and stage of cancer[5]. One fourth of patients will die due to cancer[4]. Within this cohort, it is not clear if there is a causal relationship between cachexia and death, however, it is well understood that individuals with chronic disease states are more likely to die

when they lose weight and develop progressive cachexia[16]. It is very clear that cancer cachexia reduces the survivability of cancer patients[15]. It should be noted that patients who have cancer also undergo chemotherapy treatment. Chemotherapy can disrupt muscle homeostasis even more, exacerbating muscle loss[17]. There is no cure for cancer cachexia and thus there is a justified need for a viable treatment avenue[3,5,18]. Understanding holistic and muscle specific molecular adaptations that occur as a result of cancer development can aid in understanding the etiology of the disease and the development of future therapies. This literature review will focus on the impact of cancer-induced changes to skeletal muscle with focus on the role of mitochondrial function.

2.1.2 Cancer's Development and Impact on the Host

Tumours develop when cells exhibit a myriad of different mutations that alter the cells ability to proliferate and differentiate[19]. When these cells aggregate together and develop into a mass, this can form what is commonly known as a neoplasm or a tumour. Tumours can be benign or malignant. Benign tumours are localized, non-cancerous and do not spread throughout the body[19]. These types of tumours respond well to treatment and do not lead to cancer cachexia. A malignant tumour is a cancerous growth that is often resistant to treatment and can spread throughout the body[19]. Malignant tumours are commonly classified as "cancer." This literature review will elucidate how these cancerous tumours impact its host.

Cancer cachexia can be thought of as a state of "autocannibalism." – the tumour survives at the expense of the host[20]. Cancer cachexia is multifactorial, as no one mediator contributes independently to produce the cachectic phenotype. Instead, many factors induce cachexia, some popularly investigated mediators include: circulating cytokines (either released from the tumour or the host), tumour-specific factors and neuroendocrine changes[20]. These mediators are all thought to contribute to muscle protein breakdown in cancer. Muscle can be catabolized by three

main proteolytic pathways: lysosomal systems, calpain systems and the ubiquitin-proteasome pathway[21].

Human data expresses heterogeneity in the activation of proteolytic pathways with cancer. In one study where patients had pancreatic cancer, weight loss was between 12-19% and the ubiquitin-proteasome proteolytic pathway was hyperactivated[22]. In another study whereby, early disease stage lung cancer patients had only 2.9% weight loss, individuals expressed no changes in the ubiquitin-proteasome, but discovered increased mRNA content of lysosomal protease cathepsin B[23]. This may suggest that solely one proteolytic pathway is not responsible for muscle breakdown. This could also suggest that cancer impacts muscle in a time-course manner, meaning, the longer the time period of tumour growth the more severe the protein breakdown.

Cancer type - not only stage - plays a role in dictating the extent at which muscle is damaged. Data from 3047 cancer patients demonstrate that those with pancreatic or gastric cancer have the highest frequency of weight loss (83-87%), patients with colon, prostate or lung cancer have intermediate weight loss (48-61%) and patients with breast cancer and sarcomas (cancers developing from connective tissue) have the least weight loss (31-40%)[15]. Therefore, it appears likely that both cancer type and cancer stage may dictate the extent to which cachexia is established in humans. This makes cancer cachexia literature extremely difficult to interpret as data from different rodent models may not be transferable to humans. In order to truly understand how tumours activate proteolytic pathways and change host metabolism, it is important to understand what factors are released by tumours and how this leads to a cascade of outcomes.

2.1.3 Tumour Muscle Cross-talk

Tumours can impact neighboring tissues by both releasing its own factors and forcing the host to release factors as well. Popularly investigated factors released by the tumour and host include cytokines like: tumour necrosis factor-α (TNF-α), interleukin (IL)-1 and -6, and interferon

-γ (IFN-γ)[24]. Tumour-specific products include proteolysis-inducing factor (PIF)[24]. These factors are thought to work synergistically to activate various signaling cascades that induce protein degradation or inhibit protein synthesis.

TNF-α and IL-1 from immune or tumour cells can activate nuclear factor kappa B (NF-kB), a protein complex that controls DNA transcription for cytokine production and cell survival[25]. NF- kB is thought to induce skeletal muscle atrophy in three ways: 1) augment the expression of several proteins during atrophy 2) increase the expression of inflammation-related molecules which directly or indirectly promote muscle-wasting and 3) interfere with myogenic regeneration of atrophied skeletal muscle[25]. NF-kB activity is increased 6-fold in skeletal muscle of mice bearing Lewis lung cancer carcinoma (LLC)[26]. In humans, expression of the inhibitor of kappa B alpha (IkBA), a marker of NF-kB activation, was decreased by 25% in rectus abdominis skeletal muscle of gastric cancer patients[27]. Indeed, NF-kB seems to play a role in both rodent models of cancer cachexia and human models, thus ultimately suggesting that the cytokines TNF-α and IL-1 are main facilitators of cancer cachexia via their role in increasing NF-kB activation. However, cytokine release and corresponding signaling cascades may be tumour specific. In other words, tumours in different mice models seem to release different cytokines[28]. Cancer cachexia models and their differences will be further discussed in section 2.1.6.

IL-6 regulates skeletal muscle atrophy by both inducing protein degradation and inhibiting protein synthesis. IL-6 cytokine family bind to the receptor glycoprotein 130 (gp130) which can induce downstream JAK/STAT activation[29]. JAK/STAT can increase expression of STAT3, which is a primary mediator of muscle wasting in rodent models of colon 26 adenocarcinoma (C26) cachexia[30]. In addition, IL-6 can induce suppression of mTOR[31]. Briefly, mTOR controls protein synthesis and is regulated by insulin/IGF-I signaling[32]. In a cancer cachexia rodent model of plasmid-based IL-6 over expression ($Apc^{Min/+}$), IL-6 induces a dose-dependent suppression of

mTOR signaling in skeletal muscle, suggesting a reduction in protein synthesis[31]. Therefore, IL-6 is a commonly cited cytokine responsible for inducing or contributing to cachexia in cancer.

PIF is a tumor-specific factor, originally isolated from MAC16 tumour bearing mice and urine of cachectic cancer patients[33]. PIF was first identified as a 24K proteoglycan and was distinguished from cytokines by its structure and ability to accelerate breakdown of skeletal muscle *in vitro* and *in vivo* by a process not involving anorexia[34]. PIF is detectable in the urine of all cancer cachectic patients, irrespective of cancer type[34]. There is also evidence to suggest PIF can activate NF-kB[35]. Last, PIF also activates the ubiquitin proteasome pathway in both *in vivo* and *in vitro* models of MAC16 (colon cancer carcinoma) cancer cachexia using mice gastrocnemius muscle and C2C12 myotubes[36].

Indeed, many factors that are both host specific and tumour specific seem to communicate to the muscle to induce an increase in protein breakdown and a decrease in protein synthesis. Current strategies to improve muscle health in cancer cachexia include appetite stimulants, non-steroidal anti-inflammatory drugs, exercise, and more [33,37]. If inflammatory markers were solely responsible for cachexia, then anti-inflammatory drugs would serve as a sufficient treatment plan. However, none of the above-mentioned treatment strategies seems to fully recover muscle during cancer cachexia. Thus, additional pathological mechanisms must be investigated, and new therapeutic strategies must be developed.

2.1.4 Cancer's Impact on Skeletal Muscle Atrophy Processes

Original rodent experiments suggest that the main facilitator of muscle protein breakdown in cancer cachexia is hyperactivation of the ubiquitin-proteasome pathway[38–40]. The ubiquitin-proteasome pathway is a complex system. Briefly, this system degrades proteins by using the enzymes: E1 - ubiquitin carrier protein, E2 – ubiquitin-conjugating enzyme, E3 – ubiquitin-protein ligase and 26S proteasome complex[41]. In summary, the system works through two main steps 1)

tagging the substrate by covalent attachment of multiple ubiquitin molecules and 2) degradation of the tagged protein by the 26S proteasome complex[41]. First, E1 enzymes activate ubiquitin using ATP to generate a thiol-ester intermediate[41]. Next, E2 enzymes can transfer the activated ubiquitin moiety from E1 to the protein substrate through an additional thiol-ester intermediate with the use of ATP once again[41]. This protein substrate binds to an E3 enzyme through a recognition motif[41]. The ubiquitin conjugated protein will reach the 26S proteasome, a 2.5MDa complex made up of 32 different subunits[41]. Here, with high specificity, the complex and its subunits will recognize the ubiquitin and breakdown the substrate with the help of more ATP by cleaving peptide bonds[41]. It must be noted that the ubiquitin-proteasome pathway is much more intricate and complex than described in this review. The pathway reviewed is reviewed in detail by Glickman and Ciechnover[41] and only discussed briefly in this review to help build context for cancer cachexia specific activation.

It is clear that the ubiquitin-proteasome pathway plays a large role in rodent models of cancer cachexia. What remained elusive for years in the literature was the specific changes in regulation that occur of the proteolytic pathway in muscle. Muscle RING finger 1 (MURF-1) and Muscle Atrophy F-box (MAFbx) are both E3 ubiquitin ligases expressed in skeletal muscle. Current literature suggests that the rate-limiting step in the UPS pathway for other models of cachexia is polyubiquitination which is controlled by MURF1 and MAFbx [42]. Cancer patients that exhibit cachexia also seem to have specific activation of atrogen-1 and MURF-1[43]. In a cell culture model, knockdown of atrogen-1 protected C2C12 myotubes from atrophy induced by TNF-α[44]. In addition, inhibiting myostatin promoter activity with IMB090 seemed to decrease the expression of atrogen-1 and MURF-1 and offset muscle atrophy in both cell culture and C26 murine model of cancer cachexia[45].

It seems that cancer shares a common transcriptional program for activating muscle atrophy compared to conditions like starvation, diabetes and chronic renal failure[42]. However, a growing body of literature has revealed that cancer disrupts muscle metabolism and redox homeostasis in a manner that may contribute to cachexia. The next section provides an overview of the emerging relationships between cachexia and impaired mitochondrial bioenergetics as well as potential mechanistic links that remain to be established.

2.1.5 Cancer's Impact on Muscle Metabolism

Muscle is commonly viewed as a by-stander tissue where external stimuli can induce protein anabolism or catabolism. Muscle metabolism in cancer demonstrates how alterations in the function of proteins and enzymes precedes changes in muscle turnover that lead to cachexia. A trial done on 390 cancer patients before the onset of chemotherapy evaluated their resting energy expenditure (REE) and demonstrated early hypermetabolism, negative energy balance and biological features of precachexia[46]. These patients had different types of cancer and were evaluated during early stages of cancer progression. REE encompasses the largest use of daily energy in humans. Briefly, if REE is upregulated, this can lead to weight loss if caloric intake is not properly elevated to counter the increase in REE. Moreover, individuals with hypermetabolism may be at risk of malnutrition and downstream clinical complications[46]. This increase in REE in cancer can be explained in part by upregulation of uncoupling proteins (UCPs) -particularly UCP3 in skeletal muscle[6]. However, simply providing cancer patients with better nutrition by increasing caloric intake seems to have a limited impact on cachexia[3,6,33]. In fact, stimulation of nutrient intake alone promotes weight gain, however, this results in increases in fat mass with no changes lean body muscle mass[6]. Therefore, if increasing caloric intake does not lead to better muscle health, a possible explanation may be that muscle cells are not utilizing macronutrients efficiently in cancer.

Macronutrient utilization can be explored while investigating mitochondria as these organelles are responsible for using reducing equivalents gathered from macronutrients via glycolysis and the Krebs's cycle to generate ATP and drive enzymatic processes. Recent data has demonstrated that mitochondrial dysfunction exists in muscle during cancer cachexia in both humans and rodent models[47,48]. Specific mitochondrial changes with cancer cachexia will be discussed in section 2.3 of this literature review. Interestingly, recent data in a rodent model suggests that cancer seems to induce mitochondrial dysfunction before the onset of cachexia[9]. This rodent model data matches human models. If cancer patients are exhibiting an early increase in REE and undergoing negative mitochondrial alterations that affect macronutrient utilization, this may explain why skeletal muscle is damaged after tumour bearing. A proposed model summarizing cancer's impact on skeletal muscle can be seen in Figure 1.

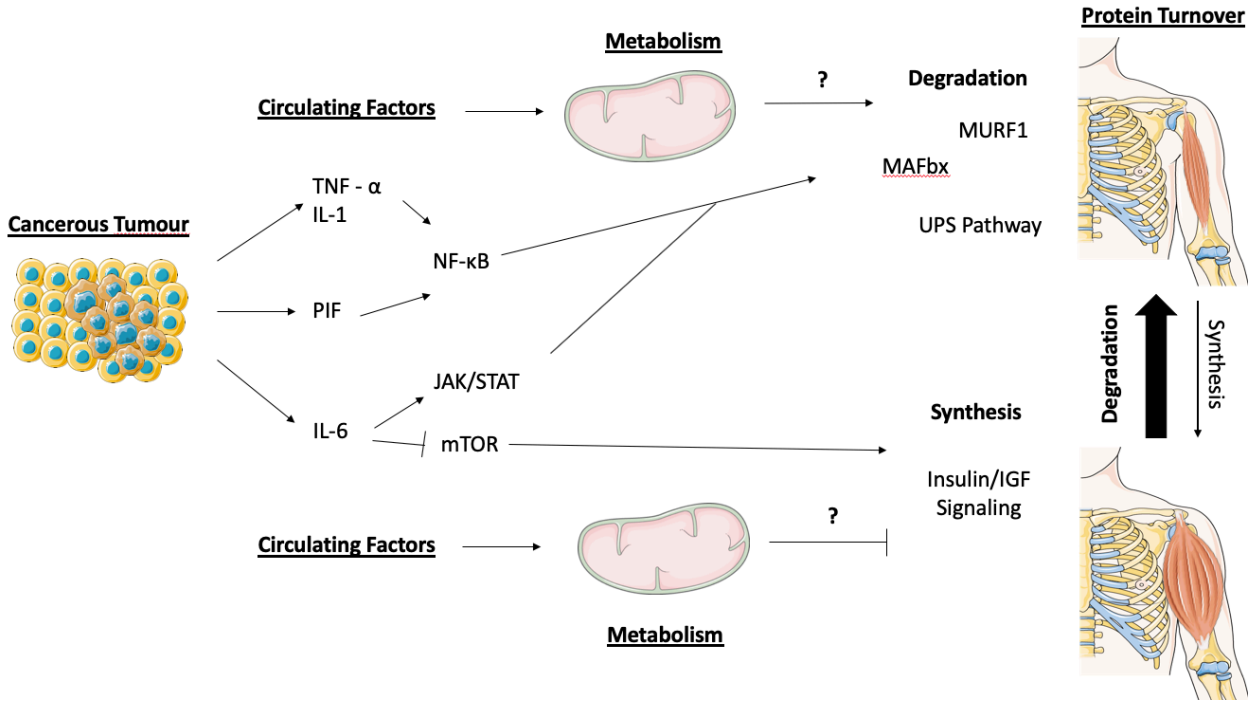

Figure 1. Proposed Model of Cancer's Impact on Skeletal Muscle Protein Content. Tumours induce muscle atrophy by both inhibiting synthesis and activating degradation. It is proposed that this is occurring due to cytokines released by the host and the tumour itself. However, much remains unknown and the role of metabolism is yet to be fully understood. **TNF-α:** Tumour Necrosis Factor-α; **IL-1:** Interleukin – 1; **PIF**: Proteolysis-Inducing Factor; **IL -6:** Interleukin – 6; **NF-kB:** Nuclear Factor Kappa B; **JAK/STAT:** Janus Kinases/Signal Transducer and Activator of Transcription Proteins; **mTOR:** Mammalian Target of Rapamycin; **MURF-1:** Muscle RING Finger 1; **MAFbx:** Muscle Atrophy F-box; **IGF-1:** Insulin-like growth factor-1.

Therefore, muscle metabolism may be playing a more active role in inducing cancer cachexia than previously thought as metabolic alterations seem to precede muscle atrophy. Although muscle's response may be ill-fated, the tissue can play a large role in combating disease by using macronutrients effectively through mitochondria. Targeting muscle metabolism through mitochondria may be an appropriate treatment plan to recovering muscle health as this may attenuate atrophy by improving nutrient utilization and enhancing lean muscle mass.

2.1.6 Models of Cancer Cachexia

As mentioned earlier in this literature review, cachexia occurs in 25-80% of all cancer patients depending on the type and stage of cancer[5]. Formatting the "perfect" model to replicate

cancer cachexia is likely impossible considering the complexity and heterogeneity that exists in this disease. In order to understand cancer cachexia as a disease, it is important to understand the strengths and limitations to the numerous cancer cachexia models.

Models of cancer cachexia are vast and can include cells, animals and human. Researchers can learn about cancer cachexia using C2C12 myoblasts[49,50]. In this model researchers can understand how cancer cells affect skeletal muscle atrophy using factors that cancers commonly release without the manipulation of a host[50]. In addition, when C2C12 myoblasts are co-cultured with cancer cells, some indications of mitochondrial dysfunction exist[49]. Indeed, this *in vitro* approach revealed evidence that cancer may induce decreased ATP synthesis ability, transient increases in reactive oxygen species (ROS) and subsequent oxidative damage[49]. Although this data is crucial to understand the fundamental mechanisms that govern alterations in skeletal muscle due to cancer, an animal model brings researchers one step closer to recapitulating human cancer cachexia.

There are many animal models of cancer cachexia. In order to induce cancer cachexia, mice or rats are either injected with cancer cells (xenograft models) or mice are genetically engineered to be immunocompromised and grow cancer spontaneously[51]. Most xenograft models are summarized by Ballarò et al.[28]. Although these models induce cancer cachexia likely in similar fashion, these models have differences in cancer cell type, injection site, tumour size, tumour development time, inflammation markers and metastasis[28]. Cancer cachexia in a spontaneous tumour model ($Apc^{Min/+}$) demonstrates yet another avenue to research cancer cachexia in an animal model[52]. Therefore, although these models all induce muscle atrophy, there are many differences within the model that can make data increasingly challenging to relate to human cancer cachexia. While the heterogeneity of these models is important, the main focus for our research design was

the presence of a mitochondrial dysfunction in cancer cachexia as it is even present in human models[47].

Each model has advantages and disadvantages and no model is perfect. Most mice-xenograft models require tumours to grow to about 10-20% body weight to induce cachexia, an extremely large size compared to human cancers. The AH130 rat model of cancer cachexia only has rat's bearing tumours for 7-8 days, an extremely unlikely timeline for cancer to induce muscle and mitochondrial adaptations in humans. Therefore, it is important to select a model based on the researcher's hypothesis and acknowledging that drawbacks may exist that can limit data interpretation. Many models of cancer cachexia demonstrate mitochondrial dysfunction [8,9,52]. Recently, a xenograft model of cancer cachexia using LLC suggests that mitochondrial dysfunction precedes cachexia[9]. C26 models of cancer cachexia also induce mitochondrial dysfunction, while maintaining modest tumuor sizes to fit animal ethical considerations[8]. This will allow us to utilize a cancer cachexia model within our laboratory.

Section 2.2: Introduction to Mitochondrial Bioenergetics

2.2.1 Overview of Mitochondrial Bioenergetics

Bioenergetics is the quantitative study of energy transductions (changes of one form of energy into another) that occurs in living cells. Mitochondria are organelles that harness the energy from carbohydrates, fats and amino acids and convert it to adenosine triphosphate (ATP). ATP is a source of energy for countless physiological reactions within the cell. Therefore, mitochondrial bioenergetics is the study of energy transduction within mitochondria.

Mitochondria are capable of harnessing energy through macronutrients by utilizing a series of electron carriers and enzymes to drive protons through its inner membrane. A natural byproduct of such energy transduction is the formation of reactive oxygen species (ROS). ROS plays a pivotal

role in a number of physiological process. The potential impact of ROS is so vast, research careers are dedicated to understanding the role of a single ROS and its impact on downstream signal transduction cascades. The following section in this literature review will discuss how exactly mitochondria harness energy from macronutrients, how ATP/ADP is shuttled between the mitochondria and the cytoplasm and how mitochondrial bioenergetics affect cellular health.

2.2.2 Oxidative Phosphorylation

Mitochondria contain two membranes, the ion permeant outer mitochondrial membrane (OMM) and inner mitochondrial membrane (IMM). In between these membranes is the intermembrane space (IMS), which is rich with key physiological proteins. Embedded in the IMM are five proteins (I-V) of the electron transport chain (ETC)[53]. Two electron carries – nicotinamide adenine dinucleotide (NADH) and flavin adenine dinucleotide ($FADH_2$) - are key regulators that catalyze the transfer of electrons through a series of redox reactions within the ETC to generate free energy[53]. The use of free energy in the production of ATP was proposed by Peter Mitchell in 1961[54]. Referred to as the chemiosmotic theory of oxidative phosphorylation, this concept explains how a series of redox reactions coupled with ions crossing the IMM and interacting with ATPases can convert free energy into ATP[54].

The five protein complexes are known as: NADH ubiquinone oxidoreductase (complex I), succinate dehydrogenase (complex II), cytochrome bc_1 complex (complex III), cytochrome oxidase (complex IV) and ATP synthase (complex V). The two electron acceptors within the IMM are known as ubiquinone and cytochrome c [55]. Through a series of redox reactions, electrons pass through complexes I-V on the IMM while simultaneously pumping hydrogen ions(H^+) from the mitochondrial matrix (negative), through the IMM and into the IMS (positive), contributing to a proton motive force (ΔP). This ΔP can energize complex V to synthesize ATP from adenosine diphosphate (ADP) and inorganic phosphate (P_i), powered by the flow of protons against the

electro-chemical gradient and into the matrix[55]. The coupling of the energy produced through oxidation and phosphorylation of ADP is known as oxidative phosphorylation (OXPHOS) and is thought to contribute to 95% of the ATP produced in the cell under basal conditions[53] (Figure 2).

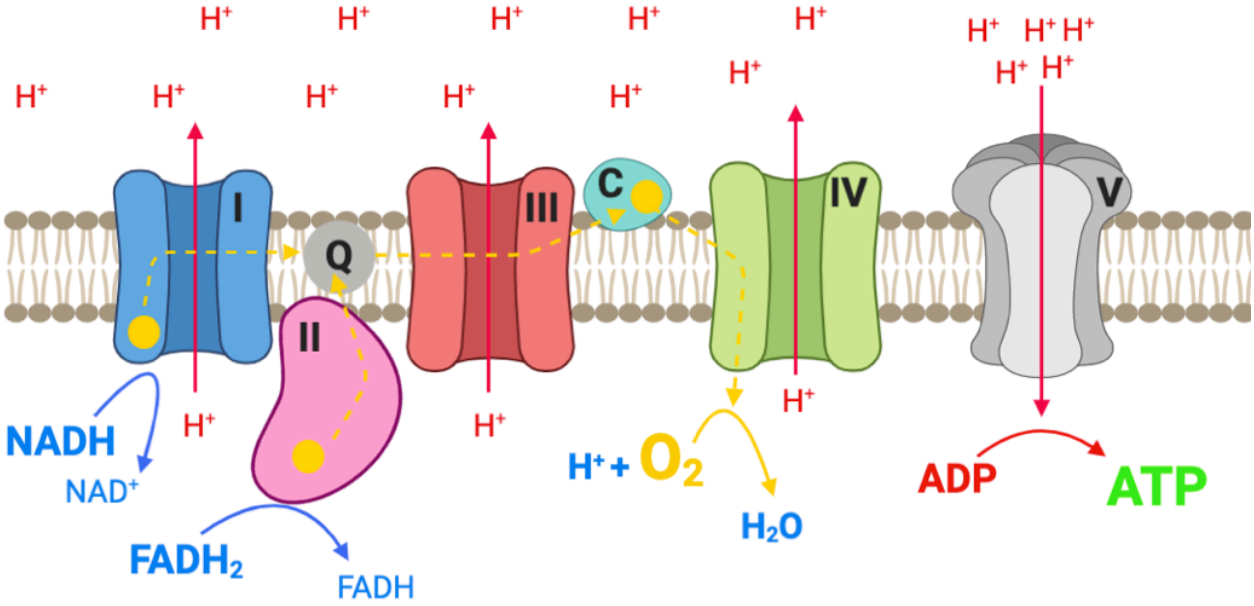

Figure 2. Schematic of Key Regulators of the ETC.
Within the IMM lies the five protein complexes (I-V) of the ETC and two mobile electron carriers (NADH and $FADH_2$). These two mobile electron carriers catalyze the transfer of electrons through redox reaction that release free energy. This process promotes complexes I, III and IV to pump protons from the matrix into the IMS, against a concentration gradient. This energy generates an electrochemical gradient in the IMS that can be used to power the phosphorylation of ADP to produce ATP at complex V.

OXPHOS is regulated in part by cellular energy demands. The more a cell requires energy to drive physiologically processes, the more the cell will upregulate OXPHOS if nutrient and oxygen supply are sufficient. Moreover, OXPHOS is largely driven by the availability of ADP and P_i as a substrates for phosphorylation[55]. As a major focus of this thesis is on the regulation of ADP sensitivity in particular, it is important to note that ATP and ADP turnover control both the rates of electron transfer and the rates of citric acid cycle and substrate oxidation in addition to glycolysis. Therefore, intracellular ADP concentrations and the mass action ratio of ATP/(ADP +

P_i) are indices of a cell's energy status[55]. Mitochondria's sensitivity to ADP can therefore elucidate the functionality of mitochondrial enzymes. Key modulators to ADP sensitivity are the proteins like adenine nucleotide translocator (ANT), voltage dependent anion channel (VDAC) and mitochondrial creatine kinase (mtCK). These proteins will be discussed further in section 2.2.4 of this literature review.

2.2.3 ROS Formation

Several steps in the path of oxygen reduction in mitochondria can produce ROS. These moieties are a natural by-product of OXPHOS. At low concentrations, ROS can function as second messengers regulating a variety of normal physiological functions depending on the cell type and location of ROS generation[7]. At high concentrations, ROS can be dangerous to the cell by initiating cell growth arrest and cell death[7].

Normally, electrons pass through the ETC to form water at complex IV. However, the primary ROS superoxide anion ($O_2^{\bullet-}$) is produced by the one electron reduction of O_2 in side reactions at multiple steps of OXPHOS before complex IV[53]. Superoxide can dismutate to form oxygen and hydrogen peroxide (H_2O_2), catalyzed by superoxide dismutase (SOD). To date, at least 11 sites that produce $O_2^{\bullet-}$ or H_2O_2 have been identified in mammalian mitochondria[56,57]. These sites include: complex I, II and III in the ETC along with oxoacid dehydrogenase complex, electron-transferring flavoprotein-ubiquinone oxidoreductase, dihydroorotate dehydrogenase in the matrix and glycerol-3-phosphate dehydrogenase in the intermembrane space[56]. Complexes I-III in the ETC are considered to be the main sources of superoxide production during OXPHOS with the highest maximal capacity[56]. In most cases, the subsequent H_2O_2 produced at these sites is rendered inactive by the action of glutathione peroxidases where a reduced glutathione peptide reduces an H_2O_2 molecule converting it to O_2 and H_2O[55].

Indeed, ROS play an important role in cell signaling, however, an imbalance of generation versus removal of ROS can result in oxidative stress. Oxidative stress can induce many irreversible changes to the cell like apoptosis, autophagy and hypoxia[57]. Perhaps the most relevant consequence of elevated ROS is the activation of the cell death pathway from within the mitochondria itself through the activation of the mitochondrial permeability transition pore (PTP)[58]. The role of the PTP in mitochondrial bioenergetics and the ability of ROS to activate it will be further discussed in section 2.2.5.

2.2.4 Phosphate Shuttling Systems

The OMM, IMS and IMM are embedded with different proteins that permit energy exchange in and out of the mitochondria. On the OMM rests VDAC, popularly known as the mitochondrial gate keeper. VDACs span the OMM, creating a medium for metabolite transportation between the mitochondria and IMS. VDAC is responsible, in part, for the translocation of ATP out of the mitochondria and ADP into the mitochondria from the cytoplasm[59]. ANT is embedded within the IMM, which facilitates the transport of ATP and ADP between the IMS and the mitochondrial matrix. ANT regulates the ADP/ATP ratio in OXPHOS, playing an essential role in bioenergetics[60]. Within the IMS lies mtCK an isoenzyme bond directly to VDAC on the OMM and cardiolipin on the IMM. Similarly to other creatine kinases, mtCK catalyzes the reaction of Mg•ATP + Cr ←→ Mg•ADP + PCr[61]. Phosphocreatine (PCr) is then shuttled out of the mitochondria through VDAC[62].

Phosphate can be shuttled in and out of the mitochondria through two main channels - the creatine dependent and creatine independent pathways - where the difference between the two systems is the activity of mtCK (Figure 3). As ATP is produced through OXPHOS, ATP exits the matrix through ANT where it has two fates. When creatine is not present, ATP can pass through the IMS and through VDAC to successfully exit the mitochondria. This ATP can then be utilized

by three main ATPases in muscle: myosin ATPase, sarco/endoplasmic reticulum Ca^{2+} ATPase and Na^{+}/K^{+} ATPase as well as a varity of kinases and other ATP-dependent pathways[21]. The regenerated ADP can then enter the mitochondria through VDAC and ANT repeating through a cyclical process. This process does not require creatine and is thus known as the creatine independent pathway. While creatine is present, ATP exits the mitochondria through ANT and binds to mtCK which can transfer a high-energy phosphate from ATP to creatine, generating PCr and ADP[61]. ADP re-enters the mitochondria, rendering ATP synthase with substrates available for more ATP synthesis while PCr exits the mitochondria through VDAC and then reacts with cytosolic creatine kinases to generate ATP[61]. As this system requires creatine to operate, it is labelled as the creatine dependent system.

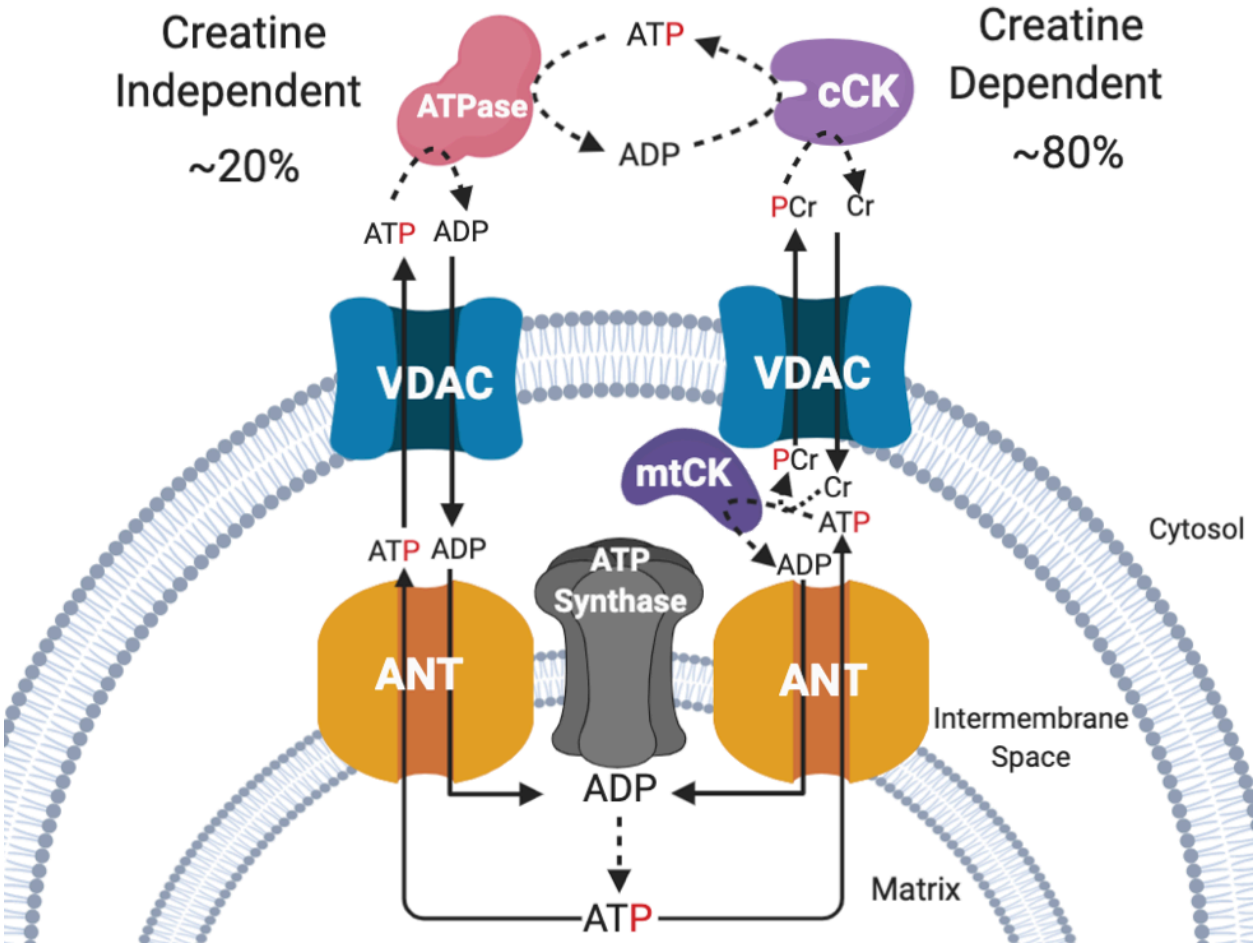

Figure 3. Model of Phosphate Shuttling Systems for Energy Exchange.
The creatine-independent model of energy exchange depicted on the left demonstrates how ADP and ATP rely solely on diffusion to shuttle in and out of mitochondria. The creatine-dependent pathway on the right uses mtCK to catalyze the transfer of a high-energy phosphate from ATP to creatine generating PCr. PCr diffuse to several creatine kinases that transfer this high energy phosphate to ADP to create ATP that fuel ATPases for muscle contraction and ion homeostasis within muscle. The Cr dependent pathway is thought to make up ~80% of energy exchange as PCr and creatine can diffuse significantly faster than ATP and ADP[63]. This emphasizes how the creatine dependent pathway is faster at energy shuttling compared to the creatine independent pathway.

In cardiomyocytes, flux control coefficients of ATP synthase, mtCK, ANT and metabolic carriers reveal that ~80% of phosphate shuttling occurs through the creatine dependent pathway[64]. Moreover, in skeletal muscle, the PCr pool is depleted to a greater extent than ATP and is classically considered to function as a storage form of high-energy phophate[61]. This is likely a result of the ability of Cr/PCr to shuttle through the mitochondria faster than ATP/ADP.

Experiments utilizing spermatozoa's single mitochondria structure reveal that PCr and creatine possess different diffusion rates compared to ADP and ATP[63]. Specifically, the diffusion flux of ADP in spermatozoa's is 2,000 times slower compared with that of creatine and the diffusion flux of ATP is 7 times slower than PCr[63].

2.2.5 Relationship Between Mitochondrial Calcium Retention Capacity and Cell Death

Ca^{2+} is an ion required for various physiological process within a cell. The main intracellular storage site of calcium is the sarcoplasmic reticulum. However, during cytosolic calcium overload, mitochondria are capable of regulating intracellular Ca^{2+} homeostasis in muscle cells[65]. In mitochondria, the matrix is negatively charged. This can drive the uptake of calcium into the mitochondria through the mitochondrial calcium uniporter (MCU)[66]. In order to prevent buildup of calcium in the mitochondria, a Na^{+}/Ca^{+} exchanger (NCLX) pumps Ca^{+} out of the matrix[66]. However, if Ca^{2+} influx exceeds Ca^{2+} efflux (a common case under pathological conditions) mitochondrial Ca^{2+} concentrations can be too high, exceeding calcium retention capacity (CRC) and triggering the PTP[67].

The PTP is thought to be made up of VDAC, ANT, ATP synthase and mitochondrial cyclophilin D (CyD), however, other components of the PTP still remain to be identified[68]. The PTP connects both the IMM and OMM and acts as a voltage dependent channel. Although PTP is activated by high Ca^{2+} concentrations in the mitochondrial matrix, PTP can be facilitated by oxidative stress, inorganic phosphate, ATP depletion and low pH[67,69]. Opening of the PTP results in osmotic swelling of the mitochondria and rupturing of the mitochondrial membranes. Ultimately, this can result in cell death cascades.

Cell death can be characterized as apoptosis or necrosis. Apoptosis, known as "cellular suicide," is an active process within the cell. Morphologically an apoptotic cell is characterized by margination and condensation of nuclear chromatin, cytoplasmic shrinkage, nuclear fragmentation

and blebbing of the plasma membrane. The cell then breaks down into membrane-enclosed fragments that are engulfed by macrophages[70]. Necrosis is not an active process. Instead, necrosis is known as an uncontrolled process whereby the cell dies due to factors external to the cell[70]. Indeed, Ca^{2+} can induce both necrosis and apoptosis, however, mitochondrial PTP activation due to calcium overload can specifically initiate apoptosis.

In isolated mitochondria, onset of the PTP initiates the release of soluble factors like cytochrome *c* and apoptosis inducing factor (AIF) from mitochondria. Consequently, this activates an apoptotic signaling cascade. Large amplitude mitochondrial swelling forces the release of proapoptotic mitochondrial factors, like cytochrome *c*[71]. Then, cytochrome *c* can bind with apoptosis-activating factor-1 (APAF-1)[72]. ATP then binds to the cytochrome *c* and APAF-1 complex, activating caspase 9, which in turn, activates caspase 3 via proteolytic cleavage of the inactive caspases[72]. Finally, caspase 3 can induce PARP cleavage, internucleosomal DNA hydrolysis, cell shrinkage, chromatin margination, and nuclear lobulation to conclude the apoptosis cascade[71]. PTP opening can also be driven by oxidants[58]. Oxidants can activate IP3Rs and RyRs on the SR/ER while inhibiting SERCA pumps and Ca^{2+} efflux through the plasma membrane, increasing Ca^{2+} concentrations in the cytoplasm[58]. This increase in free cytoplasmic Ca^{2+} can force Ca^{2+} to diffuse into mitochondria and produce more ROS as a natural byproduct of oxidative phosphorylation, resulting in induction of short PTP openings[58].

Section 2.3: Cancer's Impact on Skeletal Muscle Mitochondria

2.3.1 Mitochondrial Dysfunction in Cancer Cachexia

As discussed in section 1, cancer has significant impact on muscle metabolism in both human models and rodent models of cancer cachexia. It is proposed that inflammation induced by cancer impacts mitochondrial health by altering mitochondrial fission/fusion, autophagy and

biogenesis[48]. While this thesis will not focus on the mechanism by which cancer causes mitochondrial dysfunction in muscle, this subsection will attempt to briefly summarize the most relevant changes to mitochondrial fission/fusion, autophagy and biogenesis to demonstrate the battery of altercations that occur to mitochondria in cancer cachexia.

Maintenance of mitochondrial morphology is critical for normal cell function. Equilibrium between fission and fusion allow for maintenance of mitochondrial morphology[73]. Cancer cachexia impacts the regulation of both fission and fusion. Mitochondrial fusion is regulated by mitofusin 1 (MFN-1), mitofusin 2 (MFN-2) and optic atrophy protein 1 (OPA-1)[73]. Systemic IL-6 overexpression in the $Apc^{Min/+}$ mouse model of cachexia described above demonstrate decreased MFN-1 and MFN-2 content in cachectic muscle[52]. Decreased content of MFN-1 and MFN-2 in cachectic muscle suggests that less mitochondrial fusion may occur in cancer cachexia. However, in a rat model of cancer cachexia whereby AH-130 Yoshida ascites hepatoma cells were inoculated intraperitoneally, MFN2 mRNA content is increased, contradicting the $Apc^{Min/+}$ model and highlighting the heterogeneity in cancer cachexia models[74]. Mitochondrial fission is regulated by dynamin related protein 1 (Drp1) and mitochondrial fission protein 1 (FIS1)[73]. $Apc^{Min/+}$ mice demonstrate increased FIS1 prior to the onset of cachexia[52]. Over-expression of FIS1 can damage mitochondrial morphology by fragmenting mitochondria[73]. Dysregulation of both fission and fusion markers demonstrate how mitochondrial morphology and therefore cell function is likely compromised in cancer cachexia.

Mitochondrial autophagy (mitophagy) is the selective degradation of mitochondria and contributes to mitochondrial quality and quantity. Three models of cancer cachexia (C26, LLC, and AH130) demonstrate that muscle wasting is associated with increased autophagy evaluated by analyzing Beclin-1, LC3B and p62/SQSTM[75]. Briefly, these three markers give an approximate estimate of the extent of protein sequestration and subsequent degradation into lysosomes. Beclin-

1 is activated by NF-kB (a complex upregulated in some models of cancer cachexia) and is responsible for nucleation of autophagic vesicles, indicative of autophagy induction[76]. LC3B is a specific group of microtubule associated proteins that allow for E1, E2, and E3-like conjugation, ultimately causing the protein to associate with the membrane and serving as a marker for autophagosome abundance[76]. Last, p62/SQSTM is one of many proteins that can recognize ubiquitinated proteins by ubiquitin associated domains and thus serve as a marker for substrate sequestration and eventual degredation[76]. Changes in mitophagy seem to occur prior to the onset of muscle wasting in cancer cachexia and thus could lead to a potential therapeutic target[75].

Skeletal muscle demonstrates plasticity by their ability to regulate mitochondrial content due to a muscle fibre's energy demands. Research done half a century ago by John Holloszy, demonstrated this by the ability of muscle to increase mitochondrial oxygen uptake, respiratory enzyme activity and mitochondrial content after endurance exercise[77]. This process, whereby mitochondrial content increases due to some sort of stimuli, has since been termed mitochondrial biogenesis. The peroxisome proliferator-activated receptor gamma coactivator-1 (PGC-1) family of transcriptional coactivators are partially responsible for responding to environmental cues like temperature, nutritional status and physical activity to trigger mitochondrial biogenesis[78]. There are multiple PGC-1 isoforms, and each have an independent role in oxidative metabolism. Peroxisome proliferator-activated receptor-γ coactivator-1α (PGC-1α), a coactivator inducible by exercise training, is down-regulated in gastrocnemius and soleus muscle of *Apc* $^{min/+}$ cancer cachectic mice[52]. 5'-Adenosine monophosphate-activated protein kinase (AMPK) is an energy stress sensor that regulates oxidative metabolism once activated by PGC-1α. Interestingly, AMPK is chronically activated in the $Apc^{Min/+}$ mouse model of cancer cachexia within the gastrocnemius muscle[31]. This illustrates mechanistic insight in the dysregulation of energy control that a cancer cachectic environment can induce.

2.3.2 Cancer's Impact on Skeletal Muscle Mitochondrial Bioenergetics

It is clear that cancer cachexia can induce a myriad of alterations to skeletal muscle mitochondria. It may come as no surprise that dysfunction also exists in mitochondrial bioenergetics. Using the LLC model of cancer cachexia, Brown et al. evaluated OXPHOS prior to the onset of muscle atrophy using permeabilized muscle fibers[9]. Brown et al. reported OXPHOS efficiency with the respiratory control ratio (RCR)[9]. RCR expresses state III (ADP stimulated)/State IV (absence of ADP) respiration. A high RCR implies mitochondria have a high capacity for substrate oxidation, ATP turnover and low proton leak – while a low RCR can imply dysfunction in OXPHOS[79]. Mice that had LLC for 3 and 4 weeks experienced lower RCR compared to healthy control mice in the plantaris muscle, indicative of mitochondrial OXPHOS dysfunction even prior to the onset of cachexia[9]. In a separate study, the C26 model of cancer cachexia, mitochondrial RCR was evaluated in the soleus muscle after 4 weeks of tumour bearing[8]. This study also found a decrease in RCR in the tumour-bearing mice compared to the control[8]. In another model of cancer cachexia whereby rats were inoculated with peritoneal carcinosis (a gastrointestinal cancer that grows in the peritoneum), mitochondrial oxygen consumption was measured in isolated mitochondria of quadriceps muscle[80]. Although some mechanistic differences exist in the isolated mitochondria and permeabilized muscle fibres techniques, both methods provide accurate representations of mitochondrial OXPHOS potential. Interestingly, this model of cancer cachexia, and specifically in quadriceps, demonstrated no change in the RCR of the cancerous cohort compared to the pair-fed cohort[80]. This is contradictory as the LLC and C26 murine model found reductions in RCR[8,9]. This can potentially be due to the differences in the cancer model or the differences in the skeletal muscle selected for OXPHOS measurements. In one final example whereby mice were injected with P07 lung cancer, mitochondrial oxygen consumption was measured in the isolated mitochondria of diaphragm and gastrocnemius

muscles[81]. Although OXPHOS was not reported using the RCR, this study demonstrated depression of ETC complex content and activity in both muscles with decreased state III respiration[81]. Indeed, OXPHOS has been evaluated in a number of different muscles and a number of different cancer cachexia models, demonstrating ambiguity in either the muscle's response to cancer or the cancer's ability to impact muscle. However, researchers have not considered the potential differences in the creatine dependent and creatine independent phosphate shuttling systems to understand the relevant response of both energy transport systems to energy homeostasis in this disease model.

A common byproduct of inefficient or dysfunctional OXPHOS is ROS production. While not many cancer cachexia studies report dysfunction in OXPHOS and ROS within the same study design, two research groups did using two different models. In the LLC model, H_2O_2 emission was increased in the weeks preceding cancer cachexia in permeabilized plantaris muscle fibers[9]. Interestingly, H_2O_2 emission was not different compared to healthy control mice after 4 weeks of tumour bearing (or the onset of atrophy)[9]. Moreover, in another study, the C26 model of cancer cachexia demonstrated decreased H_2O_2 emission in the quadriceps muscle and liver mitochondria[82]. Another study utilizing the AH-130 Yoshida hepatoma cancer cachexia model demonstrated increased levels of carbonylation and 3-nitrotyosine formation while exhibiting no changes in antioxidant enzyme content in the gastrocnemius muscle[83]. Proteins with exposed cysteines are major targets for radicals and two-electron oxidants in biological systems. Carbonylation and 3-nitrotyosine formation are commonly used markers of protein oxidation by either ROS or reactive nitrogen species (RNS)[84]. Although direct measurements of mitochondrial ROS were not reported in these studies, protein carbonylation provides an index of the amount of oxidative stress present in this model. Therefore, these results potentially suggest that ROS may be elevated at some point within the development of cancer cachexia.

Therefore, this discrepancy between studies may be explained by the time point of mH_2O_2 emission collection. For example, at later stages, mitochondrial H_2O_2 emission could be down due to increased uncoupling that oxidative stress initially induced, while also prompting protein carbonylation.

While OXPHOS and mitochondrial ROS have been assessed in these prior cancer cachexia models, no research group has evaluated the impact of cancer cachexia on mitochondrial CRC. Recent literature demonstrated increased caspase 9 content in human cancer cachectic skeletal muscle[47]. Although this is not evidence of PTP activation per se, the PTP can activate apoptosis via caspases as discussed earlier in this literature review. This, along with conflicting OXPHOS and ROS data, highlights the need for more literature on cancer cachexia and mitochondrial bioenergetics.

CHAPTER 3: RATIONALE AND HYPOTHESIS

3.1: Rationale

The impact of cancer cachexia on skeletal muscle mitochondria is new and rapidly developing. It is very clear that cancer can induce muscle atrophy, but the role of mitochondria in this process still remains to be further elucidated. Much research has been done to identify alterations in autophagy, fission, fusion and biogenesis[48]. However, the role of bioenergetics in cancer cachexia remains to be fully understood. While different models of cancer cachexia demonstrate disparate results in the efficiency of mitochondrial coupling, a re-evaluation of mitochondrial bioenergetics with consideration of its central governance by ADP and creatine may reveal unique dysfunctions that unite both respiratory control and oxidant generation. No studies to date evaluate the role of mtCK in phosphate shuttling of this disease model. mtCK has been identified as dysfunctional in other pathologies like Duchenne muscular dystrophy, mitochondrial cytopathies, myophosphorylase deficiency, amyotrophic lateral sclerosis, Huntington's disease, Parkinson's and brain ischemia[10,62]. Lastly, no studies to our knowledge have determined whether mitochondrial calcium retention capacity linked to permeability transition pore is altered despite the fact that this process regulates apoptotic cell death and is decreased in other states of muscle dysfunction such as aging and Duchenne muscular dystrophy[85,86]. Therefore, in order to gain a better understanding of how cancer cachexia impacts mitochondrial bioenergetics in relation to cachexia, we employed a cross-sectional study design to assess the effect of cancer cachexia on mitochondrial respiratory sensitivity to ADP with creatine, mitochondrial H_2O_2 emission and PTP activation in different muscles.

A C26 adenocarcinoma xenograft model was employed for this thesis for several reasons. First, this model of cancer cachexia was plausible in our laboratory given animal ethics restrictions. To elicit cancer cachexia in the LLC model of cancer cachexia, tumours need to grow to about 3.5

grams in size[9]. C26 tumours can grow to ~2 grams and successfully develop cachexia[8]. Second, the C26 model demonstrates mitochondrial dysfunction in skeletal muscle [8,82]. Lastly, C26 cancer cells were easily purchased, cultured and inoculated with the trainees in the current laboratory, making a xenograft model much more plausible than a genetic model.

3.2: Specific Objectives

This thesis compared creatine dependent and creatine independent conditions that maximally activate phosphate shuttling (20mM Cr) in assessments of mitochondrial respiration, H_2O_2 emission and CRC in cancer cachectic muscle. In this context, the specific aims of this project were:

1. To determine if cancer cachexia alters mitochondrial ADP sensitivity in the context of respiration and H_2O_2 emission.
2. To determine if cancer cachexia is associated with distinct responses in the two major energy transduction pathways: creatine-dependent and -independent phosphate shuttling pathways.
3. To determine if mitochondrial bioenergetic responses to cancer are distinct in different muscles relative to muscle weakness and/or atrophy.

3.3: Hypothesis

We hypothesize that cancer cachexia will reveal impairments in mitochondrial sensitivity to ADP while evaluating respiration and H_2O_2 which may be related to differing degrees of impairments in creatine dependent vs creatine independent systems. In addition, we hypothesize that C26 cancer will impair mitochondrial bioenergetics in both the quadriceps and diaphragm.

3.4: Author Contributions

The majority of the experiments of this project were carried about by Luca Delfinis. LD cultured and injected C26 cancer cells. LD monitored all mice throughout tumour bearing period. CB performed all *in situ* and *in vitro* force production experiments. LD harvested and prepared all muscles for respiration, mH_2O_2 emission and calcium retention capacity. Due to the nature of these experiments, two people are required to efficiently complete all bioenergetic assays on fresh viable tissues. LD completed mH_2O_2 emission and calcium retention capacity while CB completed respiration protocols.

3.5: Additional Contributions

The following work encompasses the additional contributions made throughout my MSc that are not included in my thesis.

Co-Author Published:

MC Hughes, SV Ramos, PC Turnbull, IA Rebalka, A Cao, CMF Monaco, NE Varah, BA Edgett, JS Huber, P Tadi, **LJ Delfinis**, U Schlattner, JA Simpson, TJ Hawke and CGR Perry. Early myopathy in Duchenne muscular dystrophy is associated with elevated mitochondrial H202 emission during impaired oxidative phosphorylation. *Journal of Cachexia, Sarcopenia and Muscle.* 2019;10(3):643-661. doi:10.1002/jcsm.12405.

Co-Author in Progress:

SV Ramos, MC Hughes, CA Bellissimo, **LJ Delfinis**, CGR Perry. Mitochondrial bioenergetic dyfunstion in duxhenne muscular dystrophy is associated with microtubule disorganization in skeletal muscle. In Review *PLoS One*. June 2020.

CA Bellissimo, **LJ Delfinis,** MC Hughes, P Tadi, C Amaral, A Dehghani, CGR Perry. Does the mitochondrial-enhancing drug olesoxime prevent cell death and improve muscle size in duchenne muscular dytrophy?

PC Turnbull, AC Dehghani, B Deep, **LJ Delfinis,** MC Hughes, A Abdul-Sater. CGR Perry. Auranofin coupled with serine and glycine depletion selectively targets p53-null cells for ROS induced cell death through antioxidant depletion

S Gandhi, CA Bellissimo, **LJ Delfinis**, CGR Perry. A Unique clinical placement focused on screening novel drugs to improve heart function after coronary artery bypass graft surgery.

Collaborations:

JWS Jahng, CA Bellissimo, **LJ Delfinis,** CGR Perry, G Sweeney. The effects of salubrinal on muscle insulin sensitivity.

CHAPTER 4: MATERIALS AND METHODS

Animal Care

All experiments and procedures were approved by the Animal Care Committee at York University (AUP Approval Number 2019-10) in accordance with the Canadian Council on Animal Care. Eight-week old male CD2F1 mice were purchased from Charles River (Massachusetts, USA). Upon arrival, mice were housed and given a minimum of 72 h to acclimatize before cancer injections. All mice were provided access to standard chow and water ad libitum as differences in food intake is shown to not impact the C26 model of cancer cachexia[87,88].

Cell Inoculation, Functional Analysis and Surgery Procedure

Cell Inoculation

C26 cancer cells (Purchased from NCI - Frederick, MD USA) were plated at passage 2 in T-75 flasks in DMEM supplemented with 10% foetal bovine serum plus 1% penicillin and streptomycin. Once confluent, cells were trypsinized, counted and diluted in PBS. C26 cells (5 x 10^5) suspended in 100 μL sterile PBS were implanted subcutaneously to both flanks of mice at 8 weeks of age (C26)[8]. For control, one group of mice received identical subcutaneous injections but only of 100 uL sterile PBS (PBS). The tumours developed for 26-29 days to gain a cachectic phenotype and mitochondrial dysfunction[8]. Tumours were measured daily, recording the length and width of tuomurs with digital calipers using the following formula to obtain tumour volume: (4/3*π*(length/2)*(width/2)^2) provided by the York University Animal Care Committee. The same investigator was responsible for measuring tumour sizes throughout the length of the study as tumour size measurements can vary between individuals (data not shown).

Functional Analysis

In situ force production for quadriceps muscle and *in vitro* diaphragm force production have been used in this lab previously. For *in situ* force, mice were anesthetized with isoflurane and shaved of all hair on their hindlimb. An incision was made above the patella to expose the femoral tendon which was then tightly secured with suture. Once the knot was in place, the tendon was carefully severed and the suture was attached to on Aurora Scientific 305C muscle lever arm with a hook (Aurora, Ontario, Canada). The knee was secured with a vertical knee clamp immobilizing the knee joint with a 27G needle. Contraction of the quadriceps was controlled through percutaneous stimulation of the femoral nerve anterior to the hip joint. Optimal resting length (L_o) was determined using single twitches (pulse width = 0.2ms) at varying muscle lengths. Once L_o was established, force as a function of stimulation frequency was measured during isometric contractions at varying stimulation frequencies (1, 20, 40, 60, 80, 100, 120, 140 Hz). Following this force-frequency protocol, a 5-minute recovery period was provided followed by a maximum force test, performed at the frequency by which maximum force was achieved during the force-frequency curve. To induce fatigue, quadriceps muscles were stimulated at 60 Hz every second for 120 seconds. The quadriceps muscle was then harvested and weighed to allow for normalization to force production of muscle weight in mg.

For *in vitro* diaphragm force, the entire diaphragm was removed and placed in a petri dish of ~25ºC Ringer solution containing (in mM): 121 NaCl, 5 KCl, 1.8 $CaCl_2$, 0.5 $MgCl_2$ 0,4 $NaHPO_4$. 24 $NaHCO_3$, 5.5 glucose and 0.1 EDTA; pH 7.3 oxygenated with 95% O2 and 5% CO_2. Diaphragm strips were cut from the central region of the lateral costal hemidiaphragm. The strips included an adjacent section of rib on either side of the strip and part of a central tendon. Silk suture was tied to the central tendon as well the ribs, and the preparation was transferred to an oxygenated bath filled with Ringer solution, maintained at 25ºC. The suture secured to the central

tendon was then attached to a lever arm while the suture loop secured to the ribs was attached to a force transducer. The diaphragm strip was situated between flanking platinum electrodes driven by a biphasic stimulator (Model 305C; Aurora Scientific, Inc., Aurora, ON, Canada). Optimal L_o was determined using twitches (pulse width = 0.2ms) at varying muscle lengths. Once L_o was established, force as a function of stimulation frequency was measured during isometric contractions at varying stimulation frequencies (1, 10, 20, 40, 60, 80, 100, 120, 140, 200 Hz). Following this force-frequency protocol, a 5-minute recovery period was provided followed by a maximum force test, performed at the frequency by which maximum force was achieved during the force-frequency curve. Force production was normalized to the calculated CSA of the muscle strip (m/l*d) where m is the muscle mass, l is the length, and d is mammalian skeletal muscle density ($1.06 mg.mm^3$)[89].

Surgery Procedure

Quadriceps, soleus, plantaris, gastrocnemius, tibialis anterior, extensor digitorum longus, spleen and tumours were quickly collected under isoflurane anesthesia prior to euthanasia. Tissues were weighed and snap-frozen in liquid nitrogen and stored at -80°C. Quadriceps and diaphragm muscle was placed in ice cold BIOPS containing (in mM) 50 MES Hydrate, 7.23 K_2EGTA, 2.77 CaK_2EGTA, 20 imidazole, 0.5 dithiothreitol, 20 taurine, 5.77 ATP, 15 PCr, and 6.56 $MgCl_2 \cdot 6\ H_2O$ (pH 7.1) to be prepared for bioenergetic assays. Since force was collected on the quadriceps and diaphragm muscles, these muscles were selected for mitochondrial assessments. The force assessments were performed on the quadriceps from one leg while the other measures were performed on the opposite quadriceps. Likewise, force production was performed on a strip of diaphragm separate from the pieces for all other assays. In addition, both of these muscles have, to some capacity, demonstrated mitochondrial dysfunction in a cancer cachexia model[81,82].

Mitochondrial Bioenergetic Assessments

Preparation of Permeabilized Muscle Fibres

Mitochondrial bioenergetic assessment has been published using this technique from this lab before[10,90]. Briefly, the quadriceps and diaphragm from the mouse was removed and placed in ice cold BIOPS. Muscle was trimmed of connective tissue and fat and divided into small muscle bundles (~1.2 – 3.7 mg wet weight for quadricep and 0.6 – 2.1 mg for diaphragm). Each bundle was gently separated along the longitudinal axis and weighed in ~ 1.5mL of tared pre-chilled BIOPS to ensure PmFB remained relaxed. All bundles were then treated with 40 μg/mL saponin in BIOPS on a rotor for 30 min at 4°C. Bundles destined for Complex I pyruvate and malate-stimulated mH_2O_2 measurements were also treated with 35 μM 2,4-dinitrochlorobenzene (CDNB) during the permeabilization step to deplete glutathione and allow for detectable rates of mH_2O_2[91]. Following permeabilization, the permeabilized muscle fibre bundles (PmFB) that were to be used for mitochondrial respiration were washed for 15 minutes at 4°C in MiRO5 containing (in mM) 0.5 EGTA, 10 KH_2PO_4, 3 $MgCl_2 \cdot 6\ H_2O$, 60 K-lactobionate, 20 hepes, 20 taurine, 110 sucrose, and 1mg/mL fatty acid free BSA (pH 7.1). The bundles destined for mH_2O_2 were washed for 15 minutes at 4°C in Buffer Z containing (in mM) 105 K-MES, 30 KCl, 10 KH_2PO_4, 5 $MgCl_2 \cdot 6\ H_2O$, 1 EGTA, and 5mg/mL BSA (Ph 7.4). Last, the bundles destined for calcium retention capacity were placed in Buffer Y + 1mM EGTA containing (in mM) 250 sucrose, 10 tris-HCl, 20 tris-base, 10 KH_2PO_4 and 0.5 mg/mL BSA and washed on a rotor at 4°C for 10 minutes. These PmFBs were then transferred to a second wash of Buffer Y + 10μM blebbistatin (BLEB) and were washed on a rotator at 4°C until measurements were initiated.

Mitochondrial Respiration

High-resolution O_2 consumption measurements were conducted in 2 mL of respiration medium (MiRO5) using the Oroboros Oxygraph-2k (Oroboros Instruments, Corp., Innsbruck,

Austria) with stirring at 750 rpm at 37°C. Respiration medium contained 20 mM Cr to saturate mtCK and promote phosphate shuttling or no Cr to prevent the activation of mtCK[92]. For ADP-stimulated respiratory kinetics, standard procedures to determine complexes I and II-supported respiration were employed. 5 mM pyruvate and 2 mM malate were added as Complex I-specific substrates (via generation of NADH to saturate electron entry into Complex I) followed by a titration of sub-maximal ADP (25, 100 and 500 μM) and maximal ADP (5 mM in the presence of Cr or 30mM in the absence of Cr). Cytochrome *c* was added to test for mitochondrial membrane integrity. Finally, succinate (20 mM) was then added to saturate electron entry into Complex II. All experiments were conducted in the presence of 5 μM BLEB in the assay media to prevent spontaneous contraction of PmFB, which has been shown to occur in response to ADP at 37°C that alters respiration rates[92]. Polarographic oxygen measurements were acquired in 2s intervals with the rate of respiration derived from 40 data points and expressed as pmol/s/mg wet weight. PmFB were weighed in ~1.5 mL of tared pre-chilled BIOPS to ensure PmFB remained relaxed.

Mitochondrial H_2O_2 Emission (mH_2O_2)

mH_2O_2 was determined spectrofluorometrically (QuantaMaster 40, HORIBA Scientific, Edison, NJ, USA) in a quartz cuvette with continuous stirring at 37ºC, in 1 mL of Buffer Z supplemented with 10 μM Amplex Ultra Red, 0.5 U/ml horseradish peroxidase, 1mM EGTA, 40 U/ml Cu/Zn-SOD1, 5 μM BLEB and 20mM Cr. State II mH_2O_2 was induced through the addition of either 10 mM pyruvate and 2mM malate (NADH, complex I forward electron flux) or 10mM succinate ($FADH_2$ complex I via reverse electron flux from complex II). Following the induction of state II mH_2O_2, a titration of ADP was added to progressively attenuate mH_2O_2. This assay was repeated with no Cr in the assay buffer to compare ADP's effect without mtCK-mediated phosphate shuttling. All measurements were made in the presence of 5 μM BLEB to prevent ADP-induced rigor as described above. After the experiments, the fibers were rinsed in double deionized

H_2O, lyophilized in a freeze-dryer (Labconco, Kansas City, MO, USA) for > 4h and weighed on a microbalance (Sartorius Cubis Microbalance, Gottingen Germany). The rate of H_2O_2 emission was calculated from the slope of raw fluorescence (F) over time (F/min), from a standard curve established with the same reaction conditions and normalized to fibre bundle dry weight.

Calcium Retention Capacity

Mitochondrial calcium retention capacity measurements were completed spectrofluorometrically (QuantaMaster 80, HORIBA Scientific, Edison, NJ, USA) in a cuvette with continuous stirring at 37°C, in 300 µL of Buffer Y containing 1 µM membrane-impermeable Calcium Green-5N (Invitrogen), 2 µM thapsigargin, 20 mM creatine, 5 µM BLEB, and 40 µM EGTA. Prior to the initiation of each experiment, the cuvette was placed on a stir plate with 500 µL water and 10 mM EGTA. The water was then aspirated from the cuvette but not rinsed with water afterwards, leaving the EGTA coating on the cuvette walls to chelate any residual Ca^{2+} in the assay buffer. Minimum fluorescence was obtained following the addition of the PmFB and 5 mM glutamate, 2 mM malate and 5mM ADP to the assay buffer. Calcium uptake was then initiated by a single 8 nmol pulse of $CaCl_2$. Subsequent 4 nmol pulses of Ca^{2+} were added until mitochondrial permeability transition pore opening was evident. Two 0.5 mM pulses of Ca^{2+} were then added to saturate the fluorophore and establish a fluorescent maximum. Changes in free Ca^{2+} in the cuvette during mitochondrial Ca^{2+} uptake were then calculated using the known K_d for Calcium Green-5N and the equations established for calculating free ion concentrations using ion-sensitive fluorophores[93]. After the experiments, the fibres were rinsed in double deionized H_2O, lyophilized in a freeze-dryer (Labconco, Kansas City, MO, USA) for >4 h and weighed on a microbalance (Sartorius Cubis Microbalance, Gottingen, Germany). Data was expressed as nmol Ca^{2+}/mg dry weight.

Statistics

Results are expressed as mean ± SEM. The level of significance was established at $p < 0.05$ for all statistics. The D'Agostino – Pearson omnibus normality test was first performed to determine whether data resembled a Gaussian distribution. Tumour growth failed normality, therefore a Kruskal-Wallis non-parametric one-way ANOVA test followed by a Dunn's post-hoc test was performed. In addition, CRC failed normality, therefore a non-parametric Mann-Whitney t-test was performed. A two-tailed unpaired t-test was used to test for differences in muscle wet weights and specific force production between C26 tumour bearing mice and PBS injected mice. All other data were assessed with using a two-way ANOVA, with a pre-planned design to compare a given measure (e.g ADP concentration, Hz, etc.) to its corresponding value in both groups. In this way, the number of comparisons were minimized to reduce the false discovery rate by avoiding unnecessary comparisons. Fisher's Least Square Difference (LSD) post-hoc test was used to determine significant differences between individual groups when a significant interaction was identified (GraphPad Prism Software 8.4.2, La Jolla, CA, USA).

CHAPTER 5: RESULTS

The C26 Cancer Model Successfully Elicits a Cachectic Phenotype

Tumour-free body weight measurements were lower in the C26 group compared to the PBS group by week 3 (21days) and week 4 (28 days) of tumour bearing (Figure 4A). C26 tumour bearing mice lost 26.7% body weight while the PBS group gained 11.6% (Figure 4B). Tumour volume in the C26 group progressively increased throughout tumour bearing period (Figure 4C). Tumours grew up to 2.2g on average (Figure 4D). The C26 group had lower plantaris, gastrocnemius, tibialis anterior, extensor digitorum longus and quadriceps muscle wet weights compared to PBS (Figure 4E). Last, spleen weight (a marker of inflammatory disease) was significantly higher in the C26 group compared to the PBS (Figure 4F). This data confirms that this is very likely an accurate cancer cachexia model as there is body weight reductions, exponential tumour growth, and muscle wet weight reductions.

C26 Increases Normalized Force in the Quadriceps and the Diaphragm

Muscle force frequency is down in C26 quadriceps muscles specifically while stimulating at 100, 120 and 140Hz (Figure 5A). Moreover, peak tetanic force is down in C26 quadriceps muscle (Figure 5B). Interestingly, however, when muscle force in normalized to muscle weight, the opposite relationship is seen. Quadriceps and diaphragm muscle force-frequency relationship demonstrate force is higher in the C26 group compared to the PBS group (Figure 5C and 6A). Moreover, normalizing peak tetanic force to quadriceps wet weight and diaphragm cross sectional area demonstrates no difference between the C26 and PBS group (Figure 5D and 6B). Last, quadriceps muscle in C26 mice seem to recover more effectively after a fatigue protocol compared to PBS mice, however, this relationship did not exist in the diaphragm muscle (Figure 5E and 6C).

C26 Impacts -Cr and +Cr Mitochondrial Respiration Differently

We measured mitochondrial ADP sensitivity in both the creatine independent (-Cr) and creatine dependent pathway (+Cr) (Figure 7A). Surprisingly, ADP-stimulated mitochondrial respiration was increased in various ADP concentrations for both quadriceps (14.7-78.9%; $P<0.05$, Figure 6B) and diaphragm (21.8-32.9%; $P<0.05$, Figure 7C) in C26 PmFBs with -Cr. Moreover, ADP-stimulated mitochondrial respiration in the +Cr condition demonstrated no change in quadriceps muscle ($P>0.05$, Figure 7D) but increased in diaphragm muscle (28.9-50.6%; $P<0.05$, Figure 7E) within PmFB of C26 mice, illustrating differences in muscle response to cancer. This demonstrates divergent effect of C26 cancer on skeletal muscle as seen in post-fatigue assessment between quadriceps and diaphragm muscles (Figure 5E and 6C.)

C26 has Similar Impact on -Cr and +Cr Quadriceps Mitochondrial H_2O_2 Emission

We elicited complex I-supported (10 mM pyruvate & 4 mM malate) and complex-II supported (10 mM succinate) mH_2O_2 emission in the absence and presence of both ADP and Cr in the quadriceps and diaphragm muscles.

In C26 quadriceps PmFBs, complex I-supported mH_2O_2 emission in the absence of ADP is decreased in the -Cr (Figure8A) and in the +Cr condition (Figure8B). Moreover, the introduction of 25, 100 and 500 μM ADP decreases C26 mH_2O_2 emission in the -Cr (Figure 8C) and +Cr conditions (Figure 8D). However, when expressing ADP's affect to attenuate mH_2O_2 emission as a percentage of total production, the ability of ADP to decrease C26 mH_2O_2 is abolished in both the +Cr (Figure 8E) and -Cr condition (Figure 8F). In complex II-supported mH_2O_2 emission in C26 quadriceps PmFBs, a similar trend exists. In the absence of ADP mH_2O_2 emission is not different, however a trending decrease in the C26 PmFBs exists in the -Cr (Figure 9A) and in the +Cr condition (Figure 9B). Moreover, ADP decreases C26 mH_2O_2 emission in the -Cr (Figure 9C) and +Cr conditions (Figure 9D) and the ability for ADP to attenuate mH_2O_2 emission still exists

when expressed as a percentage of state II emission in the +Cr (Figure 9E) and -Cr condition (Figure 9F).

C26 Impacts -Cr and +Cr Diaphragm Mitochondrial H_2O_2 Emission Differently

A similar reduction in mH_2O_2 emission potential was not exhibited in the C26 diaphragm PmFBs. In C26 diaphragm PmFBs, complex I-supported mH_2O_2 emission in the absence of ADP was not changed in the -Cr (Figure10A) and in the +Cr condition (Figure10B). ADP did not change C26 mH_2O_2 emission in the -Cr (Figure 10C) and +Cr conditions (Figure 10D) even when expressed as a percentage of state II mH_2O_2 emission (-Cr Figure 10E; Cr Figure 10F). Similarly, complex II-supported mH_2O_2 emission in the absence of ADP is not different between C26 and PBS in the -Cr (Figure11A) and the +Cr condition (Figure11B). Interestingly, however, ADP attenuated C26 complex II-supported mH_2O_2 emission in the -Cr condition (Figure 11C), but not the +Cr condition (Figure11D). Last, while ADP's attenuation of state II mH_2O_2 emission is expressed as a percentage, the same relationship exists whereby the -Cr condition exhibits lower mH_2O_2 emission in the C26 group (Figure11E) but not the +Cr condition (Figure 11F). This battery of mH_2O_2 emission measurements further demonstrates a unique muscle response to cancer and figure 11 demonstrates diverging impact in the -Cr and +Cr conditions.

C26 Increased Mitochondrial Calcium Retention Capacity in Both Muscles

Last we measured mitochondrial CRC as an index of PTP opening. The C26 quadriceps PmFBs exhibited a ~272% increase in calcium retention ability compared to the PBS group (Figure 12A). In addition, C26 diaphragm PmFBs exhibited a ~284% increase in calcium retention capacity compared to the PBS group (Figure 12B).

C26 Impacts Cr Sensitivity in the Quadriceps and Diaphragm Differently

Cr can facilitate phosphate exchange faster due to the aid of mtCK and diffusion capabilities of phosphate compared to ADP and ATP[63] (Figure 3). Cr increased mitochondrial respiration in quadriceps of the PBS PmFBs (P = 0.062, Figure 13A) at 100 and 500 μM ADP (submaximal K_{mADP}) but not the quadriceps PmFBs of the C26 muscle (Figure 13B). This illustrates a possible mtCK impairment in cancer cachectic quadriceps muscle as Cr was not able to raise respiration in the C26 group similar to the PBS group. Interestingly, however, Cr increased mitochondrial respiration in diaphragm of the PBS PmFBs (Figure 13E) and the C26 diaphragm PmFBs (Figure 13F) as well, indicating no changes in mtCK. At 100 μM ADP (i.e., 500 μM ADP is saturating for mH_2O_2 and not sub maximal, therefore only 100 μM ADP was used), there is a trending relationship (P = 0.067; likely a result of a low sample size) whereby Cr lowers mH_2O_2 emission in the PBS quadriceps muscle, but not the C26 muscle (Figure 13C and D). Moreover, Cr does not seem to change mH_2O_2 emission in PBS or C26 diaphragm muscle (Figure 13G and 13H), disabling the ability to draw conclusions on the impact of C26 on Cr sensitivity in reference to mH_2O_2 emission.

CHAPTER 6: DISCUSSION

In this study, we questioned if cancer cachexia impairs ADP sensitivity, Cr independent/ Cr dependent phosphate shuttling and CRC in quadriceps and diaphragm skeletal muscle. To our surprise, this data set did not reveal any mitochondrial dysfunction, which should be revealed as reductions in mitochondrial respiration, increases in mH_2O_2 emission or reductions in CRC within the skeletal muscle of the C26 cancer cachexia model. In contrast, this battery of mitochondrial bioenergetic assessments actually reveals a mitochondrial enhancement in ADP sensitivity, mH_2O_2 emission, CRC and even force production. Previous models have suggested that a mitochondrial dysfunction exists in cancer cachectic skeletal muscle[8,9,80–82]. However, this evidence is expressed in different models of cancer cachexia, different skeletal muscles and using different methods of assessing mitochondrial bioenergetics.

6.1 Perspectives in Controversial Mitochondrial Function Findings

Mitochondrial dysfunction has been well documented in previous models of cancer cachexia. Considering the current data generated seems controversial, this can raise concern on the legitimacy of the model we have pioneered in this laboratory. Considering the model demonstrates similar muscle wet weight changes, body weight changes, tumour growth/time of tumour burden and muscle force changes as previously published, the reason for the unique observations in mitochondrial bioenergetics is not immediately apparent although some possibilities warrant disucssion[8,9,87]. For example, differences in how mitochondrial function is reported across studies should be considered, as could the type of cancer cachexia models or the skeletal muscle selected. It has already been thoroughly discussed in the literature review how different cancer cachexia models can produce contradictory changes between studies, therefore only comparisons to xenograft murine models of cancer will be discussed as these studies are the only ones to include measures of mitochondrial bioenergetics.

Neyroud et al. found that C26 PmFBs of soleus muscle demonstrated a decrease in ADP-stimulated mitochondrial respiration[8]. It is entirely possible that C26 skeletal muscle mitochondrial respiration is different between disparate muscles, as we have documented in our own hands between the quadriceps and diaphragm. However, Neyroud et al. report mitochondrial dysfunction using respiratory control ratio (RCR), a commonly used ratio to quantify mitochondrial respiration whereby state III(ADP stimulated)/state IV(absence of ADP)[8] is used to describe the degree of coupling oxygen consumption to ATP synthesis. Although this is a commonly-used ratio for mitochondrial respiration, this can be misleading if mitochondrial uncoupling is high despite normal ADP-stimulated respiration as this can increase state IV respiration without a change in coupled state III respiration yet still be interpreted as reduced coupling because of a lower calculated RCR. In fact, when we report RCR using maximum ADP stimulated respiration, we see no change in mitochondrial respiration in quadriceps PmFBs and a decrease in the RCR of C26 diaphragm PmFBs (Supplemental figure 1). The typical interpretation of these results would be contradictory to our reports of increased ADP-stimulated respiration in C26 cancer cachectic muscle, which is a more direct measure on its own for the ability to produce ATP. Moreover, state II respiration is significantly increased in C26 diaphragm muscle (both -Cr and +Cr) and in the -Cr condition of quadriceps muscle (Supplemental figure 2), which may indicate increased uncoupling in C26 skeletal muscle. Interestingly, increased expression of uncoupling-protein 3 (UCP-3) is reported in rat models of cancer cachectic skeletal muscle[6]. While it was not measured in the present study due to laboratory restrictions during the pandemic, future work could determine if the increased uncoupled respiration was linked to a similar elevation in UCP3. Overall, this difference in reporting mitochondrial respiration (RCR vs absolute rates) might explain the divergent interpretations between certain past and present work. Lastly, this

observation could be verified with more appropriate measures of uncoupling including membrane potential, P:O ratios (ATP produces per oxygen consumed) and proton conductance.

Regardless of ratio vs absolute, this study is the first to report mitochondrial respiration via an ADP sensitivity protocol using PmFBs in the quadriceps and diaphragm muscle. This is an important measure given ADP is a central controller of membrane potential-dependent ATP production (respiration) and H_2O_2 emission (electron slip). By comparing absolute vs relative rates of respiration and H_2O_2 emission, different conclusions can be derived about ADP sensitivity. For example, in figure 7 C, ADP lowers absolute mH_2O_2 emission but does not change relative mH_2O_2 emission. Because ADP does not lower mH_2O_2 as a percentage of the total mH_2O_2 produced, this could indicate that the trend in absolute rates only exists because the total amount of mH_2O_2 produced in C26 muscle is already lower (Figure 8A). This indicates that although ADP decreased absolute mH_2O_2 emission but did not decrease relative mH_2O_2 emission, ADP may not be governing C26 skeletal muscle efficiently. This helps researchers understand the metabolism of cancer cachectic skeletal muscle as ADP seems to govern ATP production and H_2O_2 emission.

Mitochondrial H_2O_2 emission has been reported to be increased in the weeks preceding cancer cachexia in plantaris muscle of LLC tumour bearing mice[9]. While it is possible that mH_2O_2 emission changes during the progression of tumour bearing, we expected to see an increase in mH_2O_2 emission within the C26 model. A very recent study done by Halle et al. actually demonstrate a decrease in mH_2O_2 emission in the quadriceps muscle using the C26 cancer cachexia model and a similar mH_2O_2 emission technique to our laboratory[82]. This replicates our results of decreased mH_2O_2 emission in the quadriceps muscle (Figure 8 and 9). See Table 1 for a summary of recent literature measuring mitochondrial bioenergetics in cancer cachexia.

To our knowledge, this study is the first to report CRC in a cancer cachexia model. We report nearly a 3-fold increase in mitochondrial CRC within C26 quadriceps and diaphragm

PmFBs (Figure 12). Past literature could suggest mitochondrial CRC could be decreased as typically dysfunctional mitochondria in other pathologies exhibit lower CRC and thus increase susceptibility to PTP formation and consequential cell death[94]. This thesis documents the opposite finding. Although cancer cachexia is a disease state, mitochondrial alterations in this model might seem to benefit the mitochondrial bioenergetic triad of increased respiratory control, lower mH_2O_2 governance and increased CRC as an index of reduced propensity for mitochondrial-mediated apoptosis. This is typically interpreted as "healthy" mitochondria as opposed to pathological mitochondria. A number of explanations underlie this phenomenon that might still be consistent with the muscle weakness and atrophy that were observed.

6.2 The Potential for Mitochondrial 'Compensation' During Cancer Cachexia

As noted earlier, cancer cachexia is defined as muscle loss with muscle weakness that is irreversible by dietary intervention[12]. Our data suggests that muscle loss is occurring in hindlimb muscles (Figure 4E) with decreased *in situ* quadriceps force (Figure 5A and 5B). Although muscle wet weight changes can be misleading and muscle atrophy via histological analysis of skeletal muscle fibers is not reported, the C26 cancer cachexia model has previously reported fiber cross sectional area reductions in soleus[95], extensor digitorum longus[95] and quadriceps[45] muscles. An interesting phenomenon that occurs is that *in situ* quadriceps force is decreased when evaluating raw muscle force, however, force is actually greater when normalized to muscle wet weight (Figure 5C). Indeed, muscle wasting is occurring while evaluating muscle wet weight changes and raw force production, but the results actually oppose while normalizing to muscle mass. This may be due to a number of reasons that have been previously reported in past studies and can potentially explain enhancement of mitochondrial bioenergetics as well.

One possible explanation for the increase in skeletal muscle force with cancer is fiber type shifting. In skeletal muscle, two major types of fibers exist: slow-twitch fibers (type I) whereby

muscle is designed for low-intensity, long-lasting contractions with higher mitochondrial content and fast-twitch glycolytic (type II) whereby fibers are designed for high-intensity, short-duration contractions, with less mitochondrial content albeit generally moreso in type IIb and IIx[96]. Past work indicates fiber type shifts within the cancer cachexia disease state[80,95]. Mouse soleus muscle is known to be oxidative - predominately type I and type IIA fibers[97]. Within the C26 model, soleus muscle seem to shift to a lower percentage of type I fibers and a higher percentage of type IIx and type IIb[95]. This shift in fiber type renders the soleus with less type I and type IIA fibers which are rich in mitochondria[97]. This fiber type shift may also explain the decreased respiration and mitochondrial content in the soleus muscle found in another study by Neyroud et al. employing the same C26 model[8]. To our knowledge, no C26 model has evaluated fiber type changes in quadriceps muscle, however, one rat model of cancer cachexia reports less IIb and IIa/IIx fiber types in quadriceps after tumour bearing[80]. If this fiber type shift occurred in the present study as well, there may be a higher percentage of type I oxidative fibers which could increase mitochondrial respiration and CRC as we report (Figure 7B and 12A). A review article indicates that human cancer cachectic patients exhibit selective atrophy of type II fibers[98]. Such measures will be completed once laboratory work is permitted to resume.

Another possible explanation for the force and mitochondrial changes seen is an increase in mitochondrial content. The current study measures mitochondrial force and function at 4 weeks of tumour-bearing, therefore, there is no index of mitochondrial and force alterations occurring the weeks preceding the endpoint. It may be possible that cancer induces an “energy crisis” in skeletal muscle, whereby ATP production and substrate utilization are disabled in the weeks preceding the 4-week endpoint that stimulates mitochondrial biogenesis. Mice bearing LLC demonstrate degraded mitochondrial quality in the weeks preceding muscle atrophy[9]. If a similar event is occurring in the C26 cancer cachexia model, then, it may be possible that initially ATP production

and substrate utilization is down and mH_2O_2 emission is increased. Under conditions of low energy, AMP-activated protein kinase (AMPK) can phosphorylate specific enzymes to increase ATP generation via mitochondrial biogensis[99]. Interestingly, AMPK is chronically activated in the $Apc^{Min/+}$ mouse model of cancer cachexia, a similar cancer cachexia model to the present study[31]. Measures of mitochondrial content via western blot analysis will take place once lab work is permitted and can provide further insight.

6.3 Cancer Cachexia's Impact on Phosphate Shuttling Systems of Energy Exchange

The Cr dependent pathway of phosphate shuttling is thought to make up to ~80% of energy exchange through the use of Cr and PCr diffusion capabilities[63]. This makes ATP production and mH_2O_2 emission much more efficient than the Cr independent pathway. To our knowledge, the present study is the first to evaluate the differences in the Cr dependent and Cr independent pathways in cancer cachexia skeletal muscle.

Cr improves ADP sensitivity as PCr/Cr can overcome diffusion limitations experienced by ATP/ADP, better meeting the demands of skeletal muscle (Figure 3)[63]. However, Cr does not improve diffusion at maximal [ADP], therefore, submaximal [ADP] are used to assess Cr sensitivity as past literature historically demonstrate Cr's ability to lower apparent $K_{m(ADP)}$[100]. As such 100 μM and 500 μM [ADP] are used to identify ADP sensitivity within the protocols as the $K_{m(ADP)}$ of this multienzyme system likely falls within these ranges[92,101]. 100 μM ADP is used to evaluate Cr sensitivity in mH_2O_2 emission protocols as it is submaximal within these assay conditions[10,90,102–104]. In this laboratory, K_m is not established as not all titrations fit michaelis-menten kinetics (data not shown). In quadriceps PmFBs, Cr was able to increase mitochondrial respiration at 100 μM and 500 μM ADP in PBS, however, Cr was not able to increase mitochondrial respiration in C26. This could suggest that mtCK is impaired in the quadriceps muscle of C26 mice as Cr was not able to raise respiration. Interestingly, however, the same trend

did not exist in diaphragm PmFBs. Cr was able to increase mitochondrial respiration at 100 μM and 500 μM ADP in PBS and C26 PmFBs. This could suggest that cancer impacts mtCK uniquely per skeletal muscle. One possible reason as to why +Cr respiration was impaired in the quadriceps and not the diaphragm may relate to the redox sensitivity of mtCK[62]. Since mtCK is redox sensitive and both quadriceps and diaphragm muscles have differing mH_2O_2 emission responses within this study, it may be possible that quadriceps muscles exhibited higher ROS before the end point of this study which could have resulted in oxidized mtCK. This could result in inefficiencies in the +Cr pathway as seen in respiration for C26 quadriceps. In addition, it may also be possible that the Cr independent phosphate shuttling system is upregulated in C26 muscle as opposed to a downregulation in the Cr dependent system. Instead of the originally hypothesized mtCK impairment that may be occurring, C26 may potentially be increasing the efficiency of the Cr independent pathway through changes in VDAC or ANT content in the quadriceps muscle.

It is thought that Cr lowers ROS generation by lowering membrane potential as more ADP is available to catalyze ATP synthase[105] . Evidence of Cr lowering mH_2O_2 emission is demonstrated in succinate-stimulated rat brain isolated mitochondria[105]. There is a trend in Cr's ability to attenuate mH_2O_2 emission in the quadriceps of PBS muscle (Figure13E), and no change in the C26 quadriceps. This is another likely indication that the creatine dependent pathway is impaired in C26 cancer skeletal muscle as the muscle is no longer able to attenuate mH_2O_2 in the presence of ADP. Interestingly, however, Cr is not able to attenuate mH_2O_2 emission in the diaphragm of PBS or C26 skeletal muscle. This is likely a result of being underpowered as the sample size is 8-9. In conclusion, Cr's ability to improve submaximal ADP-stimulated mitochondrial respiration is lost in the quadriceps muscle of C26 tumour-bearing mice. In addition, Cr's ability to attenuate mH_2O_2 emission in quadriceps muscle is also lost in cancer skeletal

muscle. The diaphragm does not reproduce these trends, indicating that both skeletal muscles exhibited different physiological changes to cancer.

6.4 Cancer Cachexia Induces Muscle-Unique Alterations

Many researchers have investigated the functional and mitochondrial impact of cancer on skeletal muscle. As more research emerges, it is increasingly likely muscle-specific responses to cancer exist. Even within our own data set, we see differences in quadriceps and diaphragm mitochondrial respiration and mH_2O_2 emission (Figure 8-10). Indeed, mitochondrial creatine dependent respiration seems to be impaired in C26 quadriceps PmFBs, while the same effect does not exist in diaphragm PmFBs. Moreover, C26 lowers quadriceps complex I and complex II stimulated mH_2O_2 emission but does not impact diaphragm (Figure 8-11). mtCK is susceptible to ROS-induced molecular damage[62]. Although only speculative, it is possible that mH_2O_2 emission is up in the weeks preceding cancer cachexia. This has been reported in the plantaris muscle within the LLC model of cancer cachexia[9]. Increases in mH_2O_2 emission in the weeks preceding cancer cachexia could prompt UCP-3 formation and thus result in the decreased complex I and complex II stimulated mH_2O_2 emission that we report. Thus, it is also possible that this potential increase in mH_2O_2 emission in the weeks preceding cachexia impair mtCK and thus impair creatine dependent mitochondrial respiration in C26 quadriceps PmFBs. This same trend is not seen in C26 diaphragm PmFBs. This may suggest that locomotor, skeletal muscle is more susceptible to damage compared to the diaphragm. Interestingly, CRC is increased in both skeletal muscles in response to C26. Increasing CRC could suggest that both muscles are less susceptible PTP formation and subsequent mitochondrial mediated cell death by activating Caspase 9/3.

Skeletal muscle response to cancer may be unique to fiber type. As discussed earlier in this section, C26 soleus muscle seems to shift from an oxidative phenotype to a glycolytic phenotype by increasing percentage of type IIx and IIb fibers[95]. This could potentially explain the decrease

in ADP stimulated mitochondrial respiration in the C26 cancer cachexia model[8]. Unfortunately, fiber type data is not reported within this thesis. However, although only speculation, quadriceps and diaphragm muscles may be shifting to a more oxidative phenotype. The reason for this speculation is because mitochondrial adaptations and force changes within this study suggest an increase in mitochondrial content while comparing to the PBS control. C26 muscle has increased force, ADP-stimulated mitochondrial respiration, CRC and decreased m H_2O_2 emission. This is characteristic of an oxidative shift. However, future fiber typing experiments need to be completed to verify the possibility.

CHAPTER 7: CONCLUSION AND FUTURE DIRECTIONS

7.1: Conclusion

In the current study, evaluating mitochondrial respiration in both +Cr and -Cr conditions provide a new perspective that cancer may have unique effects on different skeletal muscles. Based on the findings from the present investigation, we found that 4 weeks of cancer surprisingly enhances ADP-stimulated respiration and attenuation of mH_2O_2 emission in quadriceps and diaphragm, albeit to varying degrees depending on the muscle and whether phosphate shuttling was modelled. Specifically, in the absence of creatine, cancer increased quadriceps and diaphragm mitochondrial respiration and lowered mH_2O_2 emission in the presence of ADP, although the latter was substrate-dependent (i.e succinate). In the presence of creatine, a perplexing dichotomy was observed whereby cancer improves ADP-dependent respiration in diaphragm but not quadriceps. Whereas mH_2O_2 emission was lower in quadriceps but not diaphragm. While difficult to explain, these findings suggest that there is an overall improvement in ADP's control of respiration and mH_2O_2 emission during cancer cachexia in both muscles albeit in a substrate-dependent and muscle-specific manner.

We also observe a decrease in state II mH_2O_2 emission in quadriceps muscle which might be related to greater uncoupling (increased state II respiration), but this would require more precise measures of membrane potential and proton conductance. In addition, cancer likely increases both quadriceps and diaphragm calcium retention capacity. Given the discrepancy between quadriceps and diaphragm responses to cancer and Cr sensitivity to ADP, this thesis highlights the importance of controlling experimental parameters to model creatine dependent and independent respiration in order to gain better insight on the regulation of energy exchange and skeletal muscle function in cancer cachectic muscle.

In pre-clinical models of cancer cachexia, mitochondria are thought to be dysfunctional[8,9,52]. This study challenges the notion that mitochondrial dysfunction is associated with cancer cachexia. This highlights the need for careful consideration of the time-dependent responses of muscle to cancer. As seen in the LLC model of cancer cachexia, muscle mitochondrial alterations differ from the time of inoculation to the time of onset of muscle atrophy[9]. Similar conclusions can be made about mitochondrial dysfunction in a cell culture model of cancer cachexia[49]. By completing a time-course design for the C26 model of cancer cachexia, this would help understand the changes seen at the 4-week time point.

7.2: Future Directions & Limitations

Considering mitochondrial content may explain in part the changes in mitochondrial respiration, mH_2O_2 emission and CRC in this model of cancer cachexia, OXPHOS content in both muscles should be measured via western blot analysis. Muscles seem to respond differently to cancer; therefore, mitochondrial content changes may have muscle specific responses as well. This can aid in understanding the increase in ADP sensitivity seen in these muscles. In addition, quadriceps and diaphragm fiber typing via immunofluorescence and histochemical analysis should be employed in the C26 model to understand if muscle mitochondrial changes are due to fiber type shifts as seen in the soleus muscle[95]. Moreover, mtCK western blot analysis should be employed in quadriceps and diaphragm skeletal muscle to better understand the differences in Cr sensitivity seen in these muscles. Furthermore, UCP-3 western blot analysis should be performed to better understand the reduction in mH_2O_2 emission and increased in state IV respiration. In addition, glutathione content quantification via HPLC-UV and reduced glutathione content quantification via HPLC- fluorescence should be employed to tease out the potential role of antioxidants in attenuating mH_2O_2 emission. Last, caspase enzymatic activity assays could be employed to better understand the relationship of increased CRC and mitochondrial mediated cell death activation.

Past literature has suggested that mitochondrial dysfunction exists in C26 cancer cachectic skeletal muscle. Although our results may demonstrate mitochondrial enhancement through increased respiration, attenuation of mH_2O_2 and increased CRC, we are unaware of the mitochondrial alterations occurring the weeks preceding the 4-week endpoint. Indeed, Brown et al. report mitochondrial alterations prior to the onset of muscle atrophy in cancer cachexia using the LLC model[9]. Therefore, it is possible that our findings are misleading in that mitochondrial dysfunction still exists in the week prior to atrophy and we are solely measuring mitochondrial function of viable mitochondria after weeks of mitophagy and mitochondrial biogenesis. Future studies should look to employ a time-course design of C26 cancer cachexia as Brown et al. performed to identify time-course response to C26 tumour bearing.

Limitations to this study include the lack of a pair-feed group. PBS pair-feed mice do not seem to demonstrate muscle force changes to C26 skeletal muscle relative to PBS[87]and food consumption does not seem to change in the C26 model of cancer cachexia[88]. However, food intake can change mitochondrial function, therefore, the lack of a pair-feed group limits the study design as food intake may be changing metabolism.

CHAPTER 8: TABLES AND FIGURES

Study	Cancer Model	Age	Muscle	Respiration	mH_2O_2	CRC
Delfinis et al.	C26 (4 weeks)	12 weeks	Quadriceps ---------- Diaphragm	Increased ---------- Increased	Decreased ---------- No change	Increased ---------- Increased
Neyroud et al. 2019	C26 (4 weeks)	12 weeks	Soleus	Decreased	N/A	N/A
Brown et al. 2017	LLC (4 weeks)	12 weeks	Plantaris	Decreased	Transient increase	N/A
Halle et al. 2019	C26 (3 weeks)	13 weeks	Quadriceps ---------- Gastrocnemius	N/A ---------- Decreased	Decreased ---------- N/A	N/A ---------- N/A

Table 1: Summary of relevant cancer cachexia studies investigating mitochondrial bioenergetics to some capacity with similar cancer cells and age of mice.

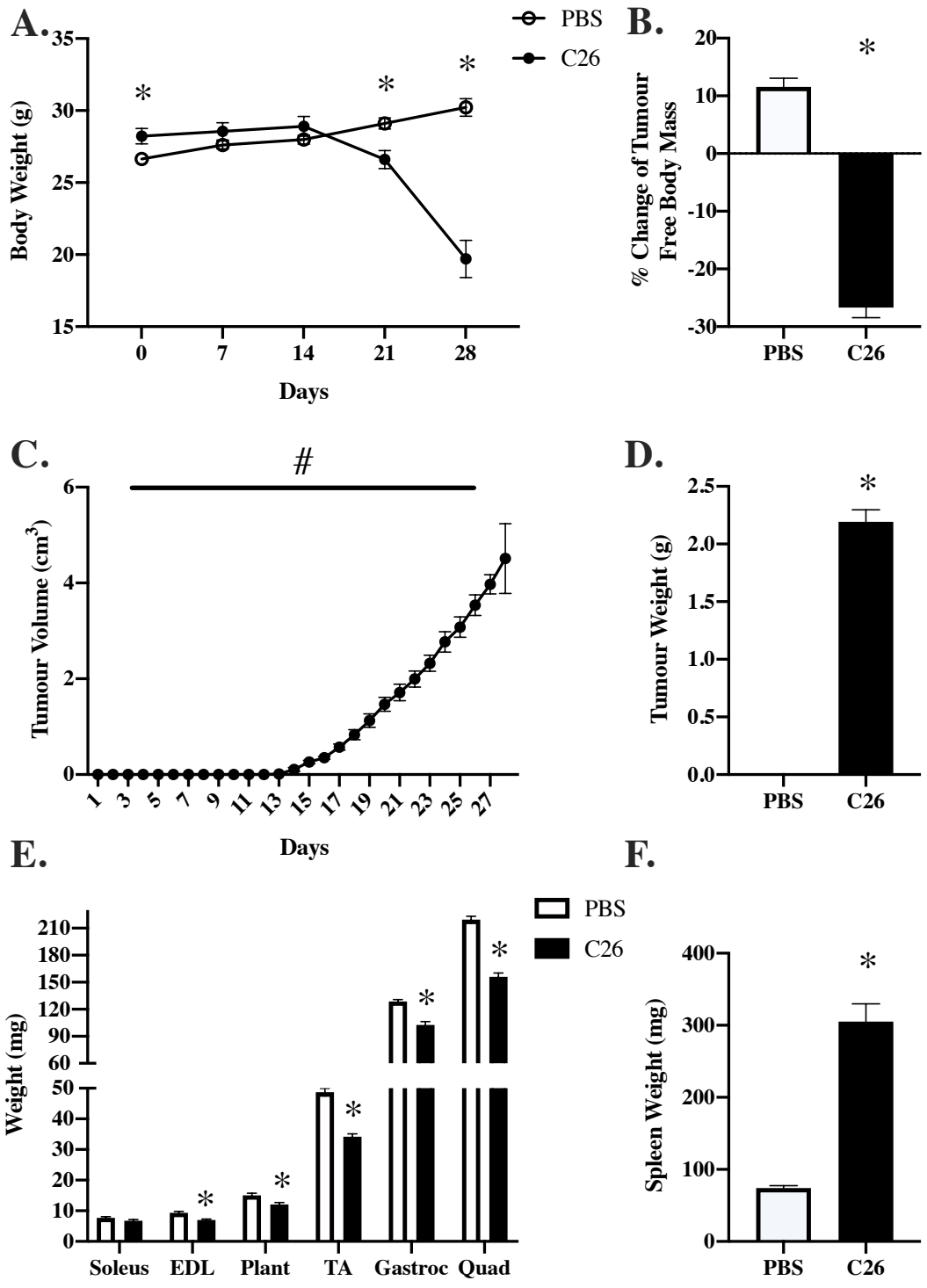

Figure 4. Impact of C26 Cancer on Mouse Phenotype.
Comparison of PBS injected and C26 injected mice weekly tumour-free body weight changes from initial day to day to endpoint **(A),** percent tumour free body mass change from initial day **(B),** tumour volume **(C),** tumour mass **(D),** muscle wet weights after tumour bearing **(E),** and spleen wet weight **(F).** Results represent mean ± SEM; n = 10-12; * P<0.05 compared to PBS at same frequency. # P <0.05 main effect of C26 compared with PBS.

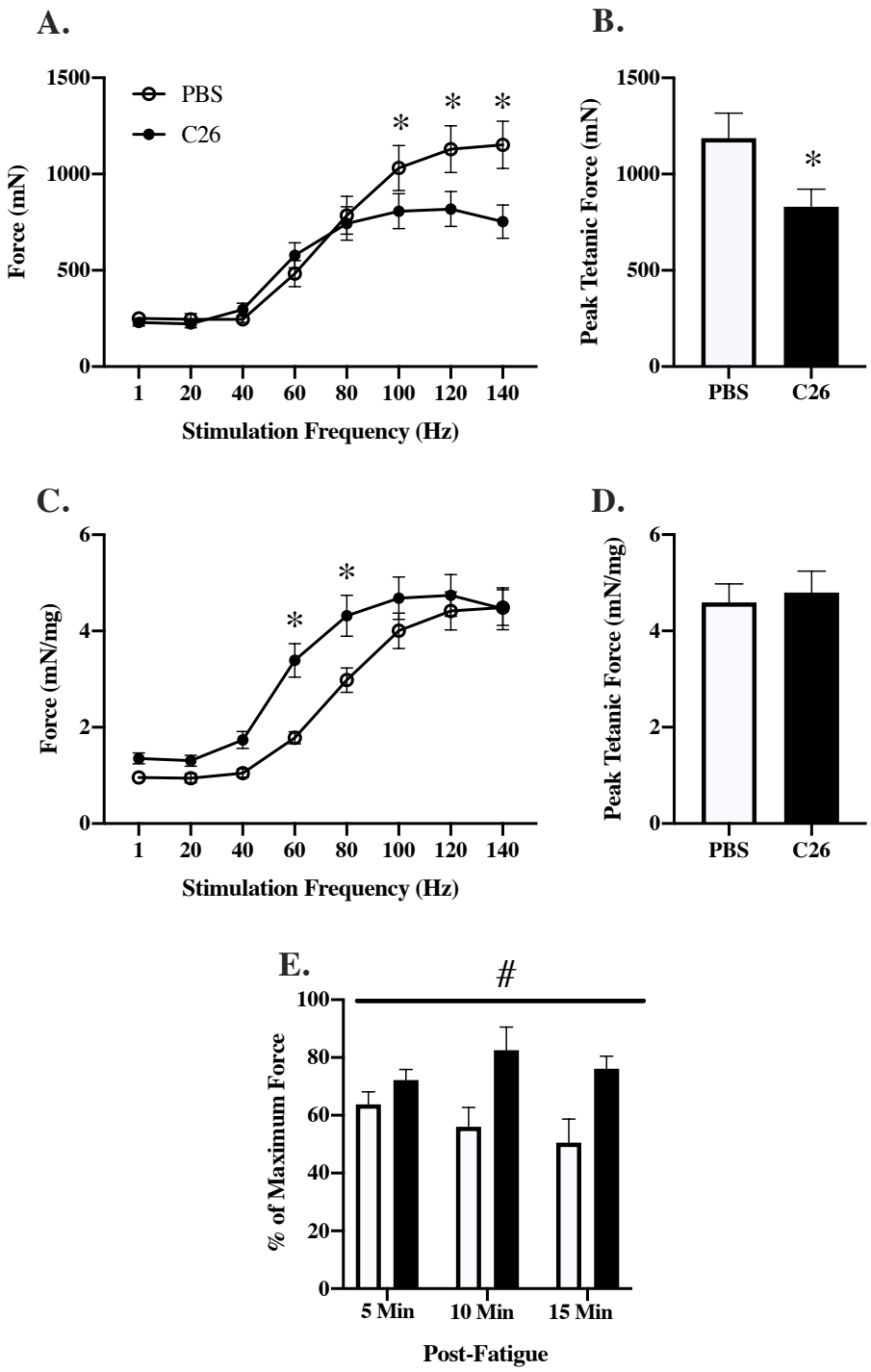

Figure 5. Impact of C26 Cancer on Quadriceps Force & Post-Fatigue.
Comparison of PBS injected and C26 injected mice force frequency in the quadriceps muscle **(A),** and peak tetanic force production **(B),** normalized force frequency in the quadriceps to quadriceps muscle wet weight **(C),** and peak tetanic force production normalized to quadriceps muscle wet weight. % maximum force 5, 10- and 15-minutes post-fatigue in quadriceps **(E).** Results represent mean ± SEM; n = 10-12; * P<0.05 compared to PBS at same frequency. # P <0.05 main effect of C26 compared with PBS.

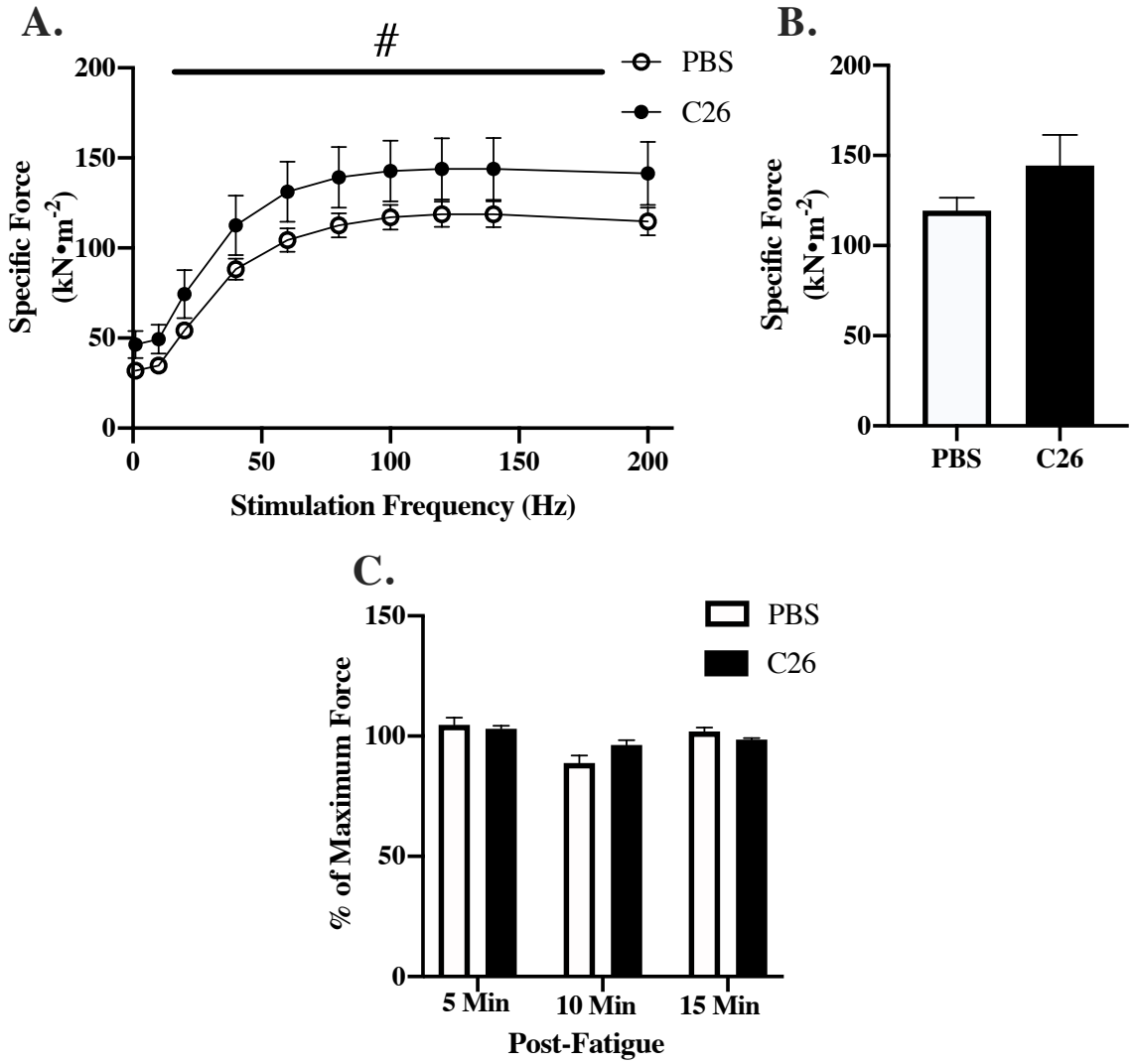

Figure 6. Impact of C26 Cancer on Diaphragm Force & Post-Fatigue.
Comparison of PBS injected and C26 injected mice force frequency in the diaphragm muscle normalized to cross-sectional area **(A),** and peak tetanic force production normalized to cross sectional area **(B),** % maximum force 5, 10 and15 minutes post-fatigue in diaphragm **(C).** Results represent mean ± SEM; n = 10-12; * P<0.05 compared to PBS. # P <0.05 main effect of C26 compared with PBS.

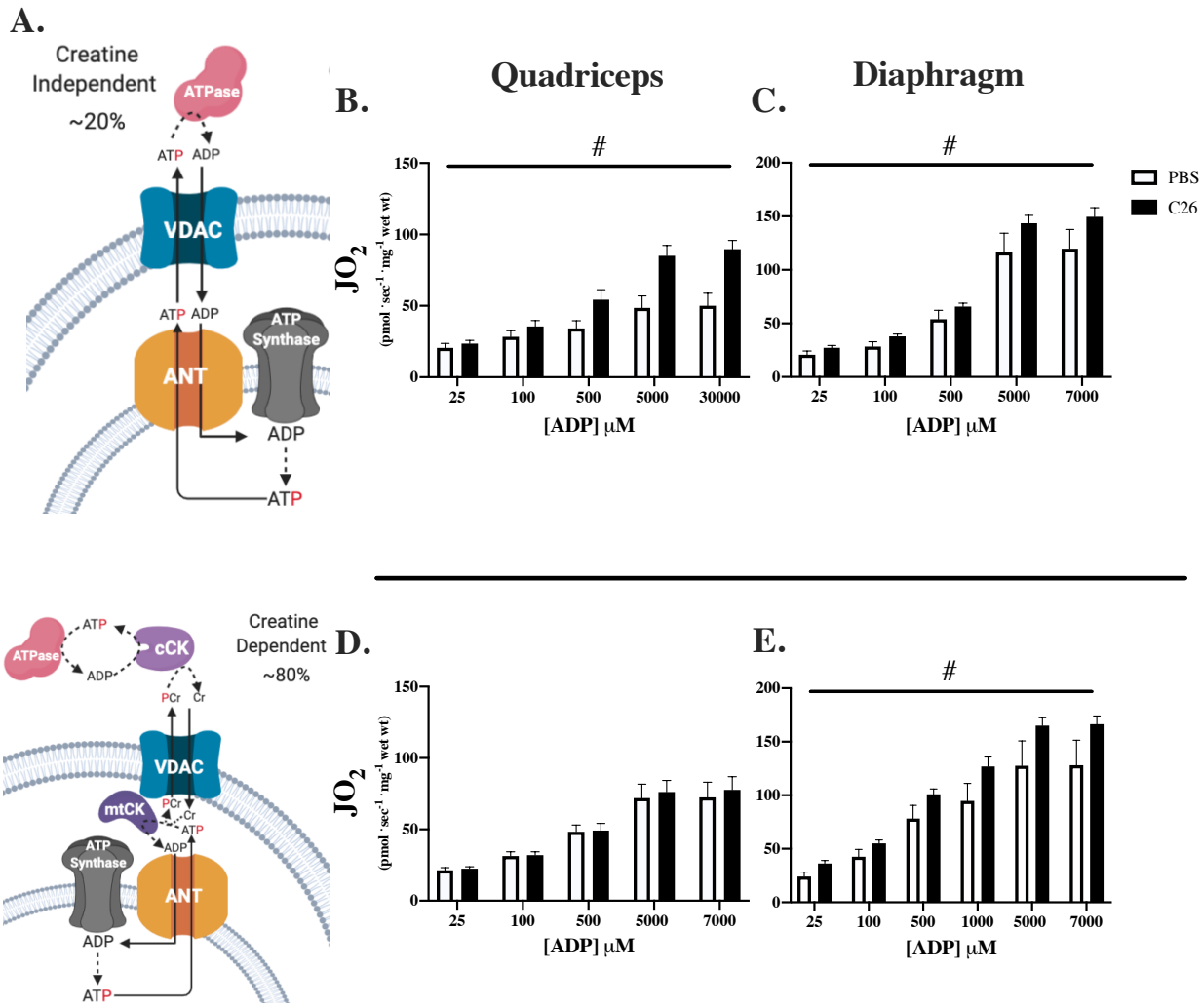

Figure 7: Impact of C26 Cancer on Quadriceps and Diaphragm Creatine Independent and Creatine Dependent Mitochondrial Respiration.
Schematic representation of both -Cr (top) and +Cr (bottom) phosphate shuttling pathways of energy exchange **(A).** -Cr mitochondrial respiration in quadriceps **(B)** and diaphragm PmFBs **(C)**. +Cr mitochondrial respiration in quadriceps **(D)** and diaphragm PmFB **(E)**. Results represent mean ± SEM; *n* = 8-12; # *P* <0.05 main effect of C26 compared with PBS.

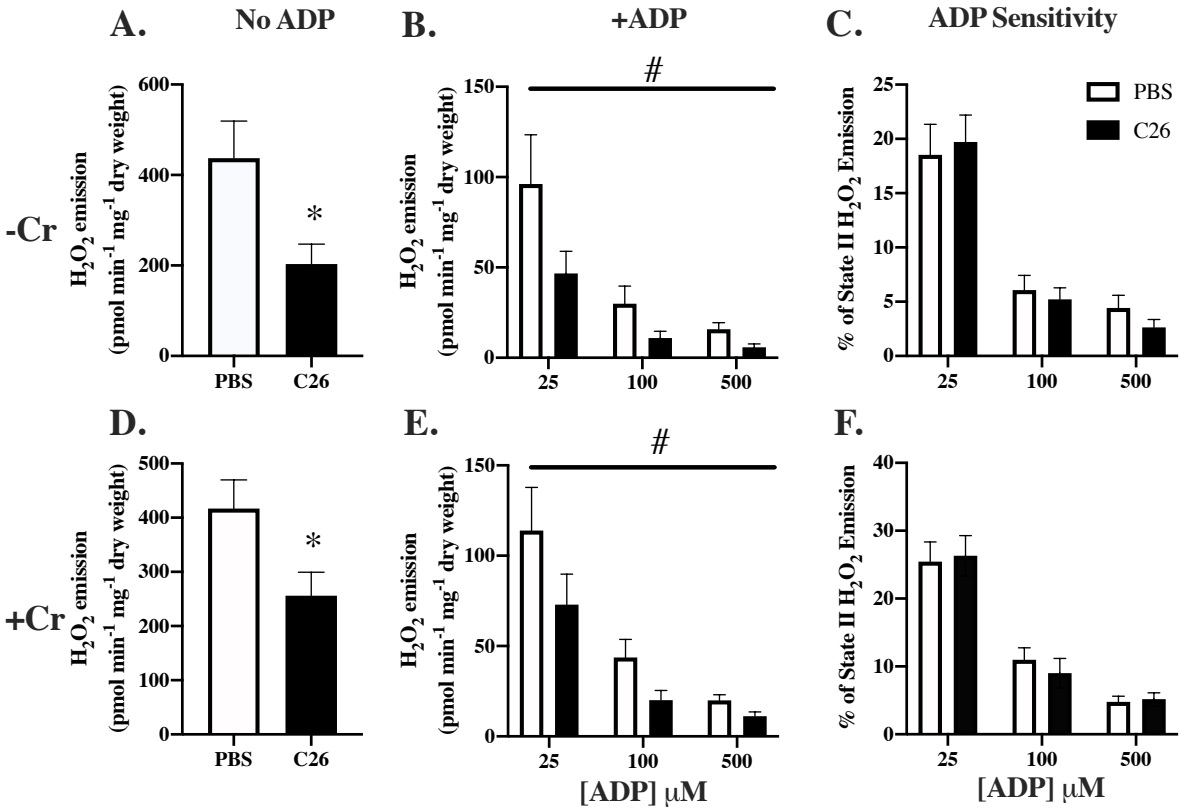

Figure 8: Impact of C26 Cancer on Quadriceps Complex I Stimulated mH_2O_2 Emission through forward electron flow from pyruvate/malate (NADH).
Comparison of PBS and C26 quadriceps pyruvate/malate stimulated mH_2O_2 emission without ADP and Cr **(A)** and with Cr **(B)**. The ability of 25, 100 and 500 μM ADP to change mH_2O_2 emission without Cr **(C)** and with Cr **(D)**. The ability for 25, 100 and 500 μM ADP to change mH_2O_2 emission expressed as a percentage of total mH_2O_2 without Cr **(E)** and with Cr **(F).** Results represent mean ± SEM; n = 9-12; # P <0.05 main effect compared with PBS. * P<0.05 compared to PBS.

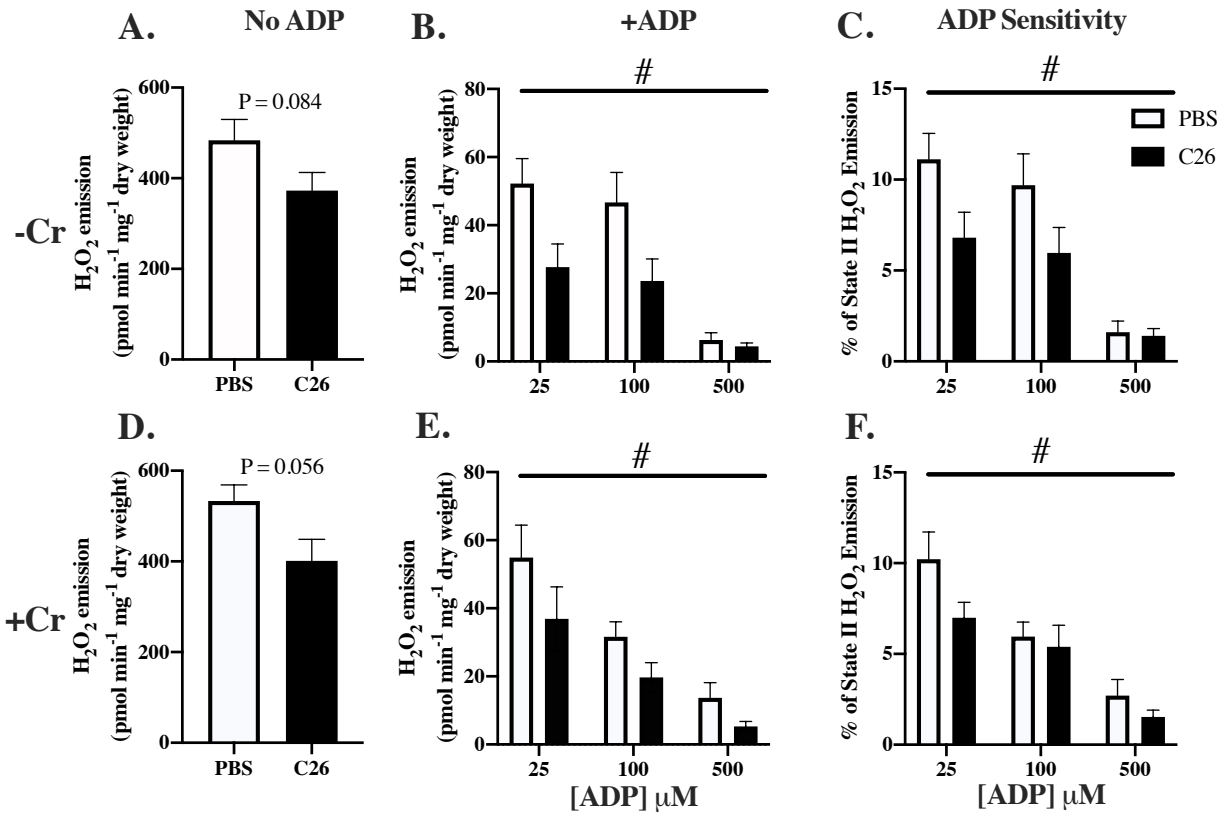

Figure 9: Impact of C26 Cancer on Quadriceps Complex I Stimulated mH_2O_2 Emission Through Reverse Electron Flow from Succinate ($FADH_2$).
Comparison of PBS and C26 quadriceps succinate stimulated mH_2O_2 emission without ADP and Cr **(A)** and with Cr **(B)**. The ability of 25, 100 and 500 u μM ADP to change mH_2O_2 emission without Cr **(C)** and with Cr **(D)**. The ability for 25, 100 and 500 u μM ADP to change mH_2O_2 emission expressed as a percentage of total mH_2O_2 without Cr **(E)** and with Cr **(F).** Results represent mean ± SEM; *n* = 8-12; # *P* <0.05 main effect compared with PBS.

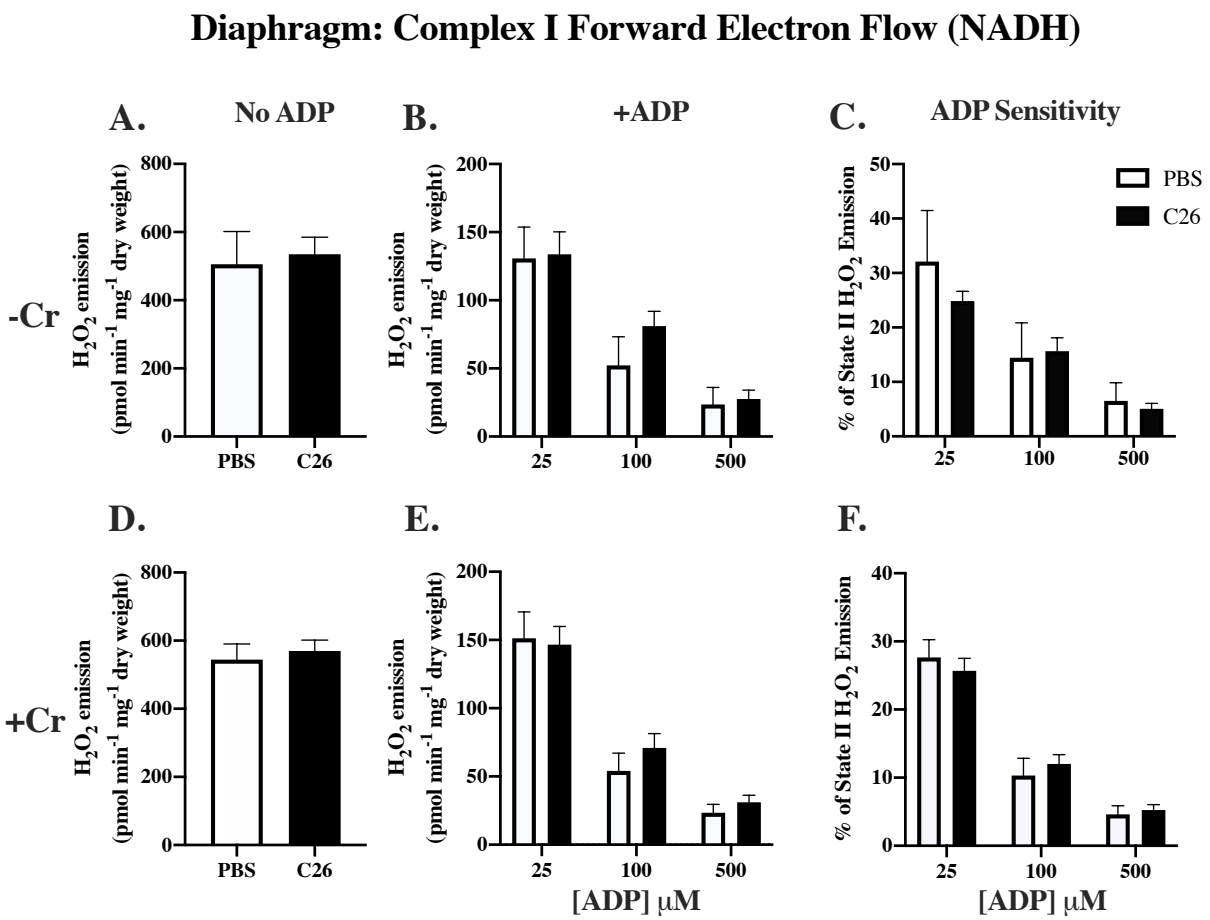

Figure 10: Impact of C26 Cancer on Diaphragm Complex I Stimulated mH_2O_2 Emission through forward electron flow from pyruvate/malate (NADH).
Comparison of PBS and C26 diaphragm pyruvate/malate stimulated mH_2O_2 emission without ADP and Cr **(A)** and with Cr **(B)**. The ability of 25, 100 and 500 u μM ADP to change mH_2O_2 emission without Cr **(C)** and with Cr **(D)**. The ability for 25, 100 and 500 u μM ADP to change mH_2O_2 emission expressed as a percentage of total mH_2O_2 without Cr **(E)** and with Cr **(F).** Results represent mean ± SEM; *n* = 6-11.

Diaphragm: Complex I Reverse Electron Flow ($FADH_2$)

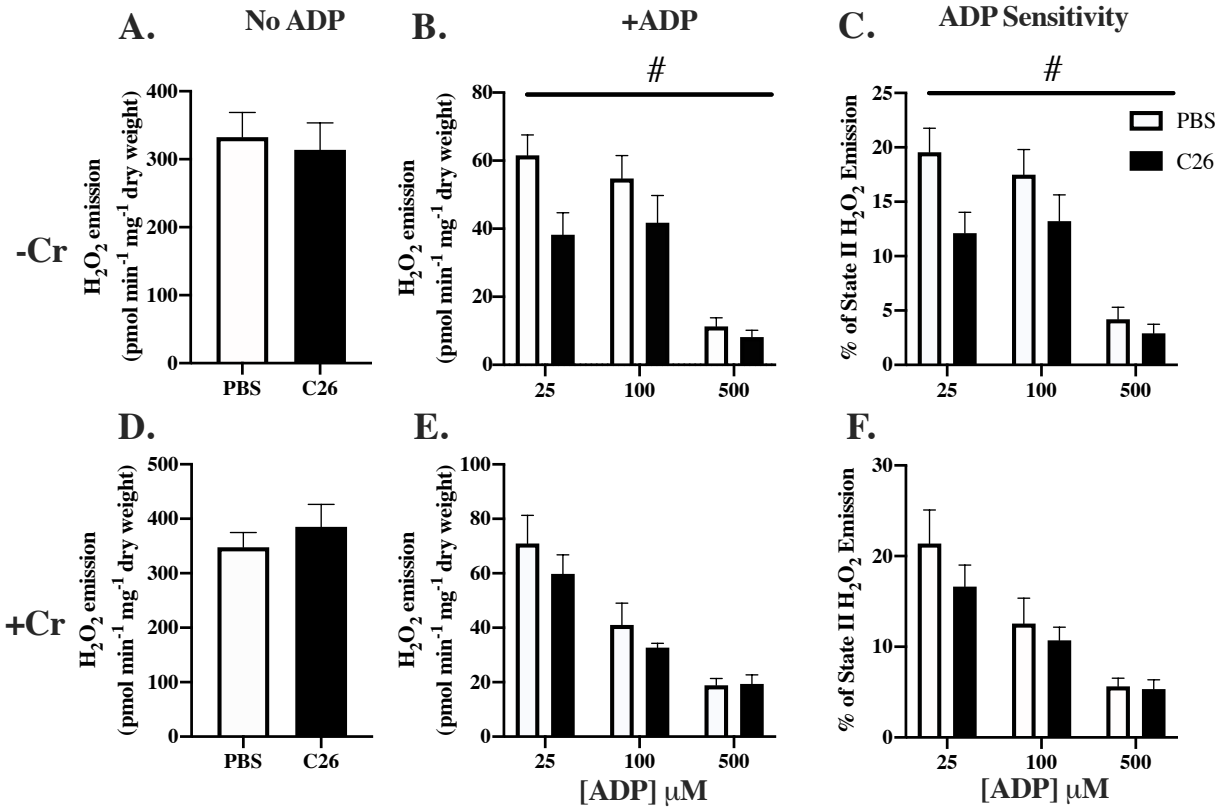

Figure 11: Impact of C26 Cancer on Diaphragm Complex I Stimulated mH_2O_2 Emission Through Reverse Electron Flow from Succinate ($FADH_2$).
Comparison of PBS and C26 diaphragm succinate stimulated mH_2O_2 emission without ADP and Cr **(A)** and with Cr **(B)**. The ability of 25, 100 and 500 μM ADP to change mH_2O_2 emission without Cr **(C)** and with Cr **(D)**. The ability for 25, 100 and 500 μM ADP to change mH_2O_2 emission expressed as a percentage of total mH_2O_2 without Cr **(E)** and with Cr **(F).** Results represent mean ± SEM; n = 8-10; # P <0.05 main effect compared with PBS.

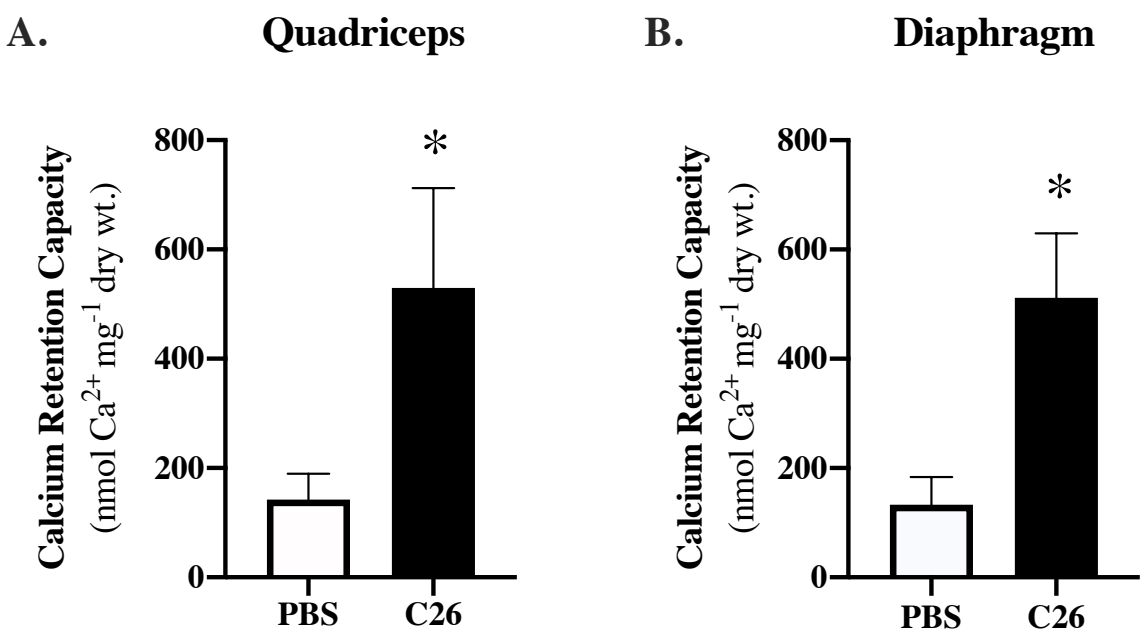

Figure 12: Impact of Cancer on Quadriceps and Diaphragm CRC.
CRC in quadriceps PmFB increased in C26 (*P<0.05)* **(A)**, CRC in diaphragm PmFB increased in C26 (*P<0.05)***(B)**. Results represent mean ± SEM; *n* = 8-12; * *P*<0.05 compared to PBS.

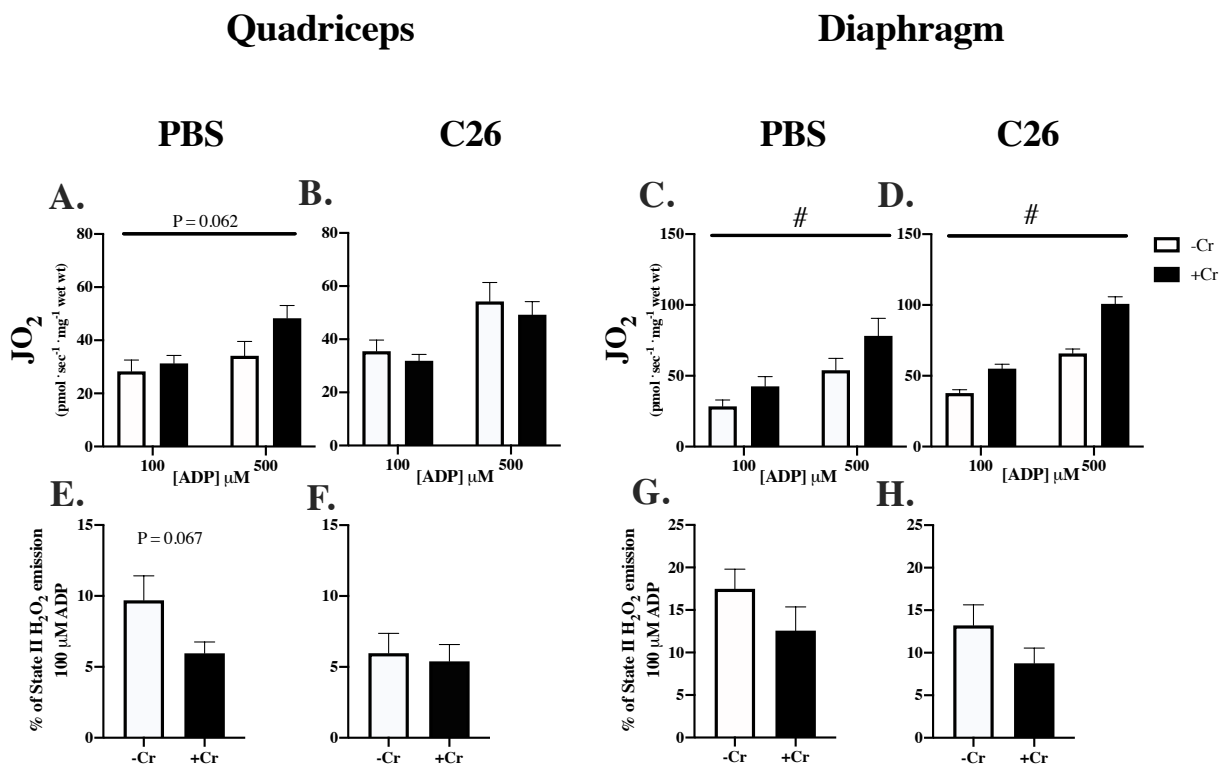

Figure 13: Impact of C26 Cancer on Cr sensitivity in Quadriceps and Diaphragm.
Data previously shown in part in Figure 6, 8 and 10. Comparison of the impact of Cr on PBS quadriceps respiration **(A)** mH_2O_2 emission **(C)** and the impact of Cr on C26 quadriceps respiration **(B**) and mH_2O_2 emission **(D).** Comparison of the impact of Cr on PBS diaphragm respiration **(E)** mH_2O_2 emission **(G)** and the impact of Cr on C26 diaphragm respiration **(F)** and mH2O2 emission **(H).** Results represent mean ± SEM; *n* = 8-12; # *P* <0.05 main effect compared with PBS.

References

1. Hanahan D, Weinberg RA. Hallmarks of cancer: The next generation. In: *Cell*. ; 2011. doi:10.1016/j.cell.2011.02.013
2. Lundholm K, Bylund AC, Holm J, Scherstén T. Skeletal muscle metabolism in patients with malignant tumor. *Eur J Cancer*. 1976;12(6):465-473. doi:10.1016/0014-2964(76)90036-0
3. Fearon K, Strasser F, Anker SD, et al. Definition and classification of cancer cachexia: An international consensus. *Lancet Oncol*. 2011;12(5):489-495. doi:10.1016/S1470-2045(10)70218-7
4. Canadian Cancer Society's Advisory Committee on Cancer Statistics. Canadian Cancer Statistics 2017. Toronto, ON. *Can Cancer Soc*. 2017. doi:0835-2976
5. Peterson SJ, Mozer M. Differentiating Sarcopenia and Cachexia among Patients with Cancer. *Nutr Clin Pract*. 2017;32(1):30-39. doi:10.1177/0884533616680354
6. Tisdale MJ. Cachexia in cancer patients. *Nat Rev Cancer*. 2002;2(11):862-871. doi:10.1038/nrc927
7. Covarrubias L, Hernández-García D, Schnabel D, Salas-Vidal E, Castro-Obregón S. Function of reactive oxygen species during animal development: Passive or active? *Dev Biol*. 2008;320(1):1-11. doi:10.1016/j.ydbio.2008.04.041
8. Neyroud D, Nosacka RL, Judge AR, Hepple RT. Colon 26 adenocarcinoma (C26)-induced cancer cachexia impairs skeletal muscle mitochondrial function and content. *J Muscle Res Cell Motil*. 2019;40(1):59-65. doi:10.1007/s10974-019-09510-4
9. Brown JL, Rosa-Caldwell ME, Lee DE, et al. Mitochondrial degeneration precedes the development of muscle atrophy in progression of cancer cachexia in tumour-bearing mice. *J Cachexia Sarcopenia Muscle*. 2017;8(6):926-938. doi:10.1002/jcsm.12232
10. Hughes MC, Ramos S V., Turnbull PC, et al. Early myopathy in Duchenne muscular dystrophy is associated with elevated mitochondrial H2O2 emission during impaired oxidative phosphorylation. *J Cachexia Sarcopenia Muscle*. 2019;10(3):643-661. doi:10.1002/jcsm.12405
11. Cooper GM, Hausman RE. *The Cell: A Molecular Approach 2nd Edition*.; 2007.
12. Evans WJ, Morley JE, Argilés J, et al. Cachexia: A new definition. *Clin Nutr*. 2008. doi:10.1016/j.clnu.2008.06.013
13. Moses AWG, Slater C, Preston T, Barber MD, Fearon KCH. Reduced total energy expenditure and physical activity in cachectic patients with pancreatic cancer can be modulated by an energy and protein dense oral supplement enriched with n-3 fatty acids. *Br J Cancer*. 2004;90(5):996-1002. doi:10.1038/sj.bjc.6601620
14. Bachmann J, Heiligensetzer M, Krakowski-Roosen H, Büchler MW, Friess H, Martignoni ME. Cachexia worsens prognosis in patients with resectable pancreatic cancer. *J Gastrointest Surg*. 2008;12(7):1193-1201. doi:10.1007/s11605-008-0505-z
15. Dewys WD, Begg C, Lavin PT, et al. Prognostic effect of weight loss prior tochemotherapy in cancer patients. *Am J Med*. 1980;69(4):491-497. doi:10.1016/S0149-2918(05)80001-3
16. Kalantar-Zadeh K, Rhee C, Sim JJ, Stenvinkel P, Anker SD, Kovesdy CP. Why cachexia kills: Examining the causality of poor outcomes in wasting conditions. *J Cachexia Sarcopenia Muscle*. 2013;4(2):89-94. doi:10.1007/s13539-013-0111-0
17. Samuels SE, Knowles AL, Tilignac T, Debiton E, Madelmont JC, Attaix D. Protein metabolism in the small intestine during cancer cachexia and chemotherapy in mice. *Cancer Res*. 2000;60(17):4968-4974.

18. Aoyagi T, Terracina KP, Raza A, Matsubara H, Takabe K. Cancer cachexia, mechanism and treatment. *World J Gastrointest Oncol*. 2015;7(4):17-29. doi:10.4251/wjgo.v7.i4.17
19. Jeff Hardin, Wayne M. Becker, Lewis J. Kleinsmith JH. *Becker's World of the Cell 9th.*; 2016. doi:10.1017/CBO9781107415324.004
20. Fearon KCH, Glass DJ, Guttridge DC. Cancer cachexia: Mediators, signaling, and metabolic pathways. *Cell Metab*. 2012;16(2):153-166. doi:10.1016/j.cmet.2012.06.011
21. Houston ME. *Biochemistry Primer for Exercise Science*. Third.; 2006. doi:10.1097/00005768-199604000-00022
22. Khal J, Hine A V., Fearon KCH, Dejong CHC, Tisdale MJ. Increased expression of proteasome subunits in skeletal muscle of cancer patients with weight loss. *Int J Biochem Cell Biol*. 2005;37(10):2196-2206. doi:10.1016/j.biocel.2004.10.017
23. Jagoe RT, Redfern CPF, Roberts RG, Gibson GJ, Goodship THJ. Skeletal muscle mRNA levels for cathepsin B, but not components of the ubiquitin-proteasome pathway, are increased in patients with lung cancer referred for thoracotomy. *Clin Sci*. 2002;102(3):353-361. doi:10.1042/CS20010270
24. Tisdale MJ. Molecular pathways leading to cancer cachexia. *Physiology*. 2005;20:340-348. doi:10.1152/physiol.00019.2005
25. Li H, Malhotra S, Kumar A. Nuclear factor-kappa B signaling in skeletal muscle atrophy. *J Mol Med*. 2008;86(10):1113-1126. doi:10.1007/s00109-008-0373-8
26. Cai D, Frantz JD, Tawa NE, et al. IKKβ/NF-κB activation causes severe muscle wasting in mice. *Cell*. 2004;119(2):285-298. doi:10.1016/j.cell.2004.09.027
27. Rhoads MG, Kandarian SC, Pacelli F, Doglietto GB, Bossola M. Expression of NF-κB and IκB proteins in skeletal muscle of gastric cancer patients. *Eur J Cancer*. 2010;46(1):191-197. doi:10.1016/j.ejca.2009.10.008
28. Ballarò R, Costelli P, Penna F. Animal models for cancer cachexia. *Curr Opin Support Palliat Care*. 2016;10(2):281-287. doi:10.1097/SPC.0000000000000233
29. Narsale AA, Carson JA. Role of interleukin-6 in cachexia: Therapeutic Implications. *Curr Opin Support Palliat Care*. 2014;8(4):321-327. doi:10.1097/SPC.0000000000000091
30. Bonetto A, Aydogdu T, Kunzevitzky N, et al. STAT3 activation in skeletal muscle links muscle wasting and the acute phase response in cancer cachexia. *PLoS One*. 2011;6(7):e22538. doi:10.1371/journal.pone.0022538
31. White JP, Puppa MJ, Gao S, Sato S, Welle SL, Carson JA. Muscle mTORC1 suppression by IL-6 during cancer cachexia: A role for AMPK. *Am J Physiol - Endocrinol Metab*. 2013;304(10):E1042-E1052. doi:10.1152/ajpendo.00410.2012
32. Glass DJ. PI3 Kinase Regulation of Skeletal Muscle Hypertrophy and Atrophy. In: Rommel C, Vanhaesebroeck B, Vogt PK, eds. *Phosphoinositide 3-Kinase in Health and Disease: Volume 1*. Berlin, Heidelberg: Springer Berlin Heidelberg; 2011:267-278. doi:10.1007/82_2010_78
33. Gordon JN, Green SR, Goggin PM. Cancer cachexia. *QJM An Int J Med*. 2005;98(11):779-788. doi:10.1093/qjmed/hci127
34. Todorov P, Cariuk P, McDevitt T, Coles B, Fearon K, Tisdale M. Characterization of a cancer cachectic factor. *Nature*. 1996;379(6567):739-742. doi:10.1038/379739a0
35. Whitehouse AS, Tisdale MJ. Increased expression of the ubiquitin-proteasome pathway in murine myotubes by proteolysis-inducing factor (PIF) is associated with activation of the transcription factor NF-kappaB. *Br J Cancer*. 2003;89(6):1116-1122. doi:10.1038/sj.bjc.6601132
36. Lorite MJ, Smith HJ, Arnold JA, Morris A, Thompson MG, Tisdale MJ. Activation of ATP-ubiquitin-dependent proteolysis in skeletal muscle in vivo and murine myoblasts in

vitro by a proteolysis-inducing factor (PIF). *Br J Cancer*. 2001;85(2):297-302. doi:10.1054/bjoc.2001.1879
37. Argilés JM, López-Soriano FJ, Stemmler B, Busquets S. Therapeutic strategies against cancer cachexia. *Eur J Transl Myol*. 2019;29(1):7960. doi:10.4081/ejtm.2019.7960
38. Temparis S, Asensi M, Estrela JM, Ferrara M, Larbaud D, Attaix D. Increased ATP-Ubiquitin-dependent Proteolysis in Skeletal Muscles of Tumor-bearing Rats. *Cancer Res*. 1994;54(21):5568-5573.
39. Llovera M, Garcia-Martinez C, Agell N, Lopez-Soriano FJ, Argiles JM. Muscle wasting associated with cancer cachexia is linked to an important activation of the atp-dependent ubiquitin-mediated proteolysis. *Int J Cancer*. 1995;61(1):138-141. doi:10.1002/ijc.2910610123
40. Baracos VE, DeVivo C, Hoyle DHR, Goldberg AL. Activation of the ATP-ubiquitin-proteasome pathway in skeletal muscle of cachectic rats bearing a hepatoma. *Am J Physiol - Endocrinol Metab*. 1995;268(5):E996-E1006. doi:10.1152/ajpendo.1995.268.5.e996
41. Glickman MH, Ciechanover A. The ubiquitin-proteasome proteolytic pathway: Destruction for the sake of construction. *Physiol Rev*. 2002;82(2):373-428. doi:10.1152/physrev.00027.2001
42. Lecker SH, Jagoe RT, Gilbert A, et al. Multiple types of skeletal muscle atrophy involve a common program of changes in gene expression. *FASEB J*. 2004;18(1):39-51. doi:10.1096/fj.03-0610com
43. Sukari A, Muqbil I, Mohammad RM, Philip PA, Azmi AS. F-BOX proteins in cancer cachexia and muscle wasting: Emerging regulators and therapeutic opportunities. *Semin Cancer Biol*. 2016;36:95-104. doi:10.1016/j.semcancer.2016.01.002
44. Yuan L, Han J, Meng Q, et al. Muscle-specific E3 ubiquitin ligases are involved in muscle atrophy of cancer cachexia: An in vitro and in vivo study. *Oncol Rep*. 2015;33(5):2261-2268. doi:10.3892/or.2015.3845
45. Liu D, Qiao X, Ge Z, et al. IMB0901 inhibits muscle atrophy induced by cancer cachexia through MSTN signaling pathway. *Skelet Muscle*. 2019;9(1):8. doi:10.1186/s13395-019-0193-2
46. Vazeille C, Jouinot A, Durand JP, et al. Relation between hypermetabolism, cachexia, and survival in cancer patients: A prospective study in 390 cancer patients before initiation of anticancer therapy. *Am J Clin Nutr*. 2017;105(5):1139-1147. doi:10.3945/ajcn.116.140434
47. de Castro GS, Simoes E, Lima JDCC, et al. Human Cachexia Induces Changes in Mitochondria, Autophagy and Apoptosis in the Skeletal Muscle. *Cancers (Basel)*. 2019;11(9):1264. doi:10.3390/cancers11091264
48. Vanderveen BN, Fix DK, Carson JA. Disrupted Skeletal Muscle Mitochondrial Dynamics, Mitophagy, and Biogenesis during Cancer Cachexia: A Role for Inflammation. *Oxid Med Cell Longev*. 2017;2017. doi:10.1155/2017/3292087
49. McLean JB, Moylan JS, Andrade FH. Mitochondria dysfunction in lung cancer-induced muscle wasting in C2C12 myotubes. *Front Physiol*. 2014;5(503):1-8. doi:10.3389/fphys.2014.00503
50. Smith HJ, Lorite MJ, Tisdale MJ. Effect of a cancer cachectic factor on protein synthesis/degradation in murine C2C12 myoblasts: Modulation by eicosapentaenoic acid. *Cancer Res*. 1999;59:5507-5513.
51. Penna F, Busquets S, Argilés JM. Experimental cancer cachexia: Evolving strategies for getting closer to the human scenario. *Semin Cell Dev Biol*. 2016;54:20-27. doi:10.1016/j.semcdb.2015.09.002
52. White JP, Baltgalvis KA, Puppa MJ, Sato S, Baynes JW, Carson JA. Muscle oxidative

capacity during IL-6-dependent cancer cachexia. *Am J Physiol - Regul Integr Comp Physiol*. 2011;300(2):R201-R211. doi:10.1152/ajpregu.00300.2010
53. Nicholls DG, Ferguson SJ. *Bioenergetics (Fourth Edition)*.; 2013. doi:10.1007/978-0-387-30411-3_1
54. Mitchell P. Coupling of phosphorylation to electron and hydrogen transfer by a chemi-osmotic type of mechanism. *Nature*. 1961;191:144-148. doi:10.1038/191144a0
55. Nelson D., Cox M. *Lehninger Principles of Biochemistry, Sixth Edition.*; 2013. doi:10.1017/CBO9781107415324.004
56. Wong H-S, Dighe PA, Mezera V, Monternier P-A, Brand MD. Production of superoxide and hydrogen peroxide from specific mitochondrial sites under different bioenergetic conditions. *J Biol Chem*. 2017;292(41):16804-16809. doi:10.1074/jbc.R117.789271
57. Brand MD. Mitochondrial generation of superoxide and hydrogen peroxide as the source of mitochondrial redox signaling. *Free Radic Biol Med*. 2016;100:14-31. doi:https://doi.org/10.1016/j.freeradbiomed.2016.04.001
58. Rasola A, Bernardi P. Mitochondrial permeability transition in Ca2+-dependent apoptosis and necrosis. *Cell Calcium*. 2011;50(3):222-233. doi:https://doi.org/10.1016/j.ceca.2011.04.007
59. Colombini M. VDAC: The channel at the interface between mitochondria and the cytosol. *Mol Cell Biochem*. 2004;256(1/2):107-115. doi:10.1023/b:mcbi.0000009862.17396.8d
60. Chevrollier A, Loiseau D, Reynier P, Stepien G. Adenine nucleotide translocase 2 is a key mitochondrial protein in cancer metabolism. *Biochim Biophys Acta - Bioenerg*. 2011;1807(6):562-567. doi:10.1016/j.bbabio.2010.10.008
61. Meyer RA, Sweeney HL, Kushmerick MJ. A simple analysis of the “phosphocreatine shuttle”. *Am J Physiol*. 1984;246(5 Pt 1):C365-77. doi:10.1152/ajpcell.1984.246.5.C365
62. Schlattner U, Tokarska-Schlattner M, Wallimann T. Mitochondrial creatine kinase in human health and disease. *Biochim Biophys Acta - Mol Basis Dis*. 2006;1762:164-180. doi:10.1016/j.bbadis.2005.09.004
63. Wallimann T, Tokarska-Schlattner M, Schlattner U. The creatine kinase system and pleiotropic effects of creatine. *Amino Acids*. 2011;40(5):1271-1296. doi:10.1007/s00726-011-0877-3
64. Guzun R, Gonzalez-Granillo M, Karu-Varikmaa M, et al. Regulation of respiration in muscle cells in vivo by VDAC through interaction with the cytoskeleton and MtCK within Mitochondrial Interactosome. *Biochim Biophys Acta - Biomembr*. 2012;1818(6):1545-1554. doi:https://doi.org/10.1016/j.bbamem.2011.12.034
65. Zulian A, Schiavone M, Giorgio V, Bernardi P. Forty years later: Mitochondria as therapeutic targets in muscle diseases. *Pharmacol Res*. 2016;113(Pt A):563-573. doi:10.1016/j.phrs.2016.09.043
66. Boyman L, Williams GSB, Khananshvili D, Sekler I, Lederer WJ. NCLX: the mitochondrial sodium calcium exchanger. *J Mol Cell Cardiol*. 2013;59:205-213. doi:10.1016/j.yjmcc.2013.03.012
67. Orrenius S, Zhivotovsky B, Nicotera P. Regulation of cell death: the calcium–apoptosis link. *Nat Rev Mol Cell Biol*. 2003;4(7):552-565. doi:10.1038/nrm1150
68. Karch J, Molkentin JD. Identifying the components of the elusive mitochondrial permeability transition pore. *Proc Natl Acad Sci*. 2014;111(29):10396 LP - 10397. doi:10.1073/pnas.1410104111
69. Orrenius S, Gogvadze V, Zhivotovsky B. Calcium and mitochondria in the regulation of cell death. *Biochem Biophys Res Commun*. 2015;460(1):72-81. doi:https://doi.org/10.1016/j.bbrc.2015.01.137

70. Zhivotovsky B, Orrenius S. Calcium and cell death mechanisms: A perspective from the cell death community. *Cell Calcium*. 2011;50(3):211-221. doi:https://doi.org/10.1016/j.ceca.2011.03.003
71. Lemasters JJ, Qian T, Bradham CA, et al. Mitochondrial dysfunction in the pathogenesis of necrotic and apoptotic cell death. *J Bioenerg Biomembr*. 1999;31(4):305-319. doi:10.1023/a:1005419617371
72. Li P, Nijhawan D, Budihardjo I, et al. Cytochrome c and dATP-dependent formation of Apaf-1/caspase-9 complex initiates an apoptotic protease cascade. *Cell*. 1997;91(4):479-489. doi:10.1016/s0092-8674(00)80434-1
73. Iqbal S, Hood DA. The role of mitochondrial fusion and fission in skeletal muscle function and dysfunction. *Front Biosci (Landmark Ed*. 2015;20:157-172. doi:10.2741/4303
74. Fontes-Oliveira CC, Busquets S, Toledo M, et al. Mitochondrial and sarcoplasmic reticulum abnormalities in cancer cachexia: Altered energetic efficiency? *Biochim Biophys Acta - Gen Subj*. 2013;(1830):2770-2778. doi:10.1016/j.bbagen.2012.11.009
75. Penna F, Costamagna D, Pin F, et al. Autophagic degradation contributes to muscle wasting in cancer cachexia. *Am J Pathol*. 2013;182(4):1367-1378. doi:10.1016/j.ajpath.2012.12.023
76. Zhang J. Teaching the basics of autophagy and mitophagy to redox biologists—Mechanisms and experimental approaches. *Redox Biol*. 2015;4:242-259. doi:https://doi.org/10.1016/j.redox.2015.01.003
77. Holloszy JO. Biochemical Adaptations in Muscle. *J Biol Chem*. 1967;242(9):2278-2282.
78. Lin J, Handschin C, Spiegelman BM. Metabolic control through the PGC-1 family of transcription coactivators. *Cell Metab*. 2005;1(6):361-370. doi:10.1016/j.cmet.2005.05.004
79. Brand MD, Nicholls DG. Assessing mitochondrial dysfunction in cells. *Biochem J*. 2011;435(2):297-312. doi:10.1042/BJ20110162
80. Julienne CM, Dumas J-F, Goupille C, et al. Cancer cachexia is associated with a decrease in skeletal muscle mitochondrial oxidative capacities without alteration of ATP production efficiency. *J Cachexia Sarcopenia Muscle*. 2012;3(4):265-275. doi:10.1007/s13539-012-0071-9
81. Fermoselle C, García-Arumí E, Puig-Vilanova E, et al. Mitochondrial dysfunction and therapeutic approaches in respiratory and limb muscles of cancer cachectic mice. *Exp Physiol*. 2013;98(9):1349-1365. doi:10.1113/expphysiol.2013.072496
82. Halle JL, Pena GS, Paez HG, et al. Tissue-specific dysregulation of mitochondrial respiratory capacity and coupling control in colon-26 tumor-induced cachexia. *Am J Physiol Regul Integr Comp Physiol*. 2019;317(1):R68-R82. doi:10.1152/ajpregu.00028.2019
83. Barreiro E, de la Puente B, Busquets S, López-Soriano FJ, Gea J, Argilés JM. Both oxidative and nitrosative stress are associated with muscle wasting in tumour-bearing rats. *FEBS Lett*. 2005;579(7):1646-1652. doi:10.1016/j.febslet.2005.02.017
84. Davies MJ. Protein oxidation and peroxidation. *Biochem J*. 2016;473(7):805-825. doi:10.1042/BJ20151227
85. Gouspillou G, Sgarioto N, Kapchinsky S, et al. Increased sensitivity to mitochondrial permeability transition and myonuclear translocation of endonuclease G in atrophied muscle of physically active older humans. *FASEB J Off Publ Fed Am Soc Exp Biol*. 2014;28(4):1621-1633. doi:10.1096/fj.13-242750
86. Godin R, Daussin F, Matecki S, Li T, Petrof BJ, Burelle Y. Peroxisome proliferator-

activated receptor γ coactivator1- gene α transfer restores mitochondrial biomass and improves mitochondrial calcium handling in post-necrotic mdx mouse skeletal muscle. *J Physiol*. 2012;590(21):5487-5502. doi:10.1113/jphysiol.2012.240390
87. Murphy KT, Chee A, Trieu J, Naim T, Lynch GS. Importance of functional and metabolic impairments in the characterization of the C-26 murine model of cancer cachexia. *DMM Dis Model Mech*. 2012;5:533-545. doi:10.1242/dmm.008839
88. Talbert EE, Metzger GA, He WA, Guttridge DC. Modeling human cancer cachexia in colon 26 tumor-bearing adult mice. *J Cachexia Sarcopenia Muscle*. 2014;5(4):321-328. doi:10.1007/s13539-014-0141-2
89. Brooks S V, Faulkner JA. Contractile properties of skeletal muscles from young, adult and aged mice. *J Physiol*. 1988;404:71-82. doi:10.1113/jphysiol.1988.sp017279
90. Ramos S V., Hughes MC, Perry CGR. Altered skeletal muscle microtubule-mitochondrial VDAC2 binding is related to bioenergetic impairments after paclitaxel but not vinblastine chemotherapies. *Am J Physiol - Cell Physiol*. 2019;316(3):C449-C445. doi:10.1152/ajpcell.00384.2018
91. Fisher-Wellman KH, Gilliam LAA, Lin C-T, Cathey BL, Lark DS, Darrell Neufer P. Mitochondrial glutathione depletion reveals a novel role for the pyruvate dehydrogenase complex as a key H2O2-emitting source under conditions of nutrient overload. *Free Radic Biol Med*. 2013;65:1201-1208. doi:10.1016/j.freeradbiomed.2013.09.008
92. Perry CGR, Kane DA, Lin C Te, et al. Inhibiting myosin-ATPase reveals a dynamic range of mitochondrial respiratory control in skeletal muscle. *Biochem J*. 2011;437(2):215-222. doi:10.1042/BJ20110366
93. Tsien RY. Fluorescent Indicators of Ion Concentrations. *Methods Cell Biol*. 1989;30:127-156. doi:10.1016/S0091-679X(08)60978-4
94. Bhosale G, Duchen MR. Investigating the Mitochondrial Permeability Transition Pore in Disease Phenotypes and Drug Screening. *Curr Protoc Pharmacol*. 2019;85(1):e59. doi:10.1002/cpph.59
95. Roberts BM, Frye GS, Ahn B, Ferreira LF, Judge AR. Cancer cachexia decreases specific force and accelerates fatigue in limb muscle. *Biochem Biophys Res Commun*. 2013;435(3):488-492. doi:10.1016/j.bbrc.2013.05.018
96. Picard M, Hepple RT, Burelle Y. Mitochondrial functional specialization in glycolytic and oxidative muscle fibers: tailoring the organelle for optimal function. *Am J Physiol Cell Physiol*. 2012;302(4):C629-41. doi:10.1152/ajpcell.00368.2011
97. Bloemberg D, Quadrilatero J. Rapid determination of myosin heavy chain expression in rat, mouse, and human skeletal muscle using multicolor immunofluorescence analysis. *PLoS One*. 2012;7(4):e35273. doi:10.1371/journal.pone.0035273
98. Ciciliot S, Rossi AC, Dyar KA, Blaauw B, Schiaffino S. Muscle type and fiber type specificity in muscle wasting. *Int J Biochem Cell Biol*. 2013;45(10):2191-2199. doi:https://doi.org/10.1016/j.biocel.2013.05.016
99. Herzig S, Shaw RJ. AMPK: guardian of metabolism and mitochondrial homeostasis. *Nat Rev Mol Cell Biol*. 2018;19(2):121-135. doi:10.1038/nrm.2017.95
100. Anflous K, Armstrong DD, Craigen WJ. Altered mitochondrial sensitivity for ADP and maintenance of creatine-stimulated respiration in oxidative striated muscles from VDAC1-deficient mice. *J Biol Chem*. 2001;276(3):1954-1960. doi:10.1074/jbc.M006587200
101. Kuznetsov A V, Tiivel T, Sikk P, et al. Striking differences between the kinetics of regulation of respiration by ADP in slow-twitch and fast-twitch muscles in vivo. *Eur J Biochem*. 1996;241(3):909-915. doi:10.1111/j.1432-1033.1996.00909.x

102. Hughes MC, Ramos S V, Turnbull PC, et al. Impairments in left ventricular mitochondrial bioenergetics precede overt cardiac dysfunction and remodelling in Duchenne muscular dystrophy. *J Physiol*. 2020;598(7):1377-1392. doi:10.1113/JP277306
103. Ydfors M, Hughes MC, Laham R, Schlattner U, Norrbom J, Perry CGR. Modelling in vivo creatine/phosphocreatine in vitro reveals divergent adaptations in human muscle mitochondrial respiratory control by ADP after acute and chronic exercise. *J Physiol*. 2016;594(11):3127-3140. doi:10.1113/JP271259
104. Hughes MC, Ramos S V, Turnbull PC, et al. Mitochondrial Bioenergetics and Fiber Type Assessments in Microbiopsy vs. Bergstrom Percutaneous Sampling of Human Skeletal Muscle. *Front Physiol*. 2015;6:360. doi:10.3389/fphys.2015.00360
105. Meyer LE, Machado LB, Santiago APSA, et al. Mitochondrial creatine kinase activity prevents reactive oxygen species generation: antioxidant role of mitochondrial kinase-dependent ADP re-cycling activity. *J Biol Chem*. 2006;281(49):37361-37371. doi:10.1074/jbc.M604123200

SUPPLEMENTAL FIGURES

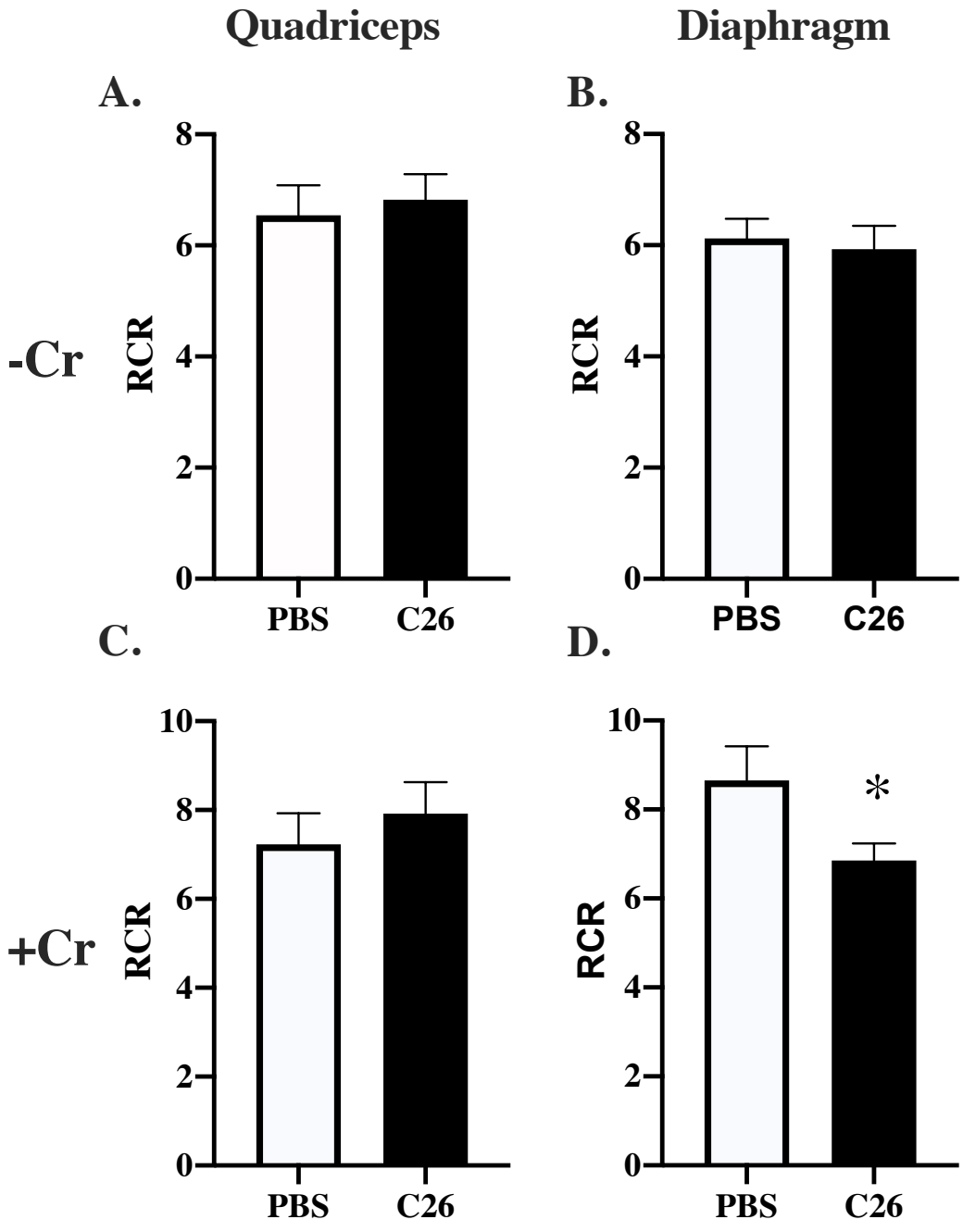

Supplemental Figure 1: Mitochondrial Respiration Expressed as RCR.
Comparison of PBS and C26 muscle RCR in -Cr quadriceps **(A)** and – Cr diaphragm **(B)** along with +Cr in quadriceps **(C)** and +Cr diaphragm **(D).** Results represent mean ± SEM; n = 8-12; * P<0.05 compared to PBS.

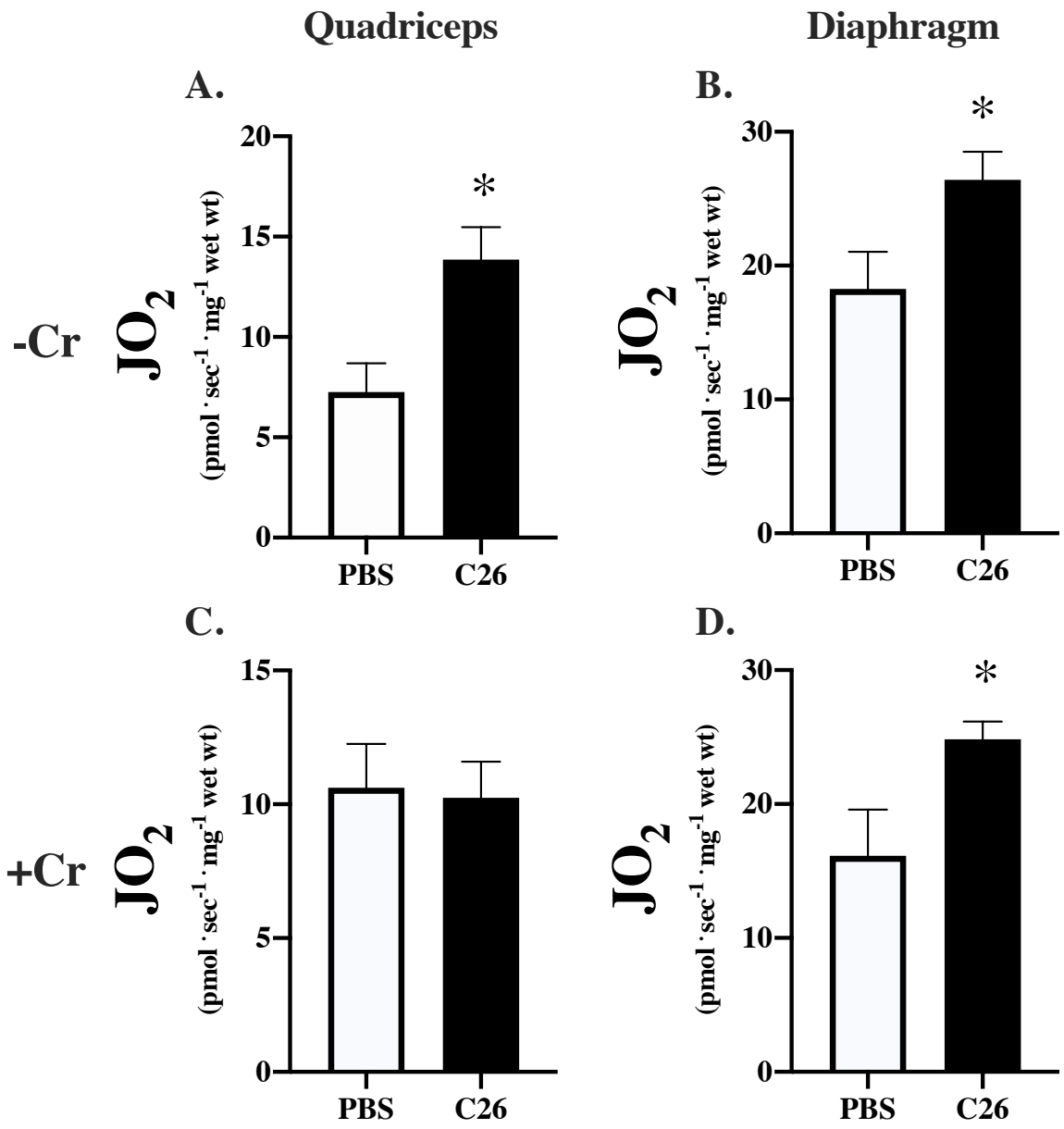

Supplemental Figure 2: State II +Cr and -Cr respiration in Quadriceps and Diaphragm. Comparison of PBS and C26 muscle state II respiration in -Cr quadriceps **(A)** and – Cr diaphragm **(B)** along with +Cr in quadriceps **(C)** and +Cr diaphragm **(D).** Results represent mean ± SEM; *n* = 8-12; * *P*<0.05 compared to PBS.

APPENDIX A: Cell Counting and Cell Inoculation

Cell Counting: LD Method

1. Complete steps 1-13 in "Cell Passaging: LD Method"
2. Go to fume hood and fill 250 uL eppendorf tube with 190 uL of Trypan Blue (Sigma. Lot #:RNBF3897; MW: 960.81 g/mol)
3. Take 10 uL out of the 3 mL Cocktail of the cells and media and put into the 190 uL of Trypan Blue (20 fold dilution). Invert up and down.
4. Take falcon tube of cell cocktail and spin down.
5. Add 10 uL of the solution onto the top and bottom of the hemocytometer

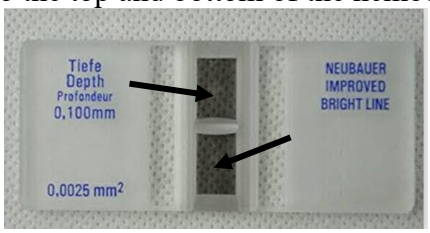

6. Apply cover slip. Make sure whole section is "filled" (you can likely only do this one side at a time -of course, this is fine because you can only count one side at a time)
7. Count cells that are "fully" in the grid. If it touches the top or left it is considered "in." If it touches the bottom or right it is considered "out."

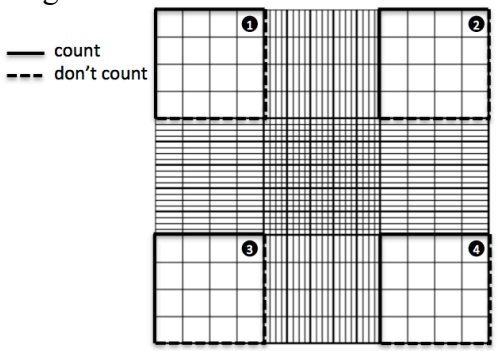

8. Add cells from grid 1, 2, 3 and 4. Take this number and divide it by 4 (average of all 4 squares). Multiply the result by 10^4 (grid represents 10, 000 cells per mL) and multiply it by 20 (dilution factor).
    a. Ex. (207 cells / 4) x 10, 000 cells/mL x 20 = 10, 350,000 cells/mL
9. Because we have 3mL of cells in suspension (from step 3), to get our total number of cells we need to multiply our result from step 8 by 3.
    a. Ex 10,350,000 cells/mL x 3mL = 31,050,000 cells
10. Take the centrifuged falcon tube and dispense the media into the waste bottle in the BSA
11. Resuspend cells in 1 mL of media (you now have a 31,050,000 cells/mL solution)
12. Re-plate cells to keep cell line growing and use remaining volume to complete any experiment needed.

Tumour Inoculation – SOP: LD

Growing and implanting C26 cells

1) Warm all C26 growth media (10%FBS, 1% P/S) to 37° in a waterbath
2) Thaw frozen vial of C26 cells in waterbath
3) Add media to flask
4) Pipette all cells (~1.5x10^6 cells) into flask and tilt to spread cells evenly.
5) Place in incubator and check ~2 hours later that cells are beginning to adhere.
6) Replace media daily for 2 days
7) On day three, ~75% confluence should be reached.
8) Remove media and rinse with PBS 2X.
9) Add trypsin (1mL for T75)
10) Incubate ~5 min
11) Gently tap plate.
12) Add at least 2ml of culture media to plate and pipet around plate to dislodge cells.
13) Collect media+cells in 15mL tube.
    (1) Add 20 uL of cell cocktail to 180 uL of tryban blue. Flick tube to mix
    (2) Count the cells by loading 10uL on hematocytometer with coverglass on top.
14) Spin down at ~250g for ~5min.
15) Remove supernatant without disturbing the pellet.
16) Add ~5mL PBS to cell pellet and mix by gentle pipetting.
17) Repeat steps 14-16 2x.
18) Re-suspend pellet in 5 x 10^6 cells/mL
    (1) Keep cells on ice and inject within 3 hours.
19) Inject
    a) 100uL of cell suspension (5x10^5 cells) into each flank.
    b) Anestitize in insoflurane box and place prone in nose cone.
        i) Shave both flanks near hindlimb
        ii) Sterilize the skin surface
        iii) Insert needle subcutaneously so that bevel is visible through surface of the skin.
        iv) Slowly inject cells so that a symmetrical bubble arises from the flank.
            (1) Do not remove needle immediately but rather wait ~15 seconds and withdraw very slowly to prevent cells from coming out of injection site.
        v) Tumor development should become obvious around 2 weeks post injection

APPENDIX B: *In situ* and *in vitro* Force Production

In Situ Quad Force Production Protocol
Updated June 16 2020 CB

A good rule of thumb is to have practiced this surgery at least 10-15 times and be able to get consistent data with previous literature. If you are doing a new model establish your own normal values in a pilot data set.

Protocol

1. Create a folder to save files for each animal - Setup: Autosave Folder, open folder you created; click "current folder"
2. Setup: Instant Stim
    a. Pulse Frequency: 1Hz
    b. Pulse Width: 0.2ms
    c. Number of Pulses: 1
    d. Train Frequency: 0.1Hz
    e. Run Time: 1 second
    ** I have a train frequency that does 3 twitches with a delay between that I find most useful for optimizing current
3. Open Live Data monitor and set time to 10 minutes
4. Optimize Current
    a. Range:10mA -100mA (if you can get the right placement this can go to 10mA, but if you struggle can go to 10% of 100mA- still 10mA)
    b. Run instant stim
    c. Adjust range to ensure all muscle fibres are being recruited – obtain 3 twitches in a row where force does not increase (run instant stim and increase current between twitches (wait about 30 seconds in between twitches)
    d. Set supramaximal current by increasing current by 15%
5. Optimize Resting Length
    a. Before officially setting optimal length, you will need to toggle the thread from the quad to the hook with forceps- this will reduce any basal tension in the line
    b. Increase/decrease length of quad until maximal twitch force is achieved, wait about 30 seconds in between twitches to avoid fatigue
    c. Time and keep basal tension about constant in the study

Once optimal current and length have been set, protocol is ready to begin

6. Load **"Quad In Situ Force Frequency"** sequence
    a. Frequencies of 40Hz, 60Hz, 80Hz, 100Hz, 120Hz, 140Hz, 160Hz,180Hz, 200Hz, 220Hz
        i. Initial Delay: 0.2ms
        ii. Pulse Frequency: ____Hz (above frequency)

iii. Pulse Width: 0.2ms
iv. Duration: 300ms

b. 45 seconds in between (can extend up to 1 min)

7. Allow 5 minutes of recovery
8. Load the tetanic protocol at the frequency that produced the highest force during step 6
9. Perform Pre Fatigue Max Force Test – make sure to save this file!
10. Allow 2 minutes recovery
11. Load "**Quad In Situ Fatigue"** sequence for your study (Fatigue protocols are varied in the literature- find one that works for your study
    a. 60 Hz, stim every second for 120 seconds (2mins)
    b. 60Hz, stim every 1.5 seconds for 120 contractions (3mins)
12. Allow 5-minute recovery from fatigue
13. Perform a second max force test at the same frequency used in step 8 – this assesses recovery from fatigue- label as **5min-post-fatigue**
14. Allow 5 minute recovery; perform another max force-label as **10min-post-fatigue**
15. Allow 5 minutes recovery; perform last max force-label as **15min-post-fatigue**
16. Harvest muscle and before freezing **MAKE SURE TO RECORD MUSCLE WEIGHT**

Data will be normalized muscle weight

In Vitro Diaphragm Force Production Protocol

Updated: June 2020 CAB

Practice of the dissection is crucial for this technique as changes in force development could be a result of technical skill of experimenter, before a study make sure you can consistently produce normal forces. When performing dissection, do so under dissection microscope in cold Tyrodes (also called Ringers) buffer on an ice pack, pining muscle when necessary. Use surgeons' knots to tie off central tendon and loop before attaching to force transducer.

Ensure you bath is filled with Tyrodes solution and oxygenated for 30mins with attached 95% O_2/ 5% CO_2 tank, with water circulator turned on and maintained at 25°C prior to start of surgery. This ensures the bath and muscle has enough oxygen since we are relying on diffusion of oxygen into the muscle and not perfusion through blood supply. CO_2 provides necessary buffering of pH during contraction. Limit strip width to 2mm (maximum 4mm) as wider strips have difficulties with diffusion limitations of O_2. 25°C is used over 37°C as oxygen has poor solubility at higher temperatures.

If you were previously doing in-vivo force

In vitro force is measured in force production (mN) not moment of Force (mN-m)—this is TORQUE

To change units: setup→ Channel set up→ force in device→ select mN

repeat with length (should appear in mm)

setup→ Channel set up →length in → select mm

Have Bath temperature to 25°C- this is to ensure oxygen stays dissolved in the bath

Protocol:

1. Create folder to save files for each animal→ File→ set up autosave folder→ open folder created→click "current folder"
2. Set up Instant Stim→ this will be used for length optimization and stim optimization
    a. Pulse Frequency : 1Hz (this is a single twitch; can increase if you want to provide tetanus stimulus)
    b. Pulse width: 0.2ms (how long the stimulus is given)
    c. Number of pulses: 3 (again giving single twitch)
    d. Train Frequency: 0.1Hz (If you are using multiple twitches this gives 10s of rest between stimuli)
    e. Run time: 1 second (amount of time of data collection)
    ** currently I have a better instant stimulation for optimizing current saved (the settings are saved in a photo on force computer)

3. Open live data monitor (File→ open live data monitor); Instant stim orange button will be available for use.
    a. Set time to 10mins (can see protocol or optimization) (screen will automatically scroll)

4. Let diaphragm strip acclimatize for 20-30mins with some tension applied (will appear at 0mm on length in monitor at the end of acclimatization)
    a. This will allow resting tension in the muscle to relax and will reduce background tension; I typically have it resting with some tension on it (6-10mm) and will give it a tetanus stimulus to fully relax the fibres before optimizing length for full data collection.

5. Optimize the current
    a. Range: **1A (50-70%)** (in vitro force stimulation requires a much higher amperage or voltage than in-situ or in-vivo force stimulation since this is a field stimulation- don't be afraid to have it at a high amperage)
    b. Run Instant Stim and check force development
    c. Increase range to ensure all fibres are recruited- if you see an increase in force development then more fibres have been recruited and you are not at a supramaximal current. Use 3 twitches in a row with increasing current (30s rest between) where force does not increase.
    d. Set supramaximal current by increasing current by 15% (this will ensure you have all fibres being activated in the muscle strip).

6. Optimize the length (necessary to make sure maximal amount of cross bridges are forming)
   YOU NEED TO RECORD THIS LENGTH AT THE END OF DATA COLLECTION
    a. Gradually increase length of diaphragm strip and apply instant stim. Provide 30s of rest to avoid fatigue.
    b. Continue to increase length of diaphragm until you obtain maximal twitch force.
    c. You will need to increase the length of the diaphragm quite considerably compared to an upright bath since this bath is flat- but be careful of drastic changes in length this will increase basal tension of diaphragm strip. Use ¼ turns of fine adjustment knob and use gross only when necessary.
    d. If you want to collect this data load a single twitch protocol in DMC software and enable autosave- this is optional but for training purposes would be beneficial to look at the shape of the twitch. Can also do this with tetanus to

e. Measure the length of the diaphragm and record, this is L_o and can be input on the main DMC screen and will be used for analysis
    i. Setup normalization- enter the reference length in mm
f. Allow some time (approx. 5min) for muscle to rest before starting force frequency curve

7. Optimal current and length have now been set, protocol is ready to begin.

8. Load "Diaphragm in-vitro force frequency" sequence
    a. Frequencies of 1 Hz, 10Hz, 20Hz, 40Hz, 80Hz, 100 Hz, 120Hz, 140Hz,160Hz & 200Hz
        i. Initial delay : 0.2ms (this is the rest period prior to stim)
        ii. Pulse Frequency: the above frequencies
        iii. Pulse Width: length of stimulus
        iv. Duration: **400ms** (inputted in s in protocol editor) *might consider increasing this but 400ms provides tension to return to baseline recording following contraction (Tupling lab uses a 1 sec- 600-800ms might be sufficient).
    b. 60s rest in between; avoids fatigue

9. Allow 5 mins recovery for the muscle to avoid fatigue in max force test
10. Load tetanic protocol at the frequency that produces the highest force during force frequency test (label this as pre-fatigue max force test)
11. Perform Pre-Fatigue Max-Force Test
12. Allow 2 mins recovery
13. Load "**Diaphragm In Vitro Fatigue**" sequence
    a. 70Hz (350ms stim, 0.2ms pulse width) every 2 seconds for 5 mins
14. Allow 5 minutes recovery from fatigue
15. Perform a second max force test at the same frequency used in Prefatigue max force test- this assesses recovery from fatigue and can be labelled as **5-min-post-fatigue max** force test.
16. Allow 5 minutes recovery
17. Perform third max force test; label as **10min-post-fatigue-max**
18. Allow 5 minutes recovery
19. Perform Fourth max Recovery test label as **15min-post-fatigue-max**
20. MAKE SURE YOU HAVE RECORDED LENGTH!!!
21. Remove muscle from bath and remove from central tendon and ribs before weighing. Obtain weight in mg.

22. Data will be normalized to Cross sectional area : mass X length X density
    a. Mammalian skeletal muscle density =1.06g/cm^3 (Mendez and key, 1960); this is commonly used in the field as it. CSA in short allows you to compare differing muscle weights and lengths of muscle. Normalizing to CSA is a way of controlling for sarcomeres in parallel and normalizing to muscle length during shortening contractions is a way of controlling for the number of sarcomeres in series.
    b. "If you need a visual -think of a rope. How strong is a single rope- now cut it in half so you have 2 shorter ropes. Lay them beside each other and glue them together. You now effectively have a new stronger rope with twice the CSA of the first rope, but it weighs the exact same (wait... forget the glue... the rope just really sticky for some reason). Cut the rope again and stick the two pieces together again. Repeat as many times as you want. You now have a rope which has a much larger CSA than the original rope, and it can handle much more load than the original rope but weighs the same and is much shorter. Replace rope with contracting muscle fibres and you probably get the idea. "- Ian Smith 2018

APPENDIX C: Preparation of PmFBs and Mitochondrial Bioenergetics

Permeabilized Fibre Preparation

Pre-surgery

1. For every fibre bundle you are going to make you will need one 0.5mL tube for wet weights one 1.5mL eppendorf tube for permeabilization and one 1.5mL tube for wash

* Keep all tubes and buffers on ice

2. In a 5mL tube, make 10mg/mL Saponin solution by dissolving a small amount of saponin in distilled water
    a. Vortex gently and place on rocker until ready for use
3. Fill all permeabilization tubes with 1.5mL of freshly thawed BIOPS (or BIOPS from fridge with fresh EGTA…see "Other Things to Consider") and *40ug/mL saponin (6uL in 1.5mL BIOPS).
    a. * different saponin concentrations may be used depending on species/tissue type but 40ug/mL is standard for rodent
4. Fill all wash tubes with 1.5mL freshly thawed MiRO (or from fridge…same as above)
5. Fill all 0.5mL tubes with 500uL of BIOPS
6. Using a 50mL falcon tube, weigh out ~ 0.05g of creatine (this number will change based on the number of chambers you need with creatine), add the correct amount of MiRO to make a 20mM Creatine MiRO Solution
    a. Place on rocker as creatine takes some time to dissolve
7. Label and fill a 5mL tube with 3.5mL BIOPS for every muscle that will be harvested during surgery
8. Proceed to "O2k Setup" Section, after O2k's are setup you are ready for surgery

Post-Surgery

1. Separate fibres in BIOPS as quickly and carefully as possible
    a. Remember to change ice block/ice pack frequently as buffer should never be allowed to warm up
2. Place separated fibres in corresponding 0.5mL tube with BIOPS and proceed to wet weight procedure

Bundle Wet Weights

1. Fill a 1.5mL tube with BIOPS until a dome of liquid covers the top
2. Place tube in holder on scale and tare the scale
3. With fine forceps remove first bundle from eppendorf and using a kim wipe, blot the bundle to remove excess liquid
    a. Try to blot no more than 3 times and try to turn the bundle the same way each time to get consistent blotting
4. Very carefully place bundle in liquid on scale, making sure the forceps to not draw up any liquid
5. Wait for scale to stabilize and record weight
6. Until accuracy is proven, do duplicates of each weight and take average if within 0.2mg, repeat weighing if weights are more variable

7. When done weighing, place back in 0.5mL eppendorf tube until all bundles have been weighed

Permeabilization

1. Once all bundles are weighed, switch bundles to permeabilization tubes (the ones that have saponin) using forceps or a gel loading pipette tip
2. Place on nutator in the fridge for 30 minutes
    a. Make sure all eppendorfs have the liquid mixing by ensuring that the air bubble is moving
    b. If air bubble appears stuck, invert eppendorf 1-2 times to allow for movement and place back on nutator
3. After 30 minutes, transfer bundles to corresponding wash tubes using gel loading pipette tip
4. Place bundles in wash back on nutator in the fridge for 15 minutes
    a. Permeabilized bundles can remain in fridge in wash for up to 2 hours but will start to lose viability after that point so use bundles ASAP
5. After 15 minute wash proceed to “Running an Experiment”

Respiration SOP

MOUSE QUAD- 20mM CR				
Substrate	**Event Code**	**STOCK**	**Titration Volume (µL)**	**Final Concentration in Chamber**
MiRO5		20mM Cr		
Lights Out	F10			
BLEB	BLEB	10 mM BLEB	1	5 µM
Fibre	Fibre			
Stop stir bar, turn on lights and verify fibre is in chamber/not stuck on side wall				
		Hit F10 (lights out)		
100% O_2	O		Injection	250-275 µM
Pyruvate	P	**2M**	**5**	5 mM
Malate	M	**1M**	**4**	2 mM
ADP	25 µM D	**5 mM**	**10**	25 µM
ADP	100 µM D	**50 mM**	**3**	100 µM
ADP	500 µM D	**50 mM**	**16**	500 µM
ADP	5 mM D	**500 mM**	**18**	5 mM
Cyto c	Cyto c	**4 mM**	**5**	10 µM
Succinate	20 mM S	**2M**	**20**	20 mM

MOUSE DIA- 20mM CR

Substrate	Event Code	STOCK	Titration Volume (µL)	Final Concentration in Chamber
MiRO5		20mM Cr		
Lights Out	F10			
BLEB	BLEB	10 mM BLEB	1	5 µM
Fibre	Fibre			
Stop stir bar, turn on lights and verify fibre is in chamber/not stuck on side wall				
		Hit F10 (lights out)		
100% O_2	O		Injection	250-275 µM
Pyruvate	P	**2M**	**5**	5 mM
Malate	M	**1M**	**4**	2 mM
ADP	25 µM D	**5 mM**	**10**	25 µM
ADP	100 µM D	**50 mM**	**3**	100 µM
ADP	500 µM D	**50 mM**	**16**	500 µM
ADP	1 mM D	**500 mM**	**2**	1 mM
ADP	5 mM D	**500 mM**	**16**	5 mM
Cyto c	Cyto c	**4 mM**	**5**	10 µM
Succinate	20 mM S	**2M**	**20**	20 mM

MOUSE QUAD- No CR

Substrate	Event Code	STOCK	Titration Volume (µL)	Final Concentration in Chamber
MiRO5		No Cr		
Lights Out	F10			
BLEB	BLEB	10 mM BLEB	1	5 µM
Fibre	Fibre			
Stop stir bar, turn on lights and verify fibre is in chamber/not stuck on side wall				
		Hit F10 (lights out)		
100% O_2	O		Injection	250-275 µM
Pyruvate	P	**2M**	**5**	5 mM
Malate	M	**1M**	**4**	2 mM
ADP	25 µM D	**5 mM**	**10**	25 µM
ADP	100 µM D	**50 mM**	**3**	100 µM
ADP	500 µM D	**50 mM**	**16**	500 µM
ADP	5 mM D	**500 mM**	**18**	5 mM
ADP	30 mM D	**1 M**	**50**	30 mM
Cyto c	Cyto c	**4 mM**	**5**	10 µM
Succinate	20 mM S	**2M**	**20**	20 mM

MOUSE DIA- No CR

Substrate	Event Code	STOCK	Titration Volume (µL)	Final Concentration in Chamber
MiRO5		No Cr		
Lights Out	F10			
BLEB	BLEB	10 mM BLEB	1	5 µM
Fibre	Fibre			
Stop stir bar, turn on lights and verify fibre is in chamber/not stuck on side wall				
		Hit F10 (lights out)		
100% O_2	O		Injection	250-275 µM
Pyruvate	P	**2M**	**5**	5 mM
Malate	M	**1M**	**4**	2 mM
ADP	25 µM D	**5 mM**	**10**	25 µM
ADP	100 µM D	**50 mM**	**3**	100 µM
ADP	500 µM D	**50 mM**	**16**	500 µM
ADP	5 mM D	**500 mM**	**18**	5 mM
ADP	7 mM D	**500 mM**	**8**	7 mM
Cyto c	Cyto c	**4 mM**	**5**	10 µM
Succinate	20 mM S	**2M**	**20**	20 mM

MOUSE Quad- No Cr - OCARN

Substrate	Event Code	STOCK	Titration Volume (µL)	Final Concentration in Chamber
MiRO5		20mm Cr		
Lights Out	F10			
Fibre (4-5 mg)	Fibre			
Stop stir bar, turn on lights and verify fibre is in chamber/not stuck on side wall				
		Hit F10 (lights out)		
100% O_2	O		Injection	250-275 µM
OCarn	200 OC	**100mM**	**4**	200 uM
Malate	M	**1M**	**4**	2 mM
ADP	5 mM D	**500 mM**	**20**	5 mM
OCarn	500 OC	**100 mM**	**6**	500 uM
Pyruvate	PYR	**2 M**	**5**	5 mM
Cyto c	Cyto c	**4 mM**	**5**	10 µM
Succinate	20 mM S	**2M**	**20**	20 mM

mH_2O_2 SOP

SUCCINATE (Complex I reverse)

SLOT	Assay Buffer	Pre-experiment		Substrates		ADP		ADP		ADP	
1	20mM Creatine 1mL	**1U HRP** 2uL of 500U/mL	3 min	**10mM Succinate** 5uL of 2M	5 min	5uL of 5mM	2min	1.5uL of 50mM	2min	0.8uL of 500mM	2min
2	No Creatine 1mL	Fibre									

PYRUVATE + MALATE (Complex I forward)

35uM CDNB (5uL of 10.5mM Stock)

SLOT	Assay Buffer	Pre-experiment		Substrates		ADP		ADP		ADP	
1	20mM Creatine 1mL	**1U HRP** 2uL of 500U/mL	3 min	**10mM Pyruvate** 5uL of 2M	1 min	5uL of 5mM	2min	1.5uL of 50mM	2min	0.8uL of 500mM	2min
2	No Creatine 1mL	Fibre		**2mM Malate** 2uL of 1M							

PYRUVATE + ROTENONE * OWN CUVETTE (For PDH complex)**

35uM CDNB (5uL of 10.5mM Stock)

SLOT	Assay Buffer	Pre-experiment		Substrates	
1	No Cr 1mL	**1U HRP** 2uL of 500U/mL	**10MIN (In QM40)**	**10mM Pyruvate** 5uL of 2M	5 min
2	No Cr 1mL	**0.5uM Rotenone** 2uL of 250uM Fibre			

Antimycin A (for Complex III)

SLOT	Assay Buffer	Pre-experiment		Substrates	
1	No Cr	**1U HRP**		**2.5uM**	
		2uL of		Antimycin	**10**
	1mL	500U/mL	3		**MIN**
			min	5uL of	
		Fibre		0.5mM	
2	No Cr				
	1mL				

** treat like succinate

CRC SOP

Procedure

* place cuvettes on stir plate and fill with ddH_2O and 10uL EGTA (0.5M stock) (minimum 10mins)

1. Harvest muscle and place in ice cold **BIOPS**
2. Separate fibres into bundles (SMALLER than those used for respiration & even more separated)
3. Permeabilize for 30 minutes in BIOPS with 30ug/mL saponin
4. WASH 1: 10 minutes in 1.5mL Buffer Y + 1mM EGTA (3uL of 0.5M)
5. Turn on fluorometer to allow lamp to heat up
6. WASH 2: 10 minutes in 1.5mL Buffer Y + 10uM BLEB (1.5uL of 10mM BLEB) **be conscience of how long bundles are in fridge for (max viability 4 hours)
7. Aspirate out water from cuvette but DO NOT RINSE (keep cuvette lined with EGTA) & add necessary ingredients according to table below and fibre
8. Select Calcium Uptake Assay Protocol on PTI Software. Make sure the following parameters are set:
    a. Excitation: 506
    b. Emission: 532
    c. Duration – 3000 seconds
    d. Slit Widths: Excitation 3nM
       Emission 3nM
    e. x-axis window: 2000 seconds
    f. y axis min and max: 200 000 and 500 000 ** this changes depending on strength of the bulb (newer bulbs may be closer 500 000 as the min)

Substrate	Stock Concentration	Addition to cuvette	Final Concentration in Cuvette
CRC Assay Buffer		300uL	
Glutamate	2M	1.5uL	10mM
Malate	1M	1.5uL	5mM
ADP	500mM	3uL	5mM
Fibre	**** make sure fibre is at the bottom of cuvette attached to stir bar****		
Collect 400 second background to establish "F-Min"			
$CaCl_2$	5mM	2.5uL	8nmol
Wait 5 minutes or until steady state			
$CaCl_2$	5mM	1.25uL	12nmol (4nmol pulse)
Wait 5 minutes in between pulses and continue pulsing until pore opens			
$CaCl_2$	50mM	5uL	0.5mM Pulse (F-Max)
Wait 3 minutes before final addition, this should establish F-Max but last addition is to make sure			
$CaCl_2$	50mM	5uL***	0.5mM Pulse (F-Max)

$CaCl_2$	50mM	Continue as necessary until flat peak	0.5mM Pulse (F-Max)

* for each addition remove cuvette from holder and ensure fibre has not been disrupted
**Make sure y axis is no more than 300 000 units or you will miss opening
*** ensure that you have F-Max by continually titrating 50mM Ca^{2+} until flat peak (need to test with SHIV)

9. Remove bundle and save for freeze drying (if applicable)

APPENDIX D: Buffers

BIOPS BUFFER (Extracellular)

Chemical	Stock Solution	Molecular Weight	Final Concentration	Addition to *2 Litre* Final Volume
CaK_2EGTA*	100mM		2.77mM	55.4mL
K_2EGTA*	100mM		7.23mM	144.6mL
Na_2ATP		555.1	5.77mM	6.41g
$MgCl_2 \cdot 6H_2O$		203.3	6.56mM	2.67g
Taurine		125.1	20mM	5.02g
Na_2Phosphocreatine		327.14	15mM	9.81g
Imidazole		68.1	20mM	2.72g
Dithiothreitol (DTT)		154.2	0.5mM	0.154g
MES Hydrate		195.2	50mM	19.52g

*__ALWAYS__ double check molecular weights for supplier-specific chemicals (n=m/M.W.)

BIOPS contains the following ion concentrations		**EXTRACELLULAR RANGE**
Ca^{2+} free	0.1uM	Rat: 7.6mM Mouse: 1.3mM
Mg^{2+} free	1mM	
Na^+	41mM	Human: 133-143mM
K^+	20mM	Human: 4.5mM
Cl^-	13mM	Rat: 160mM Mouse: 95-120mM
MgATP	5mM	
Ionic Strength	160mM	
Osmolality	295 mOsm	

*Ionic strength is the sum of all ions
*Buffers do not perfectly reflect extracellular conditions
*Species-specific extracellular ranges exist
*Ranges are expressed as mmol/L (refer to ion concentration summary chart)

CaK_2EGTA: Dissolve 2.002g of $CaCO_3$ in 100mM hot (80°C) solution of EGTA (7.608g of EGTA in 200mL ddH_2O). Add 2.3g of KOH and adjust pH to 7.0 using KOH. Freeze unused portions.

K_2EGTA: Dissolve 7.608g EGTA and 2.3g KOH into 200mL ddH_2O. Adjust pH to 7.0 using KOH. Freeze unused portions.

To make BIOPS:

1. Add approximately 1500mL of ddH_2O to 2000mL beaker
2. While constantly stirring add stock solutions of CaK_2EGTA and K_2EGTA
3. Weigh and add all powder chemicals
4. Adjust pH to 7.1 using KOH pellets
5. Using graduated cylinder, bring total volume to 2000mL
6. Filter and then aliquot into 50mL falcon tubes
7. Freeze falcon tubes

MiRO BUFFER (Intracellular)

Chemical	Stock Solution	Molecular Weight	Final Concentration	Addition to *2 Litre* Final Volume
EGTA		380.4	0.5mM	0.38g
$MgCl_2 \cdot 6H_2O$		203.3	3mM	1.22g
K-Lactobionate*	0.5M	358.3 free acid	60mM	240mL
Taurine		125.1	20mM	5.02g
KH_2PO_4		136.1	10mM	2.72g
HEPES		238.3	20mM	9.54g
Sucrose		342.3	110mM	75.3g
BSA		154.2	1g/L	2.0g

*ALWAYS double check molecular weights for supplier-specific chemicals (n=m/M.W.)

MiRO contains the following ion concentrations		**INTRACELLUAR RANGE**
Ca^{2+} free	0.0uM	Human: 30nM – 60nM SR: 5.7-20mmol/L Free Ca^{2+} in SR 0.2-0.5mM Rat: 7.76-11.11 ueq/g dry wt
Mg^{2+} free	2.1mM	
Na^+	0.0mM	Human: 6-13mM Rat: 7.10-21.9mmol/L
K^+	90mM	Human: 130 – 164mmol/L Rat: 117 – 149mmol/L
Cl^-	6mM	Rat: 4.97-16.57mmol/L
PO_4^{3-}	10mM	
EGTA free	0.46mM	
Ionic Strength	95mM	
Osmolality	330 mOsm	

*Ionic strength is the sum of all ions
*Buffers do not perfectly reflect extracellular conditions
*Species-specific intracellular ranges exist
*Ranges are expressed as mmol/L (refer to ion concentration summary chart)

K-Lactobionate: Dissolve 71.6g lactobionic acid in 300mL ddH_2O, adjust pH to 7.0, adjust final volume to 400mL with ddH_2O

To make MiRO:

1. Add approximately 1500mL of ddH_2O to 2000mL beaker
2. While constantly stirring add stock solution of K-Lactobionate
3. Weigh and add all powder chemicals
4. Adjust pH to 7.1 using KOH pellets
5. Using graduated cylinder, bring total volume to 2000mL
6. Filter and then aliquot into 50mL falcon tubes
7. Freeze falcon tubes

BUFFER Z (Intracellular)

Chemical	Molecular Weight	Final Concentration	Addition to *500mL* Final Volume
K-MES	233.33	105mM	12.26g
KCl	74.55	30mM	1.12g
KH_2PO_4	136.08	10mM	0.7g
$MgCl_2 \cdot 6H_2O$	203.3	5mM	0.51g
EGTA	380.35	1mM	0.19g
BSA		5mg/mL	2.5g

*__ALWAYS__ double check molecular weights for supplier-specific chemicals (n=m/M.W.)

Buffer Z contains the following ion concentrations		**INTRACELLULAR RANGE**
Ca^{2+}	0.0uM	Human: 30nM – 60nM SR: 5.7-20mmol/L Free Ca^{2+} in SR 0.2-0.5mM Rat: 7.76-11.11 ueq/g dry wt
Mg^{2+} (total, not free)	5mM	
Na^+	0.0mM	Human: 6-13mM Rat: 7.10-21.9mmol/L
K^+	145mM	Human: 130 – 164mmol/L Rat: 117 – 149mmol/L
Cl^-	40mM	Rat: 4.97-16.57mmol/L
PO_4^{3-}	10mM	
EGTA free	1mM	

*Buffers do not perfectly reflect extracellular conditions
*Species-specific intracellular ranges exist
*Ranges are expressed as mmol/L (refer to ion concentration summary chart)

To make Buffer Z:

1. Add approximately 400mL of ddH_2O to 1000mL beaker
2. Weigh and add all powder chemicals
3. Adjust pH to 7.4 using KOH pellets
4. Using graduated cylinder, bring total volume to 500mL
5. Filter and then aliquot into 50mL falcon tubes

6. Freeze falcon tubes